NNT/NL : 0000AIXM0000/000ED000

THÈSE DE DOCTORAT

Soutenue à Aix-Marseille Université
en cotutelle avec l'université de Rhein-Waal University of Applied Sciences
le JJ mois AAAA par

Viraj Pratap Nirwan

Electrospun Hybrid Nanofibers/Nanomats Functionalized with Ligand-Free Nanoparticles as a Platform for Biomedical Applications

Discipline
Physique et sciences de la matière

Spécialité
Matière Condensée et Nanosciences

École doctorale
PHYSIQUE ET SCIENCES DE LA MATIERE (ED 352)

Laboratoire/Partenaires de recherche
Technology and Bionics, Rhine-Waal University of Applied Sciences

Composition du jury

Tatiana ITINA	Rapporteuse
Univ Lyon, UJM-St-Etienne, Laboratoire Hubert Curien, CNRS UMR 5516, France	
Tomasz KOWALCZYK	Rapporteur
Institute of Fundamental Technological Research, Polish Academy of Sciences (IPPT PAN), Poland	
Fang YANG	Examinatrice
Department of Biomaterials, Radboud University Medical Centre, The Netherlands	
Yanqiu ZHU	Examinateur
College of Engineering, Mathematics and Physical Sciences, University of Exeter, UK	
Andrei KABASHIN	Directeur de thèse
Aix-Marseille Université, CNRS, UMR 7341, LP3, France	
Amir FAHMI	Directeur de thèse
Rhein-Waal University of Applied Sciences, Germany	
Ahmed AL-KATTAN	Co-directeur de thèse
Aix-Marseille Université, CNRS, UMR 7341, LP3, France	

Affidavit

I, undersigned, Viraj Pratap Nirwan, hereby declare that the work presented in this manuscript is my own work, carried out under the scientific direction of Prof. Dr. Andrei Kabashin, Prof. Dr. Amir Fahmi and Dr. Ahmed Al-Kattan, in accordance with the principles of honesty, integrity and responsibility inherent to the research mission. The research work and the writing of this manuscript have been carried out in compliance with both the French national charter for Research Integrity and the Aix-Marseille University charter on the fight against plagiarism.

This work has not been submitted previously either in this country or in another country in the same or in a similar version to any other examination body.

Place Kleve Germany, date 4 Mars 2021

Abstract

Nanostructured hybrid materials in particular electrospun nanofibers received significant attention due to their unique collective properties and their used in wide range of applications such as filtration membranes, superhydrophobic protective layer for clothing, nanocatalysts, and tissue engineering scaffolds. The generated hybrid nanofibers via electrospinning techniques possess large surface area to volume, superior mechanical properties, improved cavity size and porosity, flexibility and possibility of surface modifications became extraordinary functional biomaterials. Hybrid nanofibers inherit the intrinsic properties of polymer (natural or synthetic) used to incorporate new structural and chemical properties via immobilization of functional moieties such as inorganic nanoparticles, drug molecules, or inorganic polymers in their matrix.

In principle there are multiple mechanisms driving the fabrication of hybrid nanofibers which include template synthesis, self-assembly, phase-separation, and electrospinning. Compared to other methods, electrospinning is regarded as simple yet efficient mechanism for the fabrication of nanofibers. Electrospinning offers the possibility to obtain hybrid nanofibers from widely dissimilar materials. For instance, combining various polymers and functional inorganic nanoparticles to design attractive properties including biodegradability and biocompatibility.

Hybrid nanofibers possess extraordinary properties arising from nanostructure, precursor polymers. Additionally, they contain functional agents such as metallic nanoparticles which can offer remarkable optical, chemical, and electro-magnetic properties. Two different methods were used to fabricate nanoparticles. For instance, gold (AuNPs) nanoparticles obtained by wet chemistry method required several toxic chemicals throughout the process which might dampen their biocompatibility, exclusively for biological applications. Hence, pulsed laser ablation in liquid (PLAL) was preferred here for the synthesis of gold (AuNPs) and titanium nitride (TiN NPs) nanoparticles. With the applications of PLAL, it was possible to obtain ultraclean, bare (ligand-free), dispersed nanoparticles (NPs). The application of laser ablative approach avoided bio-toxic chemicals which minimised the toxicity of NPs.

In this thesis, an emphasis was given to combine the advantages of electrospun nanofibers and immobilization of metallic nanoparticles and inorganic polymers into multifunctional hybrid nanofibers. The process of obtaining uniform, non-woven hybrid nanofibers is very complex due to interdependency of multiple electrospinning parameters and properties of precursor solutions. Therefore, several optimisation studies were required for each hybrid nanofiber system. Electrospun hybrid nanofibers were analysed by a selection of techniques such as microscopy, spectroscopy, and thermal analyses, beside toxicity and bio-compatibility studies.

Here, multifunctional nanofibers were fabricated from polymers such as chitosan, poly(ethylene oxide) (PEO), polystyrene (PS), polycaprolactone (PCL) and further functionalized with gold nanoparticles (AuNPs), inorganic polymers, and titanium nitride nanoparticles (TiN NPs). First, PEO-chitosan blended nanofibers were electrospun and functionalized with AuNPs, synthesized via both wet-chemistry and pulsed laser ablation processes. Here, effects of preparation conditions and the presence of functionalisation agents on physio-chemical properties of functionalised nanofibers were investigated. Thereafter, pure chitosan (AuNPs) nanofibers were obtained from an improved formulation with higher concentrations of chitosan and bare laser-ablated AuNPs in electrospinning solution. After electrospinning, nanofibers were processed resulting in neutralisation of -NH3+ group of chitosan leading to simultaneous dissolution of PEO present in nanofibers and thus, left chitosan and AuNPs as only elements forming the scaffold matrix.

Other promising hybrid nanofibers were fabricated by blending smart inorganic polymers namely poly (ferrocenylphosphinoboranes) with synthetic homopolymers such as polystyrene (PS) and poly (ethylene oxide) (PEO) to address applications in catalysis, selective filtering, and charge transfer. Here, the electrospinning proved to be a complex, but controllable tool for the incorporation of dissimilar entities into simple nanofiber 2D-structures. Furthermore, this approach makes possible the employment of various collector types to produce efficient scaffolds for the incubation of cells in tissue-engineering applications. Finally, the thesis reports the fabrication of polycaprolactone (PCL)-based nanofibers decorated with (ultra-clean) bare laser-ablated TiN NPs. Then the nanofibers were analysed using usual physico-chemical techniques, while biological compatibility and toxicity studies showed no adverse effect on the cell growth in presence of TiN NPs in scaffolds.

This exploratory research demonstrated the feasibility of fabrication of nanofibers functionalized with laser synthesised nanoparticles for their potential application in biomedicine and tissue engineering.

Résumé

Les nanofibres hybrides sont des matériaux de choix, présentant des propriétés uniques de nanomatériaux fonctionnels. Elles sont composées de parties organique et inorganique, où la fraction organique constitue la structure de la nanofibre tandis que la faction inorganique représente la partie fonctionnelle. La méthode d'électrofilage (electrospinning) permet la fabrication de multitude de nanofibres de formulation variée avec la possibilité d'incorporer des agents fonctionnels, telles que des nanoparticules inorganiques ou encore des molécules d'intérêt. Ce procédé permet aussi la production à grande échelle de nanofibres fabriquées à partir d'une large gamme de polymères biocompatibles et biodégradables. Grâce à leurs propriétés physico-chimiques spécifiques, ces nanofibres hybrides peuvent ainsi être utilisées comme matrices pour l'immobilisation d'objets (ex., ions, métaux lourds, cellules) pour divers applications, notamment la filtration, l'ingénierie tissulaire, ou encore la théranostique.

Dans ce travail de thèse, nous nous sommes intéressés à l'électrofilage de polymères biodégradables, possédant une bioactivité élevée et une faible toxicité, en particulier pour les applications biomédicales. Ainsi en utilisant cette approche, des nanofibres multifonctionnelles ont été fabriquées à partir de polymères tels que le chitosane, le poly(oxyde d'éthylène)(PEO), le polystyrène (PS) ou encore que la polycaprolactone (PCL). Les nanofibres ont été caractérisées par diverses techniques telles que la microscopie, la spectroscopie, les analyses thermiques, en plus des études de toxicité et de biocompatibilité.

Afin d'améliorer les propriétés intrinsèques des nanofibres et/ou d'acquérir des fonctionnalités nouvelles de therapie et/ou de diagnostic, nous avons associé les nanofibres à divers types de nanoparticules (NP) comme additifs fonctionnels. Dans ce travail, nous avons ainsi choisi l'ablation laser ultra-pulsée comme technique de synthèse des NP. En effet, ce procédé permet la synthèse de NP monodisperse et ultra-propres, sans ligand, en comparaison aux méthodes de synthèses chimiques souvent utilisées. Grâce à cette approche, nous avons ainsi démontré la possibilité de fonctionnalisée des nanofibres hybrides de chitosan(PEO) avec des NP de silicium et d'or. Nous avons ainsi montré par exemples, que l'incorporation de ces NP permettait la réduction du diamètre des fibres sans aucune interférence sur leur composition. De plus, nous avons établi un protocole de neutralisation des nanofibres fonctionnalisées permettant l'obtention de nanofibres de chitosan pur (sans PEO) sans altéré la structure de la matrice fibreuse.

Dans ce travail de thèse, d'autres formulations de nanofibres ont été fabriquées en mélangeant des polymères inorganiques tels que les poly (ferrocénylphosphinoboranes) avec des homopolymères synthétiques tels que le polystyrène (PS) et le poly (oxyde d'éthylène) (PEO) pour répondre à des applications en catalyse, filtrage sélectif et

transfert de charge. Ici, le procédé d'électrofilage a permis l'association d'entités dissemblables dans de simples structures 2D de nanofibres.

Par ailleurs, nous nous sommes également interssés à la fonctionnalisation de nanofibres à base de polycaprolactone (PCL) par des NP de TiN fabriquées par procédé laser. Les nanofibres ont été analysées à l'aide de techniques physico-chimiques habituelles, tandis que les premières études de compatibilité biologique et de toxicité n'ont montré aucun effet indésirable sur la croissance cellulaire en présence de NP.

Ainsi ces matrices de nanofibres hybrides ayant la possibilité d'incorporer des NP de différentes compositions peuvent être d'un atout majeur dans l'élaboration de nanofibres multifonctionnelles pour des applications en ingénierie tissulaire, la filtration, la catalyse et la théranostique.

Acknowledgments

I would like to express sincere gratitude to my supervisors prof. Andrei Kabashin, Research Director (LP3), Aix-Marseille University, France and prof. Amir Fahmi from Rhine-Waal University of Applied Sciences, Germany along with co-supervisor Asst. Prof. Ahmed Al-Kattan from LP3, Aix-Marseille University, France for their encouragement and assistance during the research. They provided immense support and guidance for carrying out the research and writing the thesis.

I offer my sincere appreciation to prof. Amir Fahmi who has kindly offered a fascinating topic along with his insights for a successful research proposal. He has been a constant support both academically and administratively. I would also like to thank Prof. Andrei Kabashin who offered me a great depth of suggestions for improving the thesis which will only help me in the future. My sincere thanks to my co-supervisor asst. prof. Ahmed Al-Kattan who has provided me constant support and offered his kind help for preparing the French version of the abstract.

I would also like to thank the jury members prof. Tatiana Itina from University Lyon, CNRS, France (reviewer), asst. prof. Tomasz Kowalczyk from Institute of Fundamental Technological Research, Polish Academy of Sciences (IPPT PAN), Poland (reviewer), Dr. Yanqiu ZHU from College of Engineering, Mathematics and Physical Sciences, University of Exeter, UK (external examiner) and Dr. Fang Yang from Radboud University Nijmegen Medical Center, Netherlands (external examiner) for spending their time to judge and review the thesis.

It is worth mentioning the enormous effort of our collaborators who provided interdisciplinary support to the research. Prof. Evamarie Hey-Hawkins from Institute for Inorganic Chemistry, Leipzig, prof. Eva Filova from Institute of Experimental Medicine of the Czech Academy of Sciences and Dr. Souvik Pandey from Department of Chemistry, Jadavpur University have helped graciously, resulting in many fruitful publications.

Importantly, I would like to thank the Rhein Waal University of Applied Sciences for providing the complete financial support for the thesis. Additionally, I would like to thank administrative support as well as scientific staff at the Rhine-Waal University for their constant support. Furthermore, I also like to thank the researchers at LP3 whose research has provided excellent preparatory steps for the fabrication of nanoparticles.

My special gratitude to Dr. Olivier Uteza, Dr. Anne Patricia Alloncle and Dr. David Grojo from LP3 for presiding over the review committee and providing their valuable inputs.

I am immensely grateful to my colleagues and fellow researchers at Rhine Waal University of Applied Sciences with whom I had excellent exchange of research ideas. And made the duration of my thesis at the university a memorable experience.

At the end, I would like to express my immense gratitude towards to my parents, siblings, partner, family, and friends who stood by me through every endeavour. They have provided me the necessary support and always motivated me to progress. This thesis would have been impossible without the inspiration provided by supervisors, colleagues, and family.

Contents

List of Figures

List of tables

OUTLINE AND OBJECTIVES OF THE THESIS

This thesis is aimed at the development of hybrid multifunctional nanofiber systems made of a wide range of biocompatible, and biodegradable materials. The objective was to formulate novel promising formulations with distinct characteristics for biomedical applications. Here, electrospinning and laser ablation were utilised as main fabrication tools while properties of nanofibers were studied by a variety of physico-chemical and biological techniques. The fabrication, analysis, and characterisation of multifunctional materials and their constituents with respect to desired applications were performed.

Electrospinning is known as an efficient tool to fabricate multifunctional materials from dissimilar materials. This technique has been quite successful and, is currently widely used at the industrial scale. By extensive utilization of this technique and establishment of protocols for specific materials, a set of promising structures for biomedical applications can be implemented. This thesis addressed the use of electrospinning for the fabrication of biodegradable and bio-compatible polymers for mostly tissue-engineering and theranostics applications, although other applications such as catalysis and filtration were also considered. There is a vast amount of literature data related to functional nanofibers systems, where nanofibers are functionalised with chemically synthesized nano-agents. However, exhibiting many surface groups, such nano-agents typically affected the bio-activity and bio-compatibility of the nanofiber systems. In this thesis, functional nano-agents based on the use of clean, bare (ligand-free) nanomaterials, prepared by methods of laser ablation in liquids are considered for the first time. It is expected that such nano-agents can provide improved bioactivity and functionality of nanofiber platforms. Here, the research is aimed at the development of hybrid multifunctional nanofibers for biomedical applications by the combination of electrospinning and pulsed laser ablation.

Chapter 1 gives a brief overview and introduction of terminology, techniques and materials found in thesis with respect to the existing literature. In particular, it introduces tools and analysis techniques as well as briefly describes their principles and properties. This chapter also outlines the progress in the field of electrospinning and its prospects. **Chapter 2** focuses on the investigation of the impact of nanoparticle preparation techniques on physico-chemical properties of fabricated hybrid nanofibers. Both laser ablation and chemical synthesis were used for the synthesis of AuNPs which were introduced into poly(ethylene oxide) (PEO) and chitosan blends which then were electrospun to form nanofiber matrix. Thermal and morphological changes were assessed based on thermal analysis and scanning electron microscope (SEM), respectively. Electrospinning parameters and solution properties were optimised for the development of PEO/chitosan system. The research in **Chapter 3** is devoted to the development of controlled and efficient routes for the fabrication of pure chitosan nanofibers and their

functionalisation with AuNPs. This chapter also described post-processing approaches to treat nanofibers containing chitosan for their further use in biological media. Such a treatment is important to condition specific properties of nanofiber matrix for further use in tissue engineering scaffolds. **Chapter 4** presents a different paradigm of multifunctional hybrid nanofibers using an unusual combination of inorganic conductive polymers co-electrospun with organic polymer blends. Here, an elaboration of nanofibers via template electrospinning was demonstrated. **Chapter 5** describes co-electrospinning of a distinctive formulation of polycaprolactone (PCL) and titanium nitride nanoparticles (TiN NPs) as well as analysis of properties of formed nanofibers by microscopy, spectroscopy, and thermal analysis. This chapter also addresses the assessment of biocompatibility of the nanofibers and examine tissue engineering. Finally, **chapter 6** provides conclusion on project results and highlights prospects for future developments.

CHAPTER 1

Introduction to Hybrid Multifunctional Nanofibers, Materials and The Tools

Contents

1.1 Introduction

There has been a tremendous growth in technology and its influence on humans for last several decades. Traditional materials which have been used to fuel this growth initially, are no longer a viable solution for emerging technologies [1]. There has been a perpetual pursuit to develop unusual materials and upgrade production methods for new emerging technologies such as miniaturization of telephones which has resulted in development of more energy efficient processors. This improvement is made possible due to the development of advance for semi-conductor materials, micro-electronics, and related manufacturing techniques. Therefore, there has been a constant and ever-increasing demand for the development of such materials with unique properties and combinations. Nature has persistently provided such materials with distinctive combinations through millions of years of evolution. For instance, one can observe such examples in human teeth and bones or shells of brachiopods, crabs, or lobsters. These types of materials are classified as hybrid materials. They are formed gradually, due to biological processes resulting in a mixture of organic and inorganic moieties at nano-and micro-scales. Presence of both inorganics and organics within these structures provide them unique properties and multifunctionality. For instance, properties of inorganic domains provide structural strength, while organic domain provides processability. Thus, creating various structures through depositions of inorganics solubilised within organic matrix is a promising way to achieve new properties. However, the process of deposition and formation is usually slow. Furthermore, natural evolution methods are extremely slow and unrecognisable at human lifespan scale. Human have also recognised through trial and error some hybrid materials such as paints, which are colloids, containing inorganic nano-pigments. Ancient civilizations used such nano-pigments extensively, in ancient arts and potteries [2]. However, it is only recently that human civilization developed methods to reproducibly manufacture such materials at industrial scale. It became also clear we cannot engineer these processes and make them viable, by directly adopting the processes found in nature. Therefore, extensive research has been devoted to the development of novel materials and manufacturing techniques to accelerate progress [3–5]. Currently, the spotlight has been on developing hybrid materials formed from highly ordered polymers or inorganics, initially solubilised as a colloidal solution and, then restructured or modelled by various tools according to desired applications. These types of hybrid materials, which are formed by organic matrix (polymers) and inorganic nanosized transition elements (nanoparticles), are also the focus of this research. These materials emphasise the use of unique properties emerging from micro- and nano-scale, which are superior to their bulk properties at those dimensions.

1.2 Hybrid materials

Hybrid materials have been classified based on interactions of their constituents or morphologies of the products (Figure 1.1). For instance, organics are actively used as modifiers for inorganics in organically-functionalized mesoporous silica [6], while

organic surfactants are used for stabilisation of inorganic colloids, consisting of nanoparticles, nanorods, among others [7].

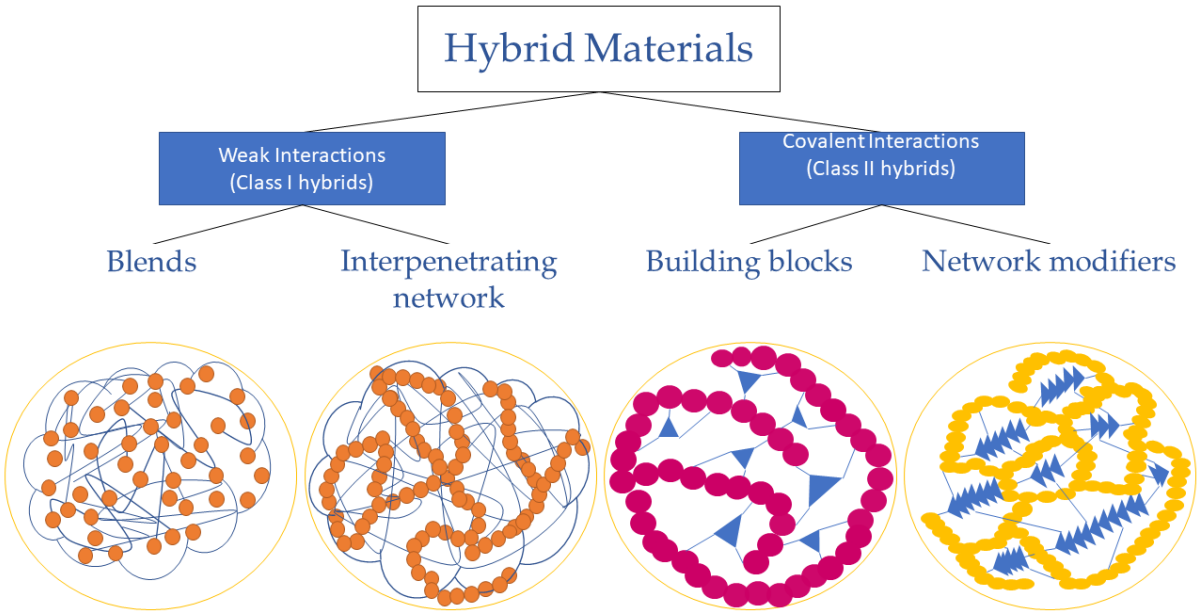

Figure 1.1: General types of hybrid materials.

Several types of hybrid materials are known, in which inorganic materials in the form of nanoparticles obtained from minerals (hydroxyapatite), metals (AuNPs, SiNPs), ceramics [8] are incorporated into organic materials including artificially synthesised (polycaprolactone) [9] or naturally obtained (chitosan) [10]. While selecting novel constituents, one can obtain hybrid materials exhibiting advanced emerging properties. Some of the advantages of such hybrid material are as follows:

Ability to fabricate unusual materials due to a wide selection of materials and processing parameters.

Matrix loaded with inorganic functional agents provide the increase in mechanical strength which is important for development of scratch resistant glass [11].

Contributing to advanced optical properties such as active or passive photochromic effect, electrochromic effect [12].

Possibility for tailor-made combinations for biomedical applications with individual specifications. For instance, the specificity of biomolecules in combination with plasmonic or superparamagnetic behaviour of inorganic part could help to realize accurate and efficient theranostics.

Development of composite polymers for light-weight and durable lithium-ion energy storage solutions to green energy sector [13].

These advantages put hybrid materials as promising candidate for biomedical systems. Hybrid materials cannot be the substitutes for materials like metals, polymers, or ceramics, but they present a combination of complementary properties. These materials are ubiquitous part of our daily life and have been constantly developed to tackle challenges of material science via the implementation of advance technologies.

1.2.1 Hybrid Multifunctional Nanofibers

Nanofibers present one of examples of hybrid systems, which can be employed in a wide range of applications, from sensors to controlled drug-delivery and release. Here, nanofibers functionalised with inorganic moieties, widely referred to as hybrid nanofibers, are especially important and discussed further. Fibers in general have been used by humans even before the beginning of civilisation, where it was primarily used for diet and textiles. Fibers were defined as natural or man-made substance, where the ratio of length to diameter is exceedingly substantial [14,15]. Fibers have been a regular part of living ecosystem. They have been found to be associated with most living systems, both plants and animals. Hence, they are also called natural fibers. Commonly, plant fibers are derived from a generic polysaccharide i.e., cellulose, found in conjugation with lignin. Cotton, hemp, dietary fibers, fibers in wood are widely known plant natural fibers [16], whereas animal fibers contain various proteins such as keratin and are present in hair, wool, or spider silk. Therefore, it is not surprising to learn that modification of natural fibers for clothing, writing materials etc., represents age old human traditions [17].

Recently, with the advancement of chemistry and polymer sciences, manufacturing synthetic or man-made fibers has seen a tremendous growth. Historically, this advancement had played a major role during industrial revolution in many economies around the world. Both synthetic and natural fibers consist of one or more type of materials, extended along the length of the fiber. Synthetic fibers were defined as fibers manufactured from various synthetic or naturally occurring materials and having modified properties, chemical structures, morphologies. They could also be obtained from a mixture of materials providing complimentary properties of components to the resulting fibers. For instance, the state-of-the-art method based on a simple strategy allows fabrication nanofibers having a highly controlled structure and morphology, as shown in Figure 1.2.

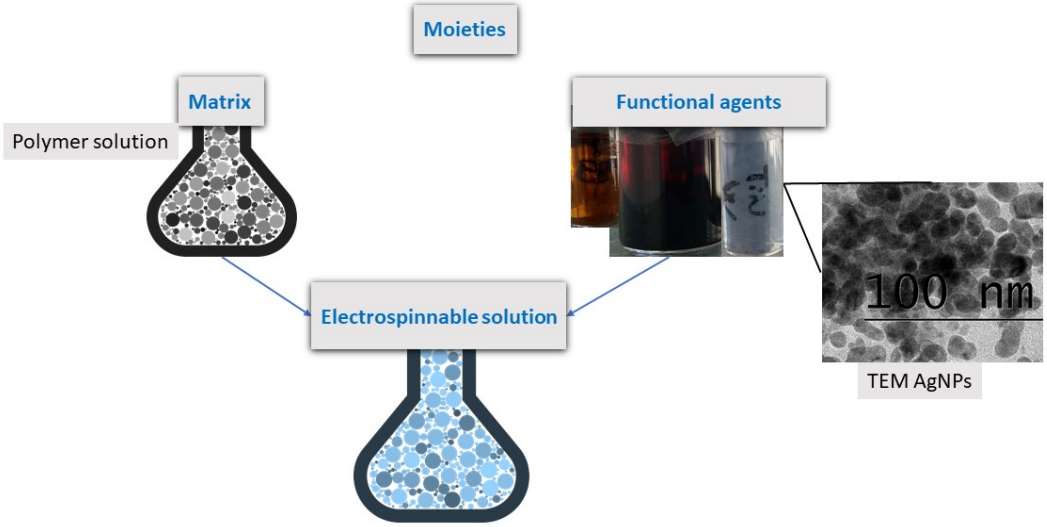

Figure 1.2: Schematics showing the preparation of electrospinning solution for the fabrication of hybrid nanofibers.

Synthetic fibers have been often classified by material in their composition such as steel fibers (metallic), carbon fibers, glass fibers, polymeric fibers. These fibers were key components in various applications such as textiles (wool, cotton, polyester), ropes (nylon), reinforcement (carbon fibers), sensors (optical fiber), filters(masks), insulation (wool, glass wool) [18].

Nanofibers present a particularly important class of fibers. Nanofibers are widely accepted as fibers with a diameter range from nanometers (50-500 nanometers) to sub-micron (above 500 nm but less than a micron). Nanofibers are mainly fabricated via electrospinning. Nanofibers provide unique morphology and properties because of their size, delivering a new class of materials. For instance, the cavity within the electrospun non-woven fibers along with the diameter and non-parallel structure increases the efficiency of fibers against impurities in filtration. Weak forces such as Van Der Waals force condition main characteristics of nanofibers, which are not possible at larger dimensions, whereas the directionality of molecule chain within fibers provides strength and elastic nature for composites. The reduced dimension also affects the wettability and surface area activity of various constituents within the fiber matrix. There have been multiple studies showing that the reduction in diameter leads to an increase in compressive properties and strength of reinforced composites [19,20]. Electrospun nanofibers are often functionalised with additional domains such as inorganic nanoparticles, drug molecules etc. Here, particularly nanoparticles can provide unique complementary functionalities such as plasmonic effect, superparamagnetism etc., along with the structural strength, to the fibers. Nanoparticles also offer similar size dependent properties to the nanofibers. Having a polymer as organic matrix and nanoparticles as functional agents, they present two widely employed domains of multifunctional hybrid nanofibers. These constituents utilised in the fabrication of nanofibers will be later discussed.

1.3 Hybrid nanofibers constituents

1.3.1 Polymers

Fibers made from polymers are especially important and present one of primary products of manufacturing industry. The polymers can be naturally or synthetically obtained, as natural or synthetic polymers have their own advantages and disadvantages. Polymers used for nanofibers are present in the form of polyamides, polyvinyl, polyesters, but can also include specifically synthesised polymers such as block polymers, conductive polymers etc. Polymers form the matrix of the fibers and condition their surface properties. Furthermore, they can also be used as functional agents by blending them in different polymer matrices, including conductive polymers to provide electron rich domains within the nanofiber mat, biodegradable polymer for wound dressing. The selection of polymer for fabrication of fibers is determined by a concrete application. Here, small number of parameters were generally considered including mechanical strength, thermal stability, processability, controlled degradability.

Several polymers have been successfully used for the fabrication of nanofibers. Poly(ethylene oxide) (PEO), chitosan, polystyrene, poly(ferrocenylphosphinoboranes), polycaprolactone are some of most popular polymers used as organic matrix for electrospinning of nanofibers. These polymers can attribute specific properties to nanofibers and can provide organic matrix for inorganic functional agents. Properties and characteristics of each polymer will be discussed in next sections.

1.3.2 Polyethylene oxide

Polyethylene oxide (PEO) or polyethylene glycol (smaller molecular weight) is a polyether compound which is water soluble and can also be dissolved in organic solvents such ethanol and toluene [21]. It is widely used in research and industrial applications, attributable to its availability in wide range of molecular weights and high processability. Due to the presence of etheric-O, it can be used to form weak interactions with dissolved metal ions or nanoparticles. Due to biodegradability and environment friendly option, it is widely be used for electrospinning [22]. Additionally, given its ability to enhance the nanofibrous structures' ionic mobility, it was used as organic matrix for co-spinning conductive polymer, as shown in following chapter. PEO can be found with molecular weight as high as 400 kD, making it easily electrospinnable. These properties of PEO presents it as a green alternative for the fabrication of nanofibers for biomedical applications. Further, its ability to mobilize both cationic and anionic ions within the composite structure, combined with processability, superior electrode/electrolyte interfacial contact, was the reason of its wide use for energy storage applications [23,24]. Thus, PEO was an ideal candidate for electrospinning and functionalising the nanofibers with nanostructures like AuNPs, SiNPs. Moreover, the nanofibers made from PEO enabled co-electrospinning of chitosan as it will be discussed in following chapters. However, water-based solubility of PEO was slightly detrimental for applications where controlled stability is one of the primary requirements for functional materials.

1.3.3 Chitosan

Chitosan is a biodegradable polymer having randomly distributed deacetylated D-glucosamine and acetylated N-acetyl-D-glucosamine, (type of saccharides). Chitosan as a polymer obtained from chitin, forms exoskeletons of crustaceans like crabs, shrimps, lobsters, and other animal groups. Therefore, putting this polymer right next to cellulose present in plants amongst the most abundant natural polymers. However, till recently, it was not utilised efficiently as a source material and tons chitosan were being disposed to natural degradation [25]. Nowadays, chitosan is in high demand biomedicine due to its biodegradability [26,27] and low environmental impact [28] as compared to synthetic polymers which are generally obtained from petrochemical refining. Chitosan and its derivatives are currently utilised for its bioactivity including anti-cancer and antioxidant options, and as substitute material in textiles and cosmetics [29]. Additionally, it has been used as a chelation agent along with polyamines [30], while its polycationic behaviour can offer effective attachment sites for inorganic moieties. Chitosan has been transformed into various structures such as hydrogels and nanoparticles [31,32]. However, the

processability of chitosan is very low, especially in the context of electrospinning as chitosan does not dissolve directly in water or organic solvents. Typically, chitosan requires a slight acidic solution for dissolution such as dilute acetic acid to convert -NH_2 group of chitosan into -NH_3^+ form. Moreover, a certain degree of acetylation can attribute to chitosan properties such as high crystallinity, low surface activity and swelling, suppressing its utilization for fabrication of nanofibers. Therefore, it often has been blended with other higher molecular weight polymers such as PEO, before electrospinning. Additionally, it requires post-processing techniques for stabilisation of -NH_3^+ present in chitosan blended nanofibers, before using them in biological medium such as saline solutions. Nevertheless, chitosan remains an attractive naturally occurring alternative for biomedical and industrial applications.

1.3.4 Polystyrene

Polystyrene (PS) is a known synthetic thermoplastic polymer made of styrene monomers. This polymer is a good candidate for electrospinning possessing excellent properties such as high durability, formability, good strength, low cost of manufacturing, hydrophobicity, and low melting point [33]. Thus, there is no surprise that PS is the most produced and utilized polymer for packaging, insulations, food containers [34,35]. Therefore, high molecular PS is ideal for electrospinning and it has been used extensively to fabricate superhydrophobic nanofibers [36]. Its nanocomposites and co-polymers have been reported for UV-shielding and electrolytic storage applications. They have also been utilized for synthesising and contributing to nanostructures such as nanopillars and nanorods. However, due to its hydrophobic nature, hydrolysis of polystyrene takes hundreds of years for decomposition [37]. Moreover, common techniques for processing of polystyrene uses hydrofluorocarbons which are known to have 1000 times stronger impact on global warming, as compared to carbon dioxide [38]. Therefore, there has been an increased focus on balancing the utilization and environment impact of PS. New methods have been developed and studied to decompose PS by natural processes, while using them as energy source for microorganisms, simultaneously [35]. These methods make possible the increase of rate of decomposition and relieve environment from piles of polystyrene depositions. Nevertheless, as an industrial polymer polystyrene remains an effective compound due to its properties. Moreover, by focusing on the recycling and developing strategies to enhance decomposition rates, the environmental impact of polystyrene can certainly be decreased.

1.3.5 Poly(ferrocenylphosphinoborane)

Poly(ferrocenylphosphinoboranes) are specially synthesised polycationic polymers, which can be synthesized by cross-decoupling methods [39]. These inorganic polymers look very appealing for catalysis [40]. The inorganic polymers employed to fabricate templated nanofibers, comprised of two types with a slight difference in their monomer structure: **Fe A** poly(ferrocenylmethylphosphinoborane) and **Fe B** poly(ferrocenyl-phosphinoboranes). The polymers have different monomer structures due the presence of an additional methyl group in **Fe A** attached to the phosphine group. Fe moiety

containing ferrocenyl part of the polymer has been widely utilized as a stabilizer for nanoparticles, and as a building block for synthesising complex hierarchical structures in dendrimers [41,42]. Although, the polymer can be dissolved in common organic solvents like chloroform or tetrahydrofuran, the molecular weight and the chain length of the polymer are not suitable for electrospinning. Therefore, they were blended with other high molecular weight polymers before electrospinning, which provided the matrix for the co-spinning of inorganic polymers in order to attribute additional surface properties to the nanofibers [43].

1.3.6 Polycaprolactone

Polycaprolactone (PCL) is one of the most promising polymers which has been widely utilised in pharmaceutical and implantable biomaterials. It is a long chain aliphatic polymer synthesised by polymerization of cyclic ester, ε-caprolactone, which is known to be degraded in nature by the action of enzymes already present in environment, via hydrolysis of ester links. Since PCL can be mixed with other polymers therefore, it has been used frequently to improve their biodegradability [44]. PCL dissolves at room temperature in organic solvents such as chloroform, dichloromethane, dimethylformamide, toluene and is insoluble in alcohols, water. Many applications of PCL and its by-products were reported. For instance, PCL is a popular for electrospinning of nanofibers for tissue engineering, which makes possible improved bio-activity, enzyme immobilizations [45–47]. Consequently, PCL presented itself as an ideal polymer to be electrospun to fabricate biomedical implants and controlled drug delivery systems. However, due to nature of solvents used to dissolve PCL, it could have slight negative impact on its bio-compatibility. Trace solvents present within the PCL nanofibers after electrospinning, could further be reduced by drying the nanofibers to improve their bio-compatibility. However, electrospinning of PCL needs a highly exceedingly controlled climate to achieve required efficiency and yield.

1.3.7 Nanoparticles

Nanoparticles (NPs) present an essential group of inorganic materials (iron, gold, copper, silver) having the size in sub-micron range. However, many organic and ceramic nanoparticles have also been synthesised such as chitosan nanoparticles, hydroxyapatite nanoparticles. These nanoparticles were generally used alone or as functional agents in combinations with organic matrices. Nanoparticles promise attractive applications in biotechnology, pharmaceuticals, and coatings as they exhibit wide range of properties based on their size and shape, as shown in Figure 1.3. Although, the term “nanoparticles” can be applied for particles with dimensions less than a micron, functional nanoparticles, typically have a narrow diameter distribution of less than 500 nm, while most nanoparticles exhibit a diameter median of 5-200 nm [48]. At such dimensions, many characteristics of NPs are due to quantum size effects. A commonly known example is quantum dot semiconductor nanocrystal, which have been used for producing colours in television. Additionally, size dependent surface plasmon effect, band gap structure and

surface enhanced Raman scattering (SERS) for bioimaging application have also been extensively researched and utilised [49,50].

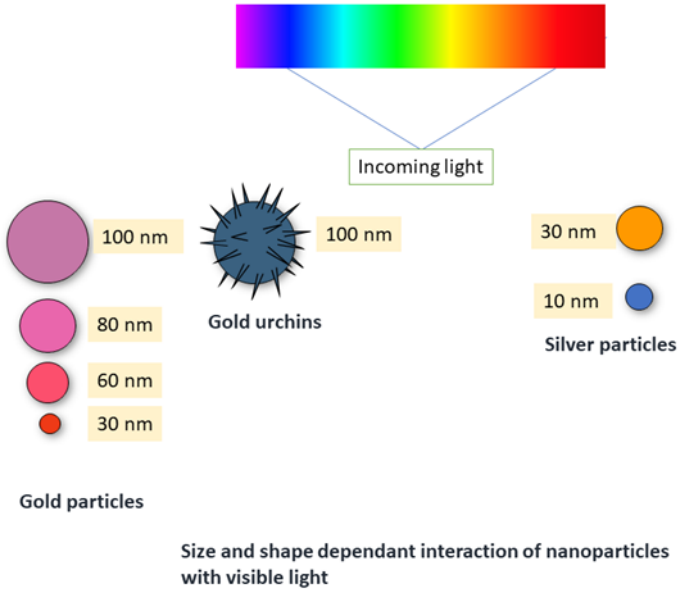

Figure 1.3: Change in colour of colloidal solution due to various size and shapes of NPs under visible light.

There exist various pathways for fabrication of NPs such as co-precipitation, biological pathways, sputtering, sol-gel templates, spark discharge [51]. Here, co-precipitation and laser ablation are in the focus of research for last years. Here, co-precipitation technique has its own advantages such as easily controllable size, possibility of particle surface modification, while working at low temperatures [52]. However, there are some disadvantages of using co-precipitation technique to synthesise NPs such as presence of trace impurities and low reproducibility. On the other hand, pulsed laser ablation in liquids can offer the solution to these problems. Compared to co-precipitation technique, laser ablation is a fast method and does not involve long reaction times, or multi-step synthesis. Moreover, it eliminates the use of toxic chemicals in the synthesis and gives relatively stable NPs colloids without presence of surfactants [53]. Some types of nanoparticles obtained by co-precipitation and laser ablation are shown in Figure 1.4.

Non-woven nanofibers were functionalised by incorporating such NPs as functional agents, providing additional complimentary properties. The nanofibers developed using the hybrid conjugation of inorganics specially NPs and biodegradable polymers provided for instance, a platform for therapy and a delivery mechanism for drugs. Some advantages offered by functionalised hybrid nanofibers included increased reactive surface area, size-dependent band gap in semiconductors, superparamagnetism (control mechanism in nanodevices, and hyperthermic treatments of cancerous cells), electron-photon transfer for catalytic activity, photochromatic effect, plasmon resonance [54–60].

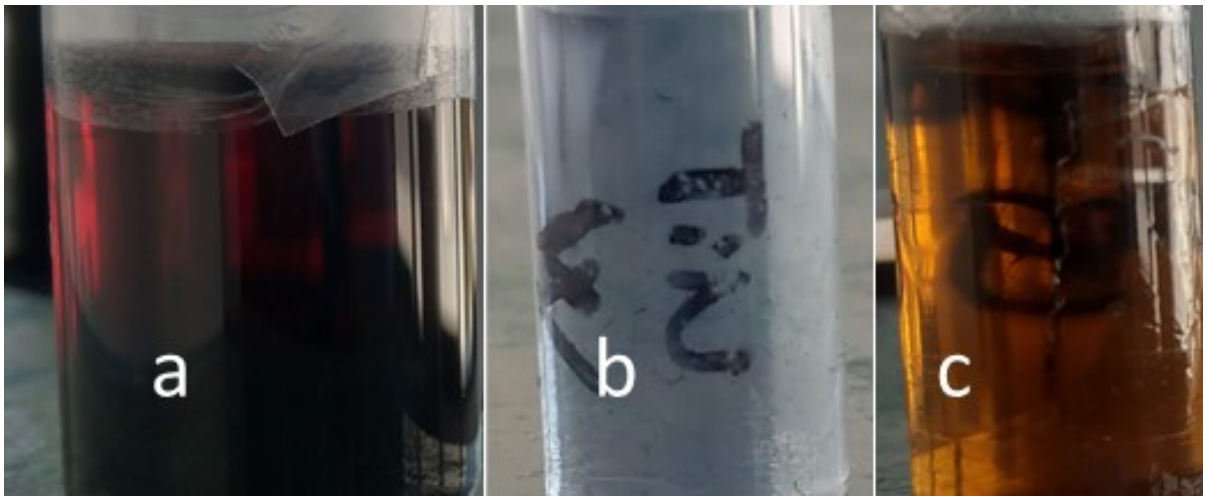

Figure 1.4: a) Gold NPs b) Titanium nitride NPs c) Silver NPs.

1.4 Tools for fabrication of multifunctional nanofibers

1.4.1 Electrospinning

Electrospinning technique for fabrication of synthetic fibres was developed in 1900s, when the first patient was filed [61]. It has been known for over 100 years that electrostatic forces could be utilized for production of synthetic fibers. Electrostatic being the driving force led to the technique being termed as electrospinning. Electrospinning works by application of two forces namely: electrostatic repulsion and surface tension. The process has been described briefly as follows: when extremely high voltage is applied to the polymer solution being pushed through a very small capillary, surface tension of polymer solution emerging out of the capillary as droplet is overwhelmed by the repulsion forces due to the applied voltage. These repulsion forces experienced by the polymer droplet leads to the ejection of polymer in the form of a jet along the electromagnetic fields stretched between the droplet and the collector. This jet is deposited as non-woven fibrous structures on collector at the other end, in the form of nanofibers (Figure 1.5). The jet which was ejected from the end of capillary called spinneret, while travelling towards collector, divides further into small fibrous structures due to Rayleigh instabilities [62].

The solvents used for solubilising the polymer evaporated completely or partially depending on the volatility of the solvent as jet travelled between spinneret and collector. A particular morphology characteristic of electrospinning process called Taylor's cone could also be observed. It was formed due to presence of an equilibrium between electrostatic repulsion and the surface tension behaviour of the polymer. As the electric field strength increased just beyond the threshold of surface tension of a polymer solution, a jet started to emerge from the Taylor's cones. This cone was described by a British physicist names Geoffrey Ingram Taylor hence, it was named as Taylor's cone [63].

A simple electrospinning set up consists of a flow controllable pump, a high voltage DC or AC source, spinneret, capillary, syringe, and a collector. Further, complicated systems have also been manufactured, allowing a control over temperature/humidity and provide attachments options for different types of collectors along with multiple spinneret set-ups (Figure1.6).

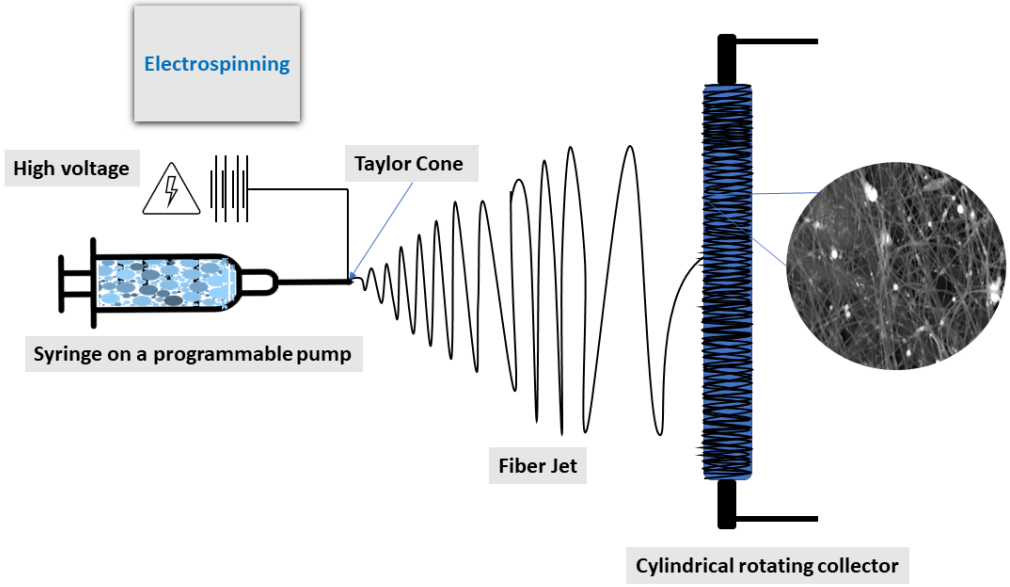

Figure 1.5: Fabrication of hybrid nanofibers via electrospinning on a rotating collector.

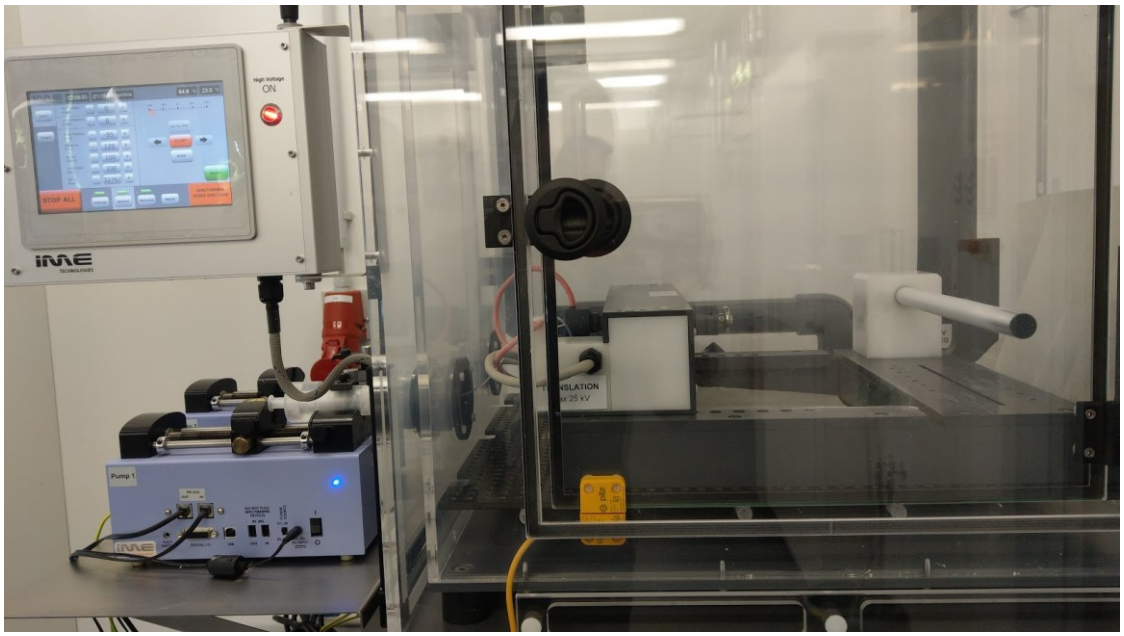

Figure 1.6: Electrospinning machine used during the research.

There were several parameters which could generally be optimised to generate nanofibers with desired characteristics. Some important parameters and their effects have been briefly defined as follows:

Voltage: An increase in the applied voltage led to reduction in diameter of the fibers initially however, beyond the threshold the diameter increased again.

Flow rate: Increase in flow rate generally increased the diameter of the fibers.

Concentration of polymer: It is one of the decisive material properties for electrospinning, which played an important role in determining electrospinnability of the solution and diameter of resulting nanofibers.

Collector distance: Increasing the distance between the collector and the spinneret caused diameter to decrease. A low collector distance gave “wet” nanofibers in form of bundles and holes on the surface of fibers, particularly when a highly volatile organic solvent was used to solubilize the polymer.

Ionic behaviour of polymer solution: The diameter of nanofibers decreased with increasing conductivity. Furthermore, nanofibers were comparatively monodispersed.

Solvents: The volatility of solvents impacted efficiency and yield of fibers. Highly volatile solvents often led to blockage of capillary.

Collector shape: The shape of collector did not influence the process of electrospinning itself, but the morphology and deposition of fibers.

Therefore, electrospinning is a complex process based on organized equilibrium of multiple parameters like material properties, electrospinning parameters, and the environment. These parameters in turn affect the morphology and properties of resulting nanofibers. Electrospinning machines come in various shapes and size. Recently, with an increased focus on electrospinning and a desire to adopt the technique for industrial scale, various production set ups have evolved. Particularly, to resolve the issue with the yield of electrospinning, deep interest has generated in manipulating spinnerets. That interest has been translated to some highly inventive and successful spinnerets seen in Figure 1.7, specifically to increase the yield.

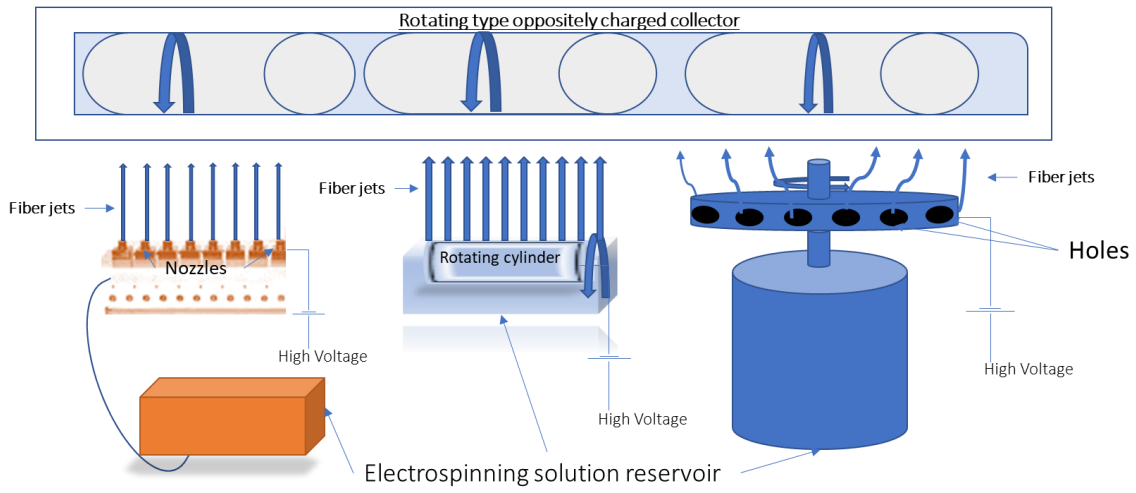

Figure 1.7: Several examples of spinnerets being used by industrial scale set ups for increasing the yield of nanofibers.

Electrospinning as a technique for the preparation of nanofibers has led to development of pioneering applications such as:

Flexibility in terms of utilisation of materials and fabrication of structure, as electrospinning allowed a wide range of materials with dissimilar properties to be fabricated as hybrid nanofibers.

Fabrication of co-axial structures and post-processing techniques led to fabrication of nanostructure from metals and polymer by using template method [64].

Electrospinning also allowed the deposition of fibers to desired surface therefore, modifying the surface properties of conventional materials such as textiles. Imparting them properties such as hydrophobicity, conductivity [65].

Nanofilters which utilises specificity for filtering biomolecules in biofluids and aerosol filters were also fabricated. Moreover, they could be used for drug-loading and act as an efficient drug-delivering structure [66].

Electrospinning provided scaffolds for tissue regeneration for bones cartilages and skin grafts. Moreover, the nanofibers could be developed in the form of cylindrical meshes, mimicking arteries and lymphatic vessels [67].

1.4.2 Laser ablation

Pulsed laser ablation in liquid (PLAL) has been a significant tool for the elaboration of ultra-clean nanoparticles (NPs) [68,69] which can offer ligand free surface. This process offered simple, rapid and adaptable synthesis of NPs for wide range of applications, including but not limited to electronics, biomedicine, energy production and storage [68,69]. Briefly, PLAL comprises elements of both top-down and bottom-up approaches. First laser radiation is used to ablate materials from a target immersed in liquid and thus form nanoclusters. Then, the nanoclusters interact with each other in the liquid medium to grow further into a colloidal NPs solution. Figure 1.8 illustrates, basic experimental geometries, which offered processability and efficiency, simultaneously. In this geometry, pulsed laser is focused, by adjustable mirrors on a target placed at the bottom of a beaker filled with liquid. Here, the target must be moved to constantly to avoid ablation from the same region [70] . In other geometry, the radiation is focused on a suspension of micro/nano particles and the suspension had to be stirred constantly therefore, offering different particulates [71] (Figure 1.8b). This PLAL offered the advantage of synthesising NPs with ultra-pure surface as compared to co-precipitation or sol gel synthesis of nanoparticles, which often involved utilization of surfactants or ligands. Moreover, PLAL eliminates the use of organic solvents, while providing a stable colloidal NPs solution.

NPs synthesized via PLAL exhibited unique surface reactive characteristics as compared to chemically-synthesised NPs. [72–76]. Furthermore, these NPs do not require additional steps for purification and stabilisation, which is often the case with chemically-synthesised NPs. Although, deionised water was generally used as medium for the ablating the target, it could also be replaced by organic solvents, polymers, to achieve a desirable chemical composition. Additionally, it gave the possibility to control the shape of NPs for instance by using media containing oils, superfluids, etc. and offered the possibility of in-situ functionalisation of NPs [69]. Another advantage is that laser-ablative

synthesis makes possible in-situ (bio)functionalization of synthesised nanomaterials [69].

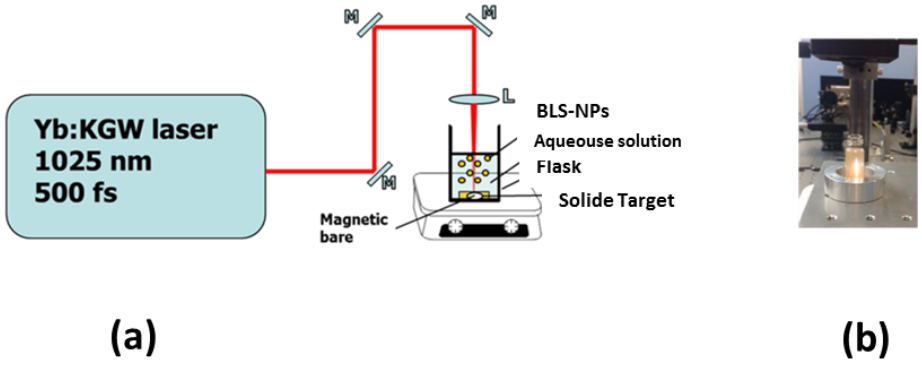

Figure 1.8: "(a) Typical PLAL setup; (b) Illustrative image of colloidal Si NPs solution prepared by femtosecond (fs) laser fragmentation" [54].

Laser ablation is a complex process which involves several phenomena such as the formation of shock waves, plasma plume, cavitation bubble, etc. During the process, temperature and pressure conditions can rise to thousands of kelvins and hundreds of pascals, respectively. Here, many simultaneous processes last for a very short duration (a few ns) and depend on laser parameters (pulses length, wavelength, fluence, etc.) [77].

Studies of laser ablation process involved multiple experimental methods such as spectroscopic analysis, acoustic measurements, x-ray imaging techniques, acoustic measurements, CCD cameras observations. Additionally, it involved investigation via theoretical modelling to comprehend the complexity of mechanism taking place during laser ablation process [78–81]. For instance, most laser ablation operations yielded polydisperse (several tens to hundreds of nm) and polymodal sized populations of NPs. During laser ablation, the sequence of ablation mechanism occurring plasma expansion and explosion of cavitation bubble have been often debated. These phenomena are vital for relatively longer nanosecond (ns) laser ablation regime. Moreover, the addition of chemical products, which enabled the control of NPs' size, often comprised the cleanliness of NPs. In contrast, ablation process at femtosecond (fs) ultrashort regime has been accepted by the larger laser ablation community as a "finer" tool. This regime restricts the transfer of radiation to cavitation bubble therefore, limiting the cavitation phenomena. Consequently, it contributes to rigorous control over NPs' size and size dispersity. [70,77].

Notably, the primary colloidal NPs solutions obtained after laser ablation either from a solid target (Figure 1.9a) or alternatively, from a micropowder suspension [71,82,83], on exposure to second laser "fragmentation" step (Figure 1.8b) [83], leads to further fragmentation. The secondary fragmentation mechanism though not fully identified yet, "photothermal evaporation" and "Coulomb explosion" are considered vital contributing mechanisms. Ultrashort (fs) laser ablation from micro/nano colloids has demonstrated itself as an efficient way to synthesise NPs with controlled size characteristics.

These characteristics validated PLAL as a reliable mechanism for synthesizing bare NPs. Furthermore, laser ablation provided control over NPs' characteristics such as desired size and size dispersity simply, by varying laser parameters.

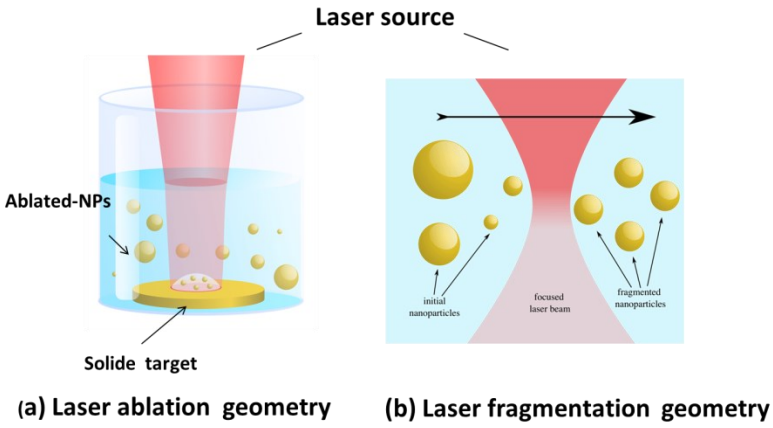

Figure 1.9: "Schematic of laser ablation (a) and laser fragmentation (b) geometries" [66].

1.5 Analysis of fabricated nanofibers

Analysis of fabricated nanofibers is done by utilizing with various materials analysis techniques. Here, these techniques with their principle are discussed briefly.

1.5.1 Scanning electron microscopy and EDX

Scanning electron microscope (SEM) primarily analyses the effectivity of electrospinning and morphology of fabricated fibers. While ImageJ® is used in conjugation with microscopy for analysis of diameter distribution in nanofiber micrographs. Micrographs obtained through SEM has following objectives:

Primarily, it helps to identify effective parameters for electrospinning to obtain desirable nanofibers from a specific polymer solution and distinguish it from simple electrospraying. Second, the micrographs obtained through SEM analyse the obtained morphology and dimensions of fabricated nanofibers.

Briefly, SEM works by scanning the samples horizontally with a high-energy focussed electron beam. Interaction of samples with the electron beam results in production of backscattered (primary) electrons, secondary electrons, and characteristics X-ray. Various detectors in the system identify, convert, and transmit the data for visualization. The electron beam is produced by a tungsten filament and mounted on the top of the instrument. These electrons are focussed and energised, by subsequent magnets and coils to an area of .50 to 6 nm, varying with the configuration of the device. The resolution of the system depends primarily on the energy of the electron beam, and the working distance from the samples. Depending on the samples, special preparation methods are required as the sample holding chamber operating at very high vacuum, which limits direct observation of liquid or organic samples. Further, the samples are ionized therefore, it is necessary for the samples to be conductive to prevent ablation of materials, damaging the instrument in process. Specifically, organic/nanofiber samples are sputtered with metals such a gold, chromium, or carbon thereby, conducting the current through the samples to the holder [84].

A secondary analytical tool known as energy dispersive x-ray spectrometer or EDX is often associated with the SEM. This device contains a detector for x-ray emissions from the samples in SEM. It characterises the elemental composition of samples by analysing the specific x-ray signatures. Briefly, as the samples are struck by high energy electron beam, some of that energy knocked peripheral shells electrons into higher energy orbits leaving behind a vacancy. However, this state is only maintained for very short duration of 10^{-15} s, and a higher energy electron transitions to lower orbit emitting characteristic x-ray photons. Therefore, it reveals elemental composition of samples by recognising the x-ray energy and translating it to corresponding energy levels [85]. Elemental map provided by EDX shows the distribution of inorganic particles, especially when present closer to the surface of nanofibers.

1.5.2 Thermogravimetric analysis

Thermogravimetry or thermogravimetric analysis (TGA) is a technique used to assess the thermal degradation behaviour of materials. In this technique, the samples are subjected to a controlled temperature increase program, beyond their degradation temperature limit. The device measures a change in mass of the samples as a function of temperature. The mass loss attributes to the presence of volatile substance within the samples. This approach is usually complemented by another thermal analysis technique called differential scanning calorimetry. TGA results are obtained as change of mass (m) against rising temperature (T). The results can also be presented in the form of derivative dm/dt, to give rate of mass loss, plotted against time or temperature. In a multicomponent sample, the loss of mass generally is obtained as two-step process within the graph [86]. The rate of heating the sample influences the rate of decomposition. For instance, at higher rate the temperature program can have disequilibrium with reactions taking place within the samples. This disbalance causes the reactions to be recorded at higher temperature than they might occur.

The device had inert atmosphere delivered by nitrogen inlet therefore, preventing combustion of the samples. The samples were kept in a ceramic crucible placed on a highly sensitive balance.

1.5.3 Differential scanning calorimetry

Differential scanning calorimetry (DSC) analysis various phase changes occurring within a sample as a function of temperature. Differential scanning calorimetry (DSC) maps phase changes which do not contribute to mass loss in samples. The data was obtained by subjecting the samples to multiple heating and cooling cycles along an empty reference. Samples are enclosed in covered aluminium pans kept in different oven chambers. The results give difference between the thermal energy required to raise equivalent temperature of sample and reference pans. This difference in energy is plotted against time or temperature. Thus, it can identify the phase changes in the samples which could be either, endothermic or exothermic [87]. Like TGA, the rate of heating has major influence on the analysis which results in phase changes occurring at unexpected temperatures. The use of DSC impacts significantly, the study of thermal behaviour of polymeric materials such as identifying degree of crystallinity, phase transition temperatures and, curing or polymerisation processes.

The DSC machine is supplemented with a cooler giving superior control over, heating and cooling cycles. Moreover, it makes possible a temperature program with wider temperature range. The heating chamber flushes with nitrogen gas throughout the program. The samples in aluminium pans are covered and crimped at the edges to creating a closed system. Similar but empty pan is used for reference. The temperature of the program is set just below the degradation initiation temperature, obtained through TGA. It is an important step for studying the behaviour of nanofibers which are functionalised with inorganic particles, which are employed as possible agents to dissipate heat throughout hybrid nanofibers effectively.

1.5.4 UV-Vis Spectroscopy

Ultraviolet-visible absorption (UV-Vis) spectroscopy is employed for the analysis of NPs. Spectroscopic analysis results are highly dependent on shape and size of NPs. It is a simple and yet effective method to quickly identify basic properties of NPs such as size range. Furthermore, it is used to determine the concentration and interaction of a specific species of NPs with its environment. On exposure to wavelengths of light between ultraviolet and visible, the samples give specific identifiable absorption or transmission spectra, based on the constituents, configurations, or state of agglomeration. For instance, AuNPs exhibits higher wavelength absorption peak when agglomerated and a sharp peak at lower wavelength around 500 nm when dispersed.

The spectral UV-Vis spectroscopy covers a very narrow spectral region. Its significance originates from the fact that the interaction of electromagnetic radiation and materials produces colours which are a part of visible spectrum. The UV-Vis spectrometer contains a light source both for visible and UV light, which is passed through a prism or diffraction grating monochromator. This light then passes through the sample which absorbs different wavelength of light depending on its constituents. The transmitted light is then analysed by the detector, and presented as graph with absorbance as function of wavelength [88]. Visible spectrum is generated in the device using tungsten halogen lamps (330-900 nm) while, ultraviolet radiation (160-375nm) is emitted from deuterium gas in deuterium lamps. However, depending on the manufacturer xenon lamps might also be used, producing radiation in complete UV-Vis range [89].

1.5.5 Fourier transform infrared spectroscopy

Fourier transform infrared (FTIR) data analysis is used to analyse the changes in chemical structure, and interaction between functional agents and organic matrix in nanofibers. FTIR is an effective tool for chemists, biologist, and material scientists, as it provides a simpler way to analyse, the presence or absence of certain functional groups in any material, by measuring absorption/transmission of light in near- to far-infrared region of electromagnetic spectrum. In contrast to UV-Vis spectrometer, it uses very broad spectral range. The resultant absorption wavenumber denotes the stretching and bending of bonds present in the material [90]. With the help of various attachments available with FTIR instrument, it is possible to analyse solids and liquids. While resulting graphs present absorption energies as function of wavenumber (cm^{-1}). Absorption spectra generated by the FTIR has been sub-divided usually into two regions, the functional group, and the fingerprint region. Functional group provides a quick and reliable information about the bending absorption of major functional groups with double, triple, or X-H bonds. While the fingerprint region is harder to read with multiple peaks superimposed, representing stretching, and bending of single bonds. Furthermore, it has unique pattern of peaks for every compound analogous to human fingerprint. The processing of data by the computer is done by algorithm based on Fourier transform hence, known as FTIR. Silicon carbide element provides the source of light transmitted at mid IR range of 4000-500 cm^{-1} to the sample [91].

Summarily, nanotechnology as described by its name is the resultant technology from the properties imparted by materials or structures, where at least of one of the dimension is less than or equal to 100 nm, has been utilized for designing, characterizing, production or application [92–94]. Nanofibers are one such example of structures or class of materials, encompassing unique characteristics and possessing average diameter of around 500 nm, while hybrid nanofibers possessed additional functional groups with certain size and shape derived properties, usually derived from transition element in the periodic table. Nanofibers have provided a multifaceted approach to biomedical technologies. They are especially advantageous for applications utilizing 2D non-woven mats or scaffolds. Nanofibers are further distinguished due to the ability of nanofibers to mimic extracellular matrix (ECM) both in terms of structure and size, providing an enormous potential to be utilised in regenerative medicine and tissue culture applications (Figure 1.10).

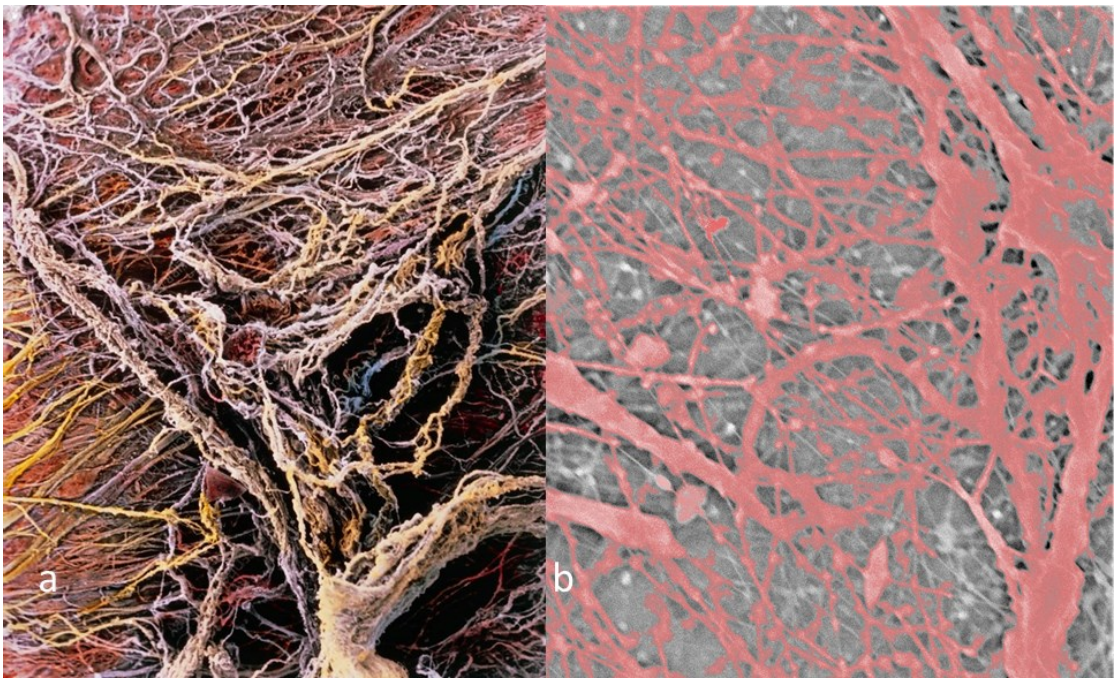

Figure 1.10 False colour images to compare the ECM to obtained nanofibers morphology. Visually identical looking (a) false colour image of ECM connective tissue courtesy *© Science Photo Library Limited 2020* and (b) coloured SEM micrograph.

Historically, nanofibers have been fabricated via plethora of techniques such as template synthesis, drawing, self-assembly [95–104]. However, it is the electrospinning which provided the ability to manipulate and control the dimensions, morphology and possessed the processability, making it an attractive and suitable option for industrial scale operations. As described earlier, electrospinning operates by employing a very high voltage for ejecting polymer solution through fine capillary towards a collector, giving polymer nanofibers in the process. The idea is very simple, the actual implementation varies greatly in complexity and scale, while still providing reproducibility to the process. It was this viability of electrospinning which has attracted a huge attention from industries and academics [105–110]. Though electrospinning was first patented in 1934,

it was designed initially as an apparatus for complementing the existing technology of thread production in textile industry [111]. Until recently, it was not considered as a serious tool to be implemented for offering solutions for disciplines as diverse as biomedicine and filtration. The data from Web of Science database of the articles, with electrospinning as keyword, reveals a well-defined picture showing a major increment in electrospinning research (Figure 1.11).

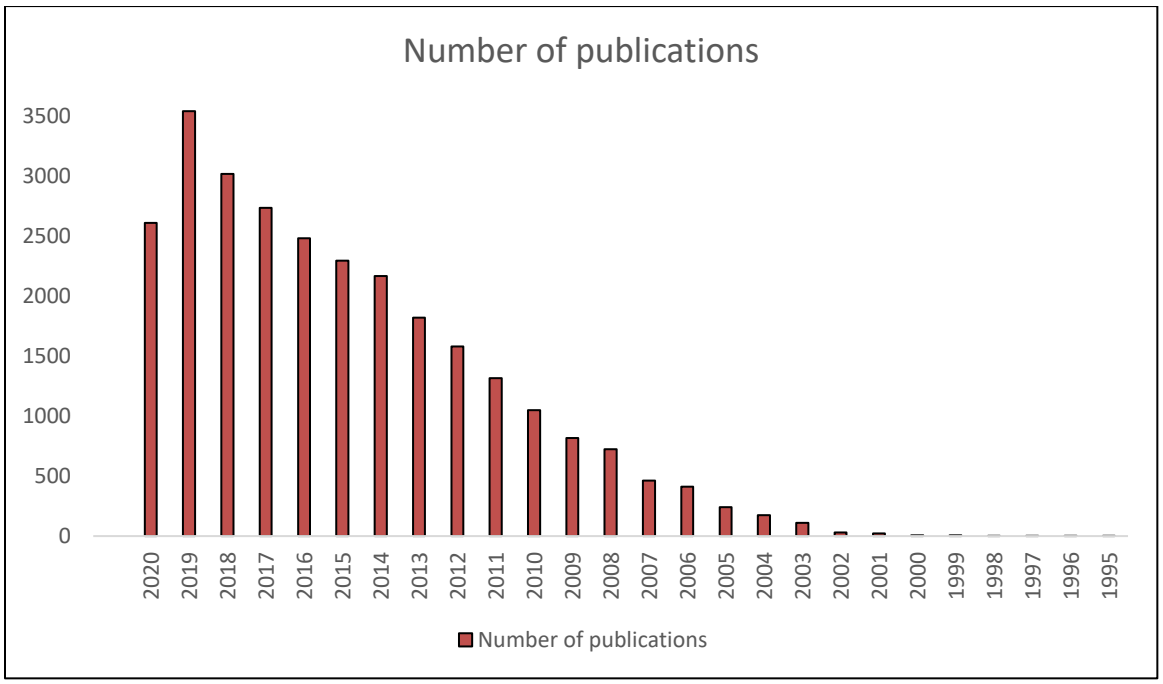

Figure 1.11 Accelerated growth in research devoted to electrospinning and nanofibers, across two decades. Web of science database was used to extract the data on various journals.

However, despite an increasing attention, the technique is still being modified, designed, and perfected to suit ever-emerging technologies. The control aspect of electrospinning has become increasingly important as it significantly influences, the properties and morphology of fabricated nanofibers. Electrospinning gives an option to control minutely parameters governing the process. Some of these parameters include applied voltage, flow rate of polymer solution through the capillary, distance between the collector and the spinneret, polymer concentration in an electrospinning solution, polymer properties, solvent properties, collector geometry, environmental conditions such as temperature and humidity, conductivity of the electrospinning solution itself and presence of additives in solution. Careful manipulation is required throughout the electrospinning process which in turn determines the rate of deposition, morphology, and alignment of fibers. There have been many studies which correlated the above-mentioned parameters to the properties of obtained nanofibers [112–116]. However, a gap still exists for establishing standardised parameter with state-of-the-art combination of materials, which have not been considered yet for supporting emerging technologies, and efficient solutions for existing technologies.

As stated earlier, there has been an increase in studies focussed on development of hybrid nanofibers. Most hybrid nanofibers are supplemented with additives and functional agents synthesised by wet-chemistry methods. These functional agents affect properties of nanofibers such as diameter, surface activity, degradation rate, and toxicity. However, by employing techniques such as laser ablation for synthesising functional agents like nanoparticles, toxicity arising from surface agents and ligands can be minimised. Therefore, requiring every concentration to be monitored and standardised, for *in situ* and *in vivo* biological models. Furthermore, designed materials must be characterized by exploring morphology and structure, with respect to their desired applications. For instance, every nanofibers system interacts differently, depending on the biological mediums for tissue regeneration or regenerative medicines. Therefore, identifying those interactions forehand and standardising becomes inherent for choosing correct materials for production. An urgency to create such platforms and establish protocols for fabrication has been evident from pace this field has acquired recently especially, given the antiquity of this technology [117].

Therefore, implementing unusual materials which showed promising properties was the objective of this research. To accomplish multiple hybrid nanofibers, systems were fabricated reflecting on the advantages of electrospinning, as a tool for fabrication of biomaterials and nanofibers. Moreover, several systems were designed containing state-of-the-art combination of materials. These materials were further tested for biological toxicity and compatibility. Secondary functional agents, namely inorganic nanoparticles, were also included for providing multifunctionality to fabricated nanofibers. Inorganic nanoparticles used to functionalise nanofibers studied intensively here, comes from a huge category of functional agents such as drug molecules, dendrimers, or other biomolecules. However, such inorganic nanoparticles were synthesised mostly via wet-chemical pathways, which had its own pros and cons. We adopted laser ablation as a method for preparation of ultra-pure bare nanoparticles and used those species of nanoparticles to decorate the nanofibers matrix, to profit from their ultra-pure surface and thus minimises toxicity, especially in biological medium. Such an approach could provide unusual combinations of materials with wide range of properties, while offering potential for scaling up for industrial use. Further, the exact process of implementing and electrospinning of laser ablated nanoparticles with polymer to produce various nanofiber system will discussed thoroughly. In next chapters, each system will be presented individually, describing the challenges and characteristics respective to the desired applications.

CHAPTER 2

Nanofibers templated with AuNPs synthesised via laser ablation and wet-chemistry

Contents

2.1 Introduction

In the framework of this chapter poly(ethylene oxide), based chitosan nanofibers functionalised with gold nanoparticles (AuNPs) were fabricated by electrospinning techniques. Here, the role of preparation techniques on physio-chemical properties nanoparticle functionalised nanofibers were investigated. AuNPs were prepared by laser ablation and chemical synthesis and then introduced into the poly(ethylene oxide) (PEO) and chitosan blend for co-electrospinning process. Wet-chemistry synthesis of nanoparticles was done at Rhine-Waal University of Applied Sciences, Germany, while ablated nanoparticles were fabricated in LP3, Aix Marseille University, France. Thermal and morphological changes highlighted in section 2.4, were the main parameters to analyse the difference in properties of nanoparticles functionalised as compared to unmodified ones. This work has been adopted from results published in **LoP-7.**

2.2 Context

Chitosan is one polymer which has been used extensively to develop new biomaterials, especially for biomedical applications [118–120]. There are various reasons for its widespread utilization including its ability to dissolve in water due to -NH_2 protonation in acidic conditions, eliminating any possible toxicity of solvents. Additionally, biodegradability of chitosan opens avenues for the development of novel biomaterials. Moreover, possessing anti-microbial properties and antifungal properties favours its use for electrospinning nanofibers [121]. However, these promising properties are compromised by poor processability of chitosan [122,123] as it is often difficult to characterize and solubilize it in order to form electrospinnable solution. Due to this reason chitosan is blended with other polymers to obtain nanofibers. Polyethylene oxide (PEO) provides an optimum platform for the co-spinning of chitosan. In this work, AuNPs were used as functional agents. Such nanoparticles were synthesized by Turkevich's method [124] and pulsed laser ablation in liquid [125]. These nanoparticles have theranostics properties mainly due to plasmonic resonance, in addition they promise improvement of properties of polymer nanofibers, promote proteins adsorption, and cell adhesion [126]. Combining these properties and comparing the effect of preparation of nanoparticles on the characteristics of functionalised nanofibers, one can have an insight on the development of promising systems. Here, the multifunctionality of the system increases its potential to be used in a wide range of applications such as contrasting agent, tissue-regeneration platform, or drug attachment modality. Majority of currently used nanoparticles are obtained by conventional chemical methods using hazardous raw materials such as nitrate salts or citrate ligands, which can provide additional attachment sites for drug and ligands. However, it has disadvantage of provoking nanoparticle surface contamination (e.g., residual anions) and leading to residual toxicity of final products [127]. Alternatively, laser ablation provides a "green" alternative to chemical synthesis as it avoids the use of toxic by-products [128].

2.3 Materials and methods

2.3.1 Materials

Poly (ethylene oxide) was used for electrospinning which acted as template for co-spinning of Chitosan and matrix for gold nanoparticles. PEO was obtained from Sigma Aldrich having a medium molecular weight of 300,000 g mol^{-1}. Chitosan was also obtained from Sigma Aldrich with a medium molecular weight. The bare gold nanoparticles used were obtained by laser ablation prepared in LP3 lab, Aix-Marseille University, France [70,83,125]. Turkevich's method was used to prepare chemically synthesized gold nanoparticles with citrate attached. Hydrogen tetrachloroaurate (III) [$HAuCl_4 \cdot 3H_2O$] used as gold precursor for Turkevich's method along with trisodium citrate dihydrate [$HOC(COONa)(CH_2COONa)_2 \cdot 2H_2O$] used as reducing agent were obtained from Sigma Aldrich. Acetic acid 99-100% was obtained from SCS GmbH.

2.3.2 Chemical synthesis of AuNPs

The gold nanoparticles used in this study were prepared using two methods namely, laser ablation and chemical reduction of gold precursor using trisodium citrate dihydrate (Turkevich's method). Turkevich's method is a simple two-step process which allowed formation of 10-20 nm sized, monodisperse gold nanoparticles. Trisodium citrate acted as both reducing and capping agent. Citrate ions have high affinity for new nuclei thereby, attaching to them, and reducing overall surface energy. Thus, prevented attachment to other nuclei, resulting in control over the size of nanoparticles. The resulting nanoparticle solution was centrifuged to remove excess citrate, and the volume of solution was reduced 5 folds from 100 to 20 ml, which was then used directly to dissolve PEO. The nanoparticles were also analysed under visible spectra to observe their characteristic absorption peak.

2.3.3 Laser ablated AuNPs

AuNPs obtained from LP3, were prepared using femtosecond (fs) radiation from a Yb:KGW laser (Amplitude Systems, 1025 nm, 480 fs, 1 kHz), under ambient conditions. With the help of a 75 mm lens, radiation was focused on the surface of target (1 cm*1 cm), the target was moved continually at the speed of 0.5 mm s^{-1}. Concentration of AuNPs could be determined by the weight loss of the target during the ablation process.

2.3.4 Preparation of electrospinning solutions

The solution for electrospinning was prepared by mixing PEO powder in 10 ml dist. water, keeping the total concentration of polymer 8% (w/v) compensating for addition of 2 ml AuNPs solution. Chitosan solution was prepared by dissolving 3% (w/v) of the polymer in acetic acid solution, 10% (v/v). The solutions were prepared at room temperature under magnetic stirring for 48 hours. Chitosan and PEO polymer solutions were mixed under constant stirring with a ratio of 1:3, respectively. 2ml of concentrated laser ablated bare AuNPs were added to the solution under sonication to ensure

homogenous distribution and remove air bubbles from the electrospinning solution. While using the AuNPs synthesized by chemical method, PEO polymer was dissolved in the nanoparticles solution itself and chitosan solution was added with similar 3:1 ratio, respectively. The solutions were quite stable, showed no signs of precipitation or coagulation until a week.

2.3.5 Electrospinning

Climate controlled electrospinning machine from IME technologies was used to preform electrospinning. 3 ml syringes with Leur-lock were filled with electrospinning solution and placed on controlled pump to achieve a flow rate of 0.3 ml hr^{-1}. Rotating cylindrical collector with variable rotation speed was used; wrapped with aluminium foil and connected to negative potential. The set-up used for electrospinning included rotating target collector with variable rotation speeds. The syringe was then fitted with PTFE tube and 0.8 mm blunt needle which was attached to spinneret. Spinneret provided interaction with high voltage to the needle applied through device. Set-up was initiated with 14 kV at the positive end and -1 kV at collector end. These parameters were standardized and optimised based on literature [76]. The flow rate was kept at 0.3 ml hr^{-1}., humidity and temperature were kept at 25% and 28°C, respectively. The distance between needle tip and collector was kept constant at 15 cm. The electrospinning set up ran till the total volume of solution in syringe was consumed. Fibers were peeled off the aluminium foil and stored in petri dishes for analysis. For SEM analysis, simply pieces of aluminium were cut from different parts of fiber mat and used for analysis.

2.3.6 Characterization analysis of Nanofibers and Nanoparticles

JSM-IT100 InTouchScope™ Scanning Electron Microscope from Joel was the primary device used for analysing and verifying the samples after electrospinning. The samples were deposited on aluminium thin sheets were around 1*1 cm. Other than confirming formation of fibers by SEM using ImageJ®, diameter of nanofibers was also analysed.

For thermal analysis, TGA device from Perkin Elmer were used to measure change of mass over the time with increasing temperature, and difference in heat required to increase the temperature of sample and reference, respectively. Therefore, providing data about the thermal stability of materials before and after electrospinning with nanoparticles.

Chemically synthesized nanoparticles were characterized using the visible spectroscopy to determine the absorbance peak and variation as the particles grow, and after each dilution. PerkinElmer lambda 25 UV-Vis spectrometer was used to determine the absorption wavelength with variation of time and various rates of dilution as represented in Table 2.2.

2.4 Results and discussions

Electrospinning of solution comprising of Chitosan (PEO)/ NPs were prepared with high percentage of Chitosan and Gold nanoparticles. AuNPs prepared by different techniques were characterized to assess their interaction within nanofibers and the impact on nanofibers' properties. Non-woven nanofibers were collected on rotating collector wrapped with aluminium foil and connected as counter electrode with negative potential. Chitosan was electrospun at high ratio blending of 1:3 with PEO. Chitosan was best dissolved with 10% (v/v) acetic acid and the formed homogenous colloid when added to PEO and AuNPs. The fibers could be peeled off from aluminium foil and were slightly charged from the electrospinning process.

2.4.1 Morphology and diameter of nanofibers

When observed under scanning electron microscope, the fibers were homogenous and without beads. They were present with no fiber alignment in the form of non-woven mat (Figure 2.2). The diameter of the fibers was analysed with the help of ImageJ®. There was not much difference between diameter of nanofibers having laser-ablation synthesized bare AuNPs, or chemically-synthesized AuNPs with citrate as capping agent (Figure 2.1). The diameter of fibers was average of 393 nm for nanofibers with bare laser AuNPs and 400 nm for chemically synthesized AuNPs (Table 2.1).

Sample name	Mean (nm)	Standard Deviation (nm)	Min. Diameter (nm)	Max. Diameter (nm)
Fibers with Laser AuNPs	393.94	223.02	30.30	757.58
Fibers with Cit-AUNPs	400	228.04	20	780

Table 2.1: Physical characteristics of chitosan nanofibers functionalized with AuNPs.

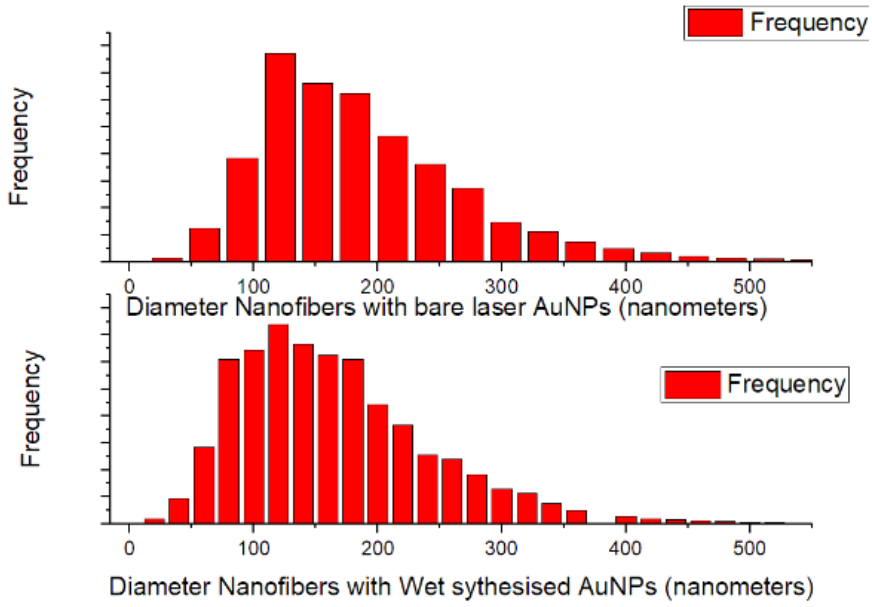

Figure 2.1: Distribution of nanofiber functionalized with bare laser and chemically synthesized AuNPs.

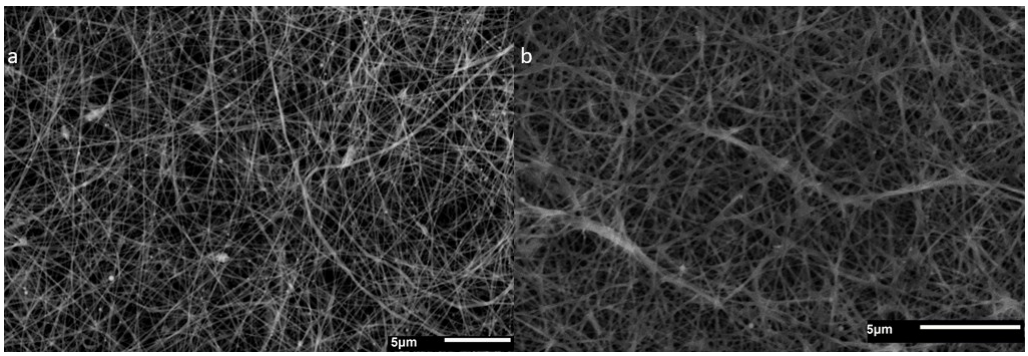

Figure 2.2: Micrographs of Chitosan nanofibers functionalized with a) bare laser AuNPs and b) chemically synthesized AuNPs.

2.4.2 Thermal Analysis

Thermal characterization was done to analyse influence of functionalization on thermal stability and degradation curve. When heated to a temperature higher than the melting point of the polymer the nanofibers functionalized with AuNPs showed higher degradation initiation point for both types of nanoparticles. On comparing the functionalized nanofibers with reference using thermogram in Figure 2.3, the initiation temperature for reference containing chitosan (PEO), is around 350°C with maximum rate of degradation at 421.54°C. While the initiation peak for functionalized nanofibers is shifted up to 20°C further, and maximum degradation temperature is at 422.3°C, 425.76°C for nanofibers functionalized with bare laser synthesized and chemically synthesized AuNPs, respectively (Figure 2.3).

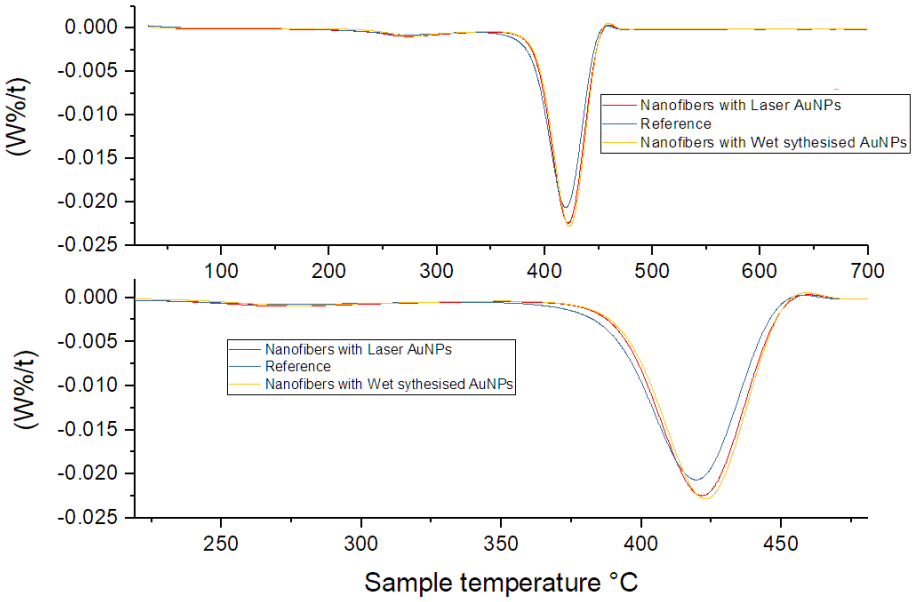

Figure 2.3: Thermogram of Chitosan nanofibers and Nanofibers functionalized with AuNPs.

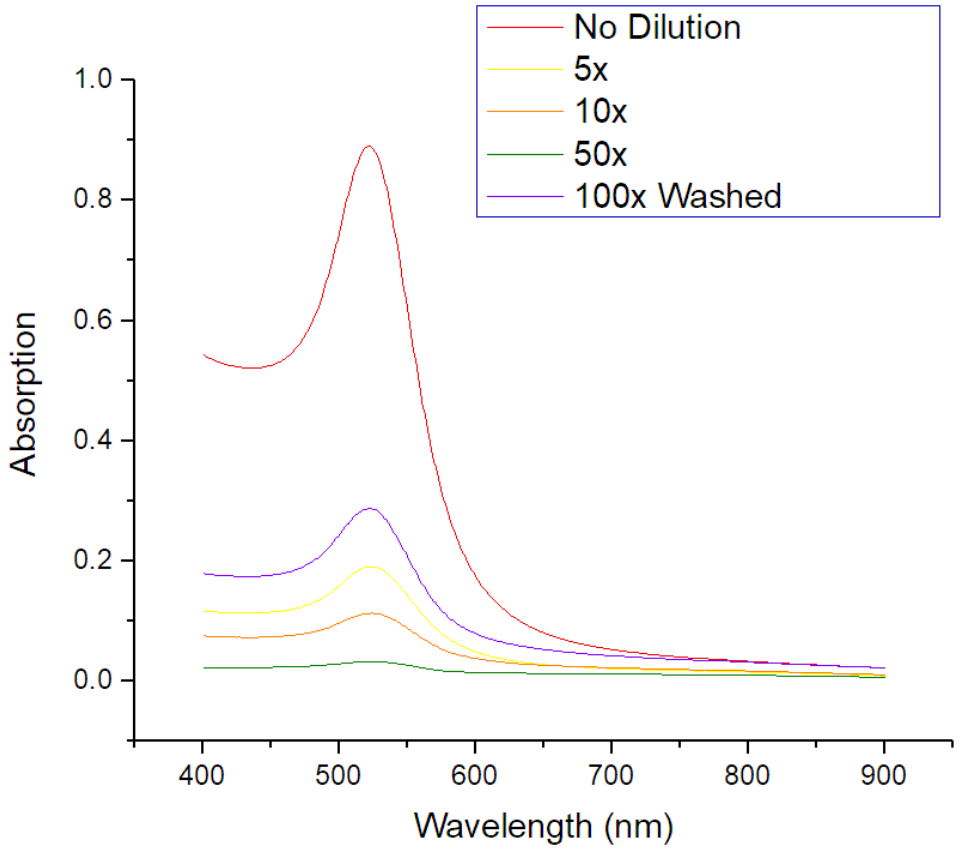

Figure 2.4: Absorption spectrum of chemically synthesized nanoparticles.

2.4.3 Spectroscopic study of chemically synthesized nanoparticles

Nanoparticles synthesized using Turkevich's method were analysed using visible spectroscopy to detect their standard absorbance peak confirming their plasmonic behaviour. Table 2.2 identifies various variables maintained for each sample such as dilution, reduction time and washing with distilled H_2O. As shown in Figure 2.4, the undiluted sample demonstrates maximal absorbance, while the washed sample diluted 100x had higher absorbance compared to other dilutions before washing process. This could be attributed to absence of non-coordinated citrate ions which might have interfered with the absorbance before washing. However, the absorption wavelength for the samples does not show much variation and they lie between 522 to 524 nm (Figure 2.4).

Colloidal solution before the washing process		
UV-Vis Absorption		
5d	No dilution	Medium peak at 522 nm
5min	5x diluted	Medium peak at 523.5 nm
5min	10x diluted	Medium peak at 524 nm
5min	50x diluted	Medium peak at 524 nm
Colloidal solution after the washing process		
UV-Vis Absorption		
5min	100x diluted	Medium peak at 522 nm

Table 2.2: Absorption spectrum of chemically synthesized AuNPs with variation of time.

2.5 Conclusions

Optimised parameters for electrospinning chitosan (PEO) nanofibers functionalised by AuNPs were established. Here functionalisation of nanofibers was done using laser ablated and chemically synthesised nanofibers resulted in variations in their physio-chemical properties. Functionalised nanofibers were uniform and showed a similar average diameter distribution for laser and chemically-synthesised AuNPs. Electrospinning with AuNPs led to increase in degradation temperature in TGA analysis. The effect was prominent on functionalising with chemically synthesised NPs.

The results showed no major difference in physico-chemical properties of nanofibers functionalised either by bare laser-ablated or chemically synthesised nanoparticles. However, bare laser AuNPs had the advantage possessing a ligand free surface which is expected to have positive affect on interaction with biological systems.

CHAPTER 3

Electrospinning and post-processing to obtain stable chitosan-AuNPs nanofibers

Contents

3.1 Introduction

This chapter continues the investigation started in the previous chapter and addressed the elaboration of controllable route to fabricate chitosan (PEO) nanofibers functionalised with bare laser ablated AuNPs. The chapter has two main objectives. The first objective is related to template fabrication of hybrid multifunctional nanofibers from highly unprocessable chitosan, and their functionalisation with AuNPs (section 3.3.3 and 3.3.4). The second objective was related to the processing of functionalised nanofibers to prevent their dissolution in aqueous medium by neutralising $-NH_3^+$ (section 3.3.7). Results presented in this chapter are published in **LoP-4**.

3.2 Context

The elaboration of artificial scaffold platforms, capable of replacing and/or repairing failing tissues or full organs, is still challenging for the scientific community [129–132]. Most efforts are devoted to the fabrication of nanostructured scaffolds, which could mimic mesoporous morphologies of a real extracellular matrix (ECM) and offer additional therapy and diagnostics (theranostics) modalities [76,133,134]. In contrast to conventional techniques such as solvent casting and particle leaching, electrospinning is now extensively explored to elaborate structured biocompatible and biodegradable nanofibrous scaffolds. Such a technique can offer a series of advantages over traditional methods:

Possibility of working with a variety of materials, including synthetic and natural polymers and their composites

Capability of generating micro- to nano-scale nanofibers having sophisticated special 3D designs [135].

Electrospun nanofibers have been employed as matrices for the encapsulation of drugs, as well as the incorporation of biological materials (e.g., proteins, DNA, etc.) and as nanofunctional elements in multiple studies [54,136–139].

Chitosan has been exploited extensively among naturally derived biopolymers. This polymer is widely used to develop innovative electrospun nanofibrous matrices for a variety of biomedical applications, including anti-microbial, antifungal, wound healing, drug, and gene delivery [140–144]. Chitosan is characterized by a good biocompatibility and biodegradability, while the presence of $-NH_2$ groups on a chitosan nanofiber surface makes it suitable for the immobilization of enzymes and negatively-charged proteins. Moreover, a highly reactive chitosan surface can offer additional opportunities for its functionalization with nano-engineered particles to improve physicochemical characteristics (e.g., electrical and mechanical properties) and enable biological (e.g., antibacterial) or other theranostic functionalities [76,145]. However, the spinnability of chitosan polymer is relatively poor due to the presence of hydrogen bonds between polysaccharide chains, leading to its high crystallinity and a weak solubility in most solvents. Therefore, acid solutions, such as acetic acid, trifluoroacetic acid (TFA), and ionic liquids are typically employed to facilitate the dissolution of chitosan. Moreover, due to a

relative shortness of the chitosan chain, a polymer-stretching effect during electrospinning process is ineffective, which results in the formation of discontinued jets. To ensure the jet continuity and uniformity, chitosan has been electrospun often together with poly(ethylene oxide) (PEO) polymer [146–148]. Here, low molecular weight chitosan (102 kDa) was a preferable solution to ensure its complete dissolution, which required a high concentration of PEO to enable co-electrospinning of polymers, resulting in a low concentration of chitosan in the matrix. On the other hand, the use of chitosan having very high molecular weight (>310 kDa) resulted in the formation of gel structures not suitable for electrospinning [149]. The employment of chitosan having reasonably high molecular weight (~200 kDa) looked a good compromise, but such a choice required the elaboration and optimization of electrospinning procedure [150]. Various chitosan/PEO formulations have been implemented successfully to develop homogenous electrospun nanofibers with different characteristics [144,149–152].

Fabrication of chitosan/PEO nanofibers containing a relatively high molecular weight chitosan (200 kDa) and decoration with laser-synthesized Si and Au nanoparticles (SiNPs and AuNPs) as functional additives has already been demonstrated [76,145]. This procedure was based on the co-spinning of chitosan/PEO formulations (1% (w/v) of chitosan, ratio 1:4), together with nanoparticles prepared by methods of laser ablation, commonly described in literature [70,71,75,83,153–158]. The uniqueness of laser-synthesized nanoparticles was provided by their bare (ligand-free) and uncontaminated surface, which offered a series of advantages for applications, including cancer diagnoses and therapies under external stimuli [75,155–157], biofuel cells [71], and Surface Enhanced Raman Spectrometry (SERS) [158], etc. Some studies [76,145] have established, the incorporation of functional additives, such as Au and Si nanoparticles, into the chitosan/PEO matrix can provide a series of advantages, including:

A decrease of fiber size, which promises the improvement of its surface reactivity.

An improvement of thermal stability at a high temperature

The possibility for enabling additional theranostic modalities based on unique properties of laser-synthesized nanomaterials [76].

However, the total concentration of chitosan in the structure of nanofibrous usually has been relatively low compared to the co-spinning agent (ratio 1:4), which reduced the efficiency of the chitosan matrix and could lead to an unacceptably high rate of dissolution of chitosan/PEO nanofibers in an aqueous environment due to the presence of NH_3^+ [56,149,159].

In this chapter, a further advancement of the electrospinning procedure to improve the properties of the formed AuNPs-decorated hybrid chitosan/PEO nanofibers is reported. Here, an increasing concentration of 200 kDa chitosan up to 3% (w/v) using 10% (v/v) acetic acid with a chitosan/PEO ratio of 1:3 was electrospun, which rendered possible the solution of the dissolubility problem. However, it resulted in protonated NH_3^+ on nanofibers consequentially, the nanofibers were highly soluble in aqueous media. To solve this problem a neutralisation protocol based on washing nanofibers in the alkaline/alcoholic solution of 5 M NaOH or 1 M K_2CO_3 is also described and compared, to ensure the structural stability of nanofiber membranes in biological media. Resulting

formulation of chitosan/PEO functionalized with bare laser-synthesized AuNPs, delivering a promising platform for tissue engineering applications.

3.3 Materials and Methods

3.3.1 Materials

A medium molecular weight chitosan (200 kDa) and a PEO powder with the molecular weight of 300 kDa were purchased from Sigma-Aldrich (Darmstadt, Germany). A target (1 cm × 1 cm) of high purity Au (99.999%) was purchased from GoodFellow (Cambridge, United Kingdom) to fabricate bare AuNPs. Chitosan was solubilized using acetic acid (99–100%) purchased from SCS GmbH (Sigmarszell, Germany). For the neutralization stage, methanol (99.9%), ethanol (99.5%), and K_2CO_3 were purchased from Carl Roth (Karlsruhe, Germany), while NaOH was purchased from VWR International GmbH (Langenfeld, Germany).

3.3.2 Laser-Ablative Synthesis of Bare AuNPs

Bare laser-synthesized AuNPs were prepared in LP3, using methods of femtosecond ablation and fragmentation in deionized water [70,71,75,83]. Briefly, a gold target (99.99%, GoodFellow, Cambridge, United Kingdom) was placed at the bottom of the glass vessel filled with deionized water (18.2 MΩ cm). A 2.3 mm diameter beam from a Yb:KGW laser (Amplitude Systems, 1025 nm, 480 fs, 1 kHz) was focused with a 75 mm lens on the surface of a target. The target was moved constantly in the focusing plane with a speed of 0.5 mm/s, while keeping the same thickness of the liquid (1 cm) above the target. The concentration of AuNPs was determined by the calculation of the weight loss of the target during the ablation process.

3.3.3 Preparation of Electrospinning Solutions

A total of 2 mL of medium molecular weight chitosan was dissolved at a concentration of 3% (w/v) using 10% (v/v) acetic acid. In a separate cuvette, we prepared 4 mL of PEO with a concentration of 8% (w/v). The solutions were then mixed in the ratio of 1:3, respectively. A concentrated AuNPs solution was added to the polymer solution and ultra-sonicated for 2 h, which ensured the removal of bubbles and a homogenous dispersion of nanoparticles. Concentration of bare laser ablated AuNPs was measured to be 0.15 g L^{-1}. The nanoparticle solution was concentrated before the addition to the electrospinning solution by holding it at 30°C in an oven for several hours. Such a procedure led to 3-fold decrease in the volume. A total of 2 mL of the concentrated solution 0.45 g L^{-1} was used to functionalize the electrospinning polymer solutions. This sample was denoted as Ch-AuNPs. A second sample of nanofibers without AuNPs (Ch-0) was prepared as a reference for comparative studies. In this case, 2 mL of AuNP solutions were replaced by 2 mL of PEO. The procedure was carried out in such a way that the final concentration of the polymer was the same as in the main sample (1:3 final ratio by volume). All steps of the preparation protocol are presented in Table 3.1.

Main Sample Ch-AuNPs	Reference Sample Ch-0
3% (w/v) chitosan in 10% (v/v) acetic acid	3% (w/v) chitosan in 10% (v/v) acetic acid
8% (w/v) PEO in 2 mL conc. AuNPs in deionized water + 2mL deionized water	8% (w/v) PEO in 4 mL deionized water
1:3 final ratio by volume	1:3 final ratio by volume.

Table 3.1: Description of preparation steps for main and reference samples.

3.3.4 Electrospinning Hybrid Multifunctional Nanofibers

The fabrication of nanofibers was done using specialized equipment purchased from IME medical electrospinning technologies. A climate-controlled setup was employed to ensure constant environmental conditions and fixed parameters during the process. An electrospinning setup contained a rotating cylinder set at 2300 rpm. Electrospinning solutions were transferred into a 5 mL syringe, which was connected to a programmable pump providing the constant feed rate of 0.3 mL h^{-1}. The pump was connected via a Leur-Lock and PTFE (Polytetrafluoroethylene) tube with a blunt 0.8 mm-diameter needle at one end of a spinneret, where 14 kV was applied to the solution. The distance between the collector and spinneret was kept at 15 cm. The collector had a negative voltage of −1 kV and was wrapped in aluminium foil to collect the fibers. Climate conditions were fixed for all experiments at 25°C temperature and 50% of humidity.

3.3.5 Morphological and Physicochemical Analysis

A high-resolution transmission electron microscopy (HR-TEM) system (JEOL JEM 3010, Croissy Sur Seine, France) was used to characterize laser-synthesized AuNPs. Using ImageJ software (National Institutes of Health (NIH), Bethesda, MA, USA), statistic measurements were performed on more than 200 AuNPs to determine diameter size distribution. A scanning electron microscope was used as a primary analysis method to verify formation of nanofibers after electrospinning. Due to the limited charging effect on samples, it was unnecessary to proceed to the sputter coating step. Size distributions and morphology of fibers were characterized using scanning electron microscopy (SEM), and a subsequent treatment of micrographs using ImageJ® software. JSM-IT100 InTouch-Scope™ system (Tokyo, Japan) operating at 5–20 kV accelerating voltages was the main microscope used at lower magnifications. A DSM 982 Gemini Zeiss system (Marly le Roi, France) operating at accelerating voltage of 20 kV was used to produce higher magnification micrographs. Both SEM systems were coupled to energy dispersive X-ray analysis. Chemical characteristics were evaluated by Fourier transform infrared (FTIR) spectroscopy (Perkin–Elmer, Cambridge, MA, USA) equipped with a universal attenuated total reflection (ATR) sampling accessory. The measurement histogram was performed by analysing 2 micrographs; one from centre of the collector, where most of the fiber deposition takes place, and another from the edge of the collector. The frequency

distribution, as obtained using integrating ImageJ results with the origin, ranged from 100 to 15,000.

Thermal properties of nanofibers were studied with the help of thermogravimetric analysis (TGA, Perkin–Elmer TGA 4000 system, Billerica, MA, USA) and differential scanning calorimetry (DSC, Perkin–Elmer DSC 8000 system, Billerica, MA, USA). A total of 7 mg and 5 mg of nanofibers were used for each TGA and DSC measurement, respectively. A TGA heating chamber was flushed with nitrogen at 20 mL min^{-1}, preventing the combustion of the samples, and heated at the rate of 10°C min^{-1}. Similarly, DSC was carried out under a nitrogen environment with a constant flow rate of 21 mL min^{-1} and heating rate was kept at 5°C min^{-1}. The operation temperature was between 30 and 700°C during TGA studies and between 30 and 180°C during DSC analysis.

3.3.6 Neutralization of Chitosan/PEO Nanofibers

A total of two protocols were investigated based on two solutions of 1M K_2CO_3, dissolved in 15 mL of ethanol (70%), and 5M NaOH dissolved in 15 mL of methanol (70%). The nanofibers were immersed in the solutions for a total of 20 h at ambient conditions. The immersion process was repeated 3 times by changing solutions after every immersion step to ensure effective neutralization. The samples were then washed with distilled water and dried at room temperature for 24 h, before SEM-EDX and FTIR analyses to assess their structural stability and chemical composition.

3.4 Results and Discussions

The electrospinning of pure chitosan is quite challenging due to its poor solubility and short chain length. In most cases, 1% (w/v) concentration of chitosan was used at variable chitosan/PEO ratios. Therefore, to increase the available bioactivity of functional chitosan, new formulations were tested. The increased concentration of chitosan 3% (w/v) at chitosan/PEO ratio of 1:3, was used for forming electrospinning solution. 10% (v/v) aqueous of acetic acid solution used to dissolve chitosan. Structural analyses by SEM measurements, revealed that the nanofibers are homogenous without observable beads possessing mean diameter of 189 ± 100 nm (Figure 3.1a, b). Thus, this composition of chitosan/PEO was used to prepare a unique solution containing highly concentrated AuNPs (0.09 mg mL^{-1} in electrospinning solution). A typical HR-TEM image of AuNPs synthesised by laser ablation and corresponding AuNPs size distribution is given in Figure 3.2. SEM-EDX examinations of chitosan/PEO nanofibers functionalized with AuNPs revealed a homogenous network of cylindrical nanofibers without any beads.

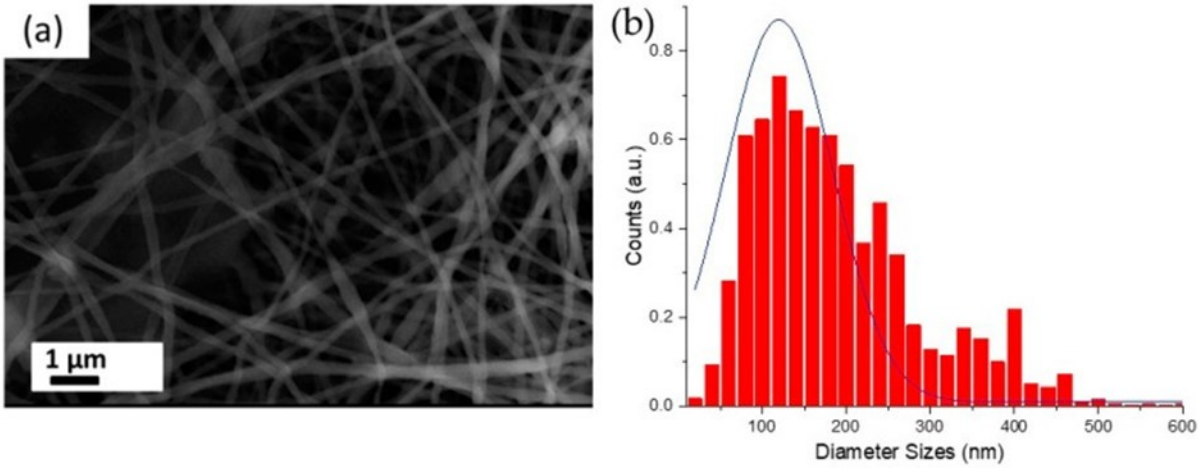

Figure 3.1: SEM image of hybrid chitosan/poly(ethylene oxide) (PEO) nanofibers (a) and corresponding size distribution for nanofiber thicknesses (b).

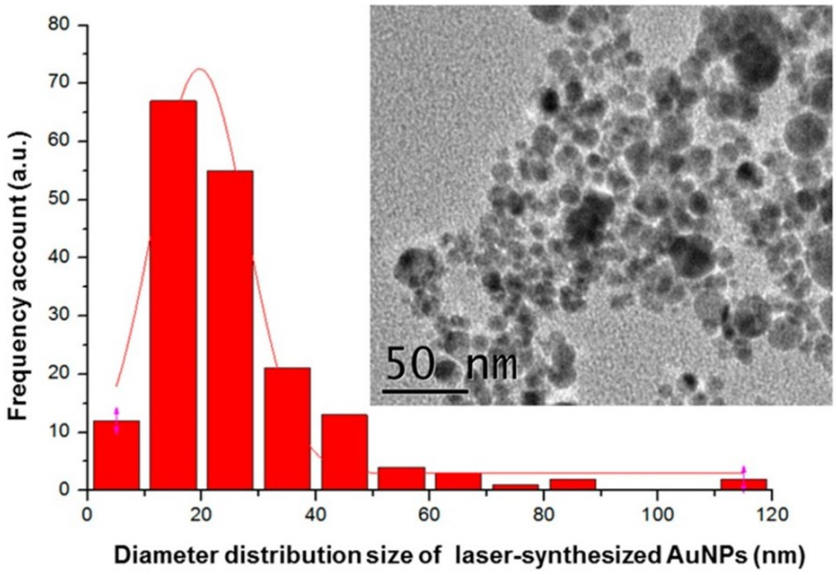

Figure 3.2: Typical high-resolution transmission electron microscopy (HR-TEM) image (inset image) of laser-synthesized AuNPs and corresponding nanoparticle size distribution.

These results were consistent with literature [76], which demonstrated similar morphologies of fibers electrospun with and without bare AuNPs. In addition, the fibers exhibited a mean diameter of 189 ± 86 nm, as measured on micrographs from different sample regions, using ImageJ® software and fitted with a Gaussian approximation (blue curve) (Figure 3.3). AuNPs were clearly resolvable on the fiber surface, while the fiber matrix was still homogeneous. Energy-dispersive X-ray spectroscopy (EDX) confirmed the metallic nature of the bare laser AuNPs. The observed affinity between the nanofibers and the AuNPs was likely due to electrostatic interactions between the polycationic fiber surface possessing positively charged NH_3^+ groups, and negatively charged (–23.1 ± 2.61 mV) Au nanoparticles [70,71,75,83,155]. A 3.5-fold decrease of fiber diameter in compared to literature was observed [76,145]. Such nanofiber surface promised higher reactivity as this result was obtained with 1:3 ratio of chitosan/PEO.

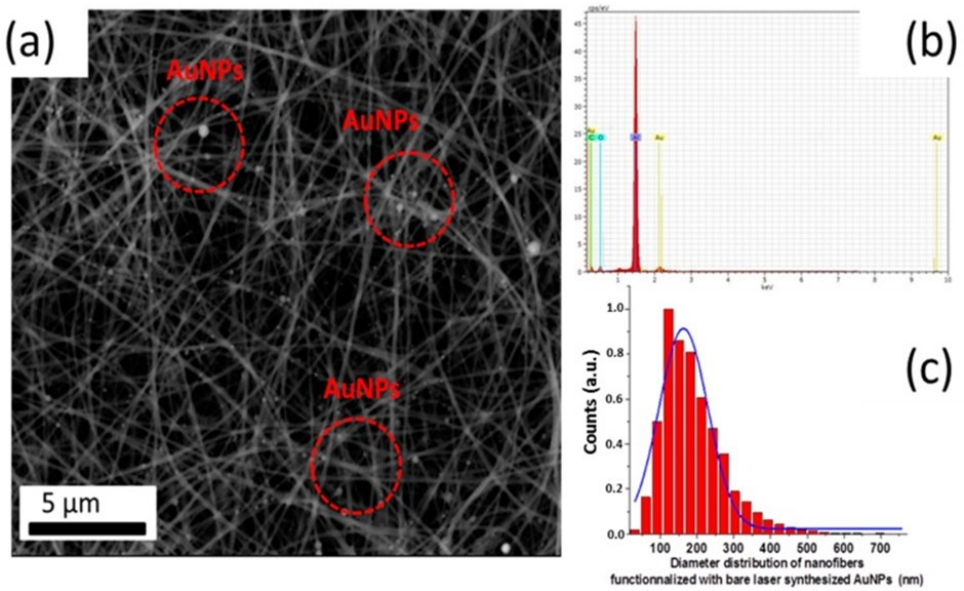

Figure 3.3: SEM image of hybrid chitosan/PEO nanofibers functionalized with bare laser-synthesized AuNPs (a); corresponding energy-dispersive X-ray spectrometry (EDX) spectrum (b); and size distribution of functionalized hybrid chitosan/PEO-AuNPs complex (c).

TGA and DSC was used to examine thermal properties of formed nanofibers and the impact of AuNPs on them. TGA curve (Figure 3.4a) revealed that both Ch-0 and Ch-AuNPs exhibited the same degradation behaviour. However, it was interesting to note that almost 10% weight of the reference (Ch-0) remained after the heating cycle, while 5% weight of the functionalized nanofibers (Ch-AuNPs) left after the program ended. This was likely due to the incorporation of AuNPs that acted as heating spots leading to maximal degradation of the polymer. The derivative curve of the TGA analysis is shown in Figure 3.4b. When heated beyond their melting point, the nanofibers demonstrated a loss of weight. The weight loss region was observed for both nanofibers functionalized with AuNPs (Ch-AuNPs) and no-functionalized nanofibers denoted as the reference sample (Ch-0) after 250°C, which could be interpreted as the initialization of mass loss and could be attributed to the breaking of tertiary bonds in the polymer structure. The major weight loss region started at 347°C and 366°C for Ch-0 and Ch-AuNPs samples, respectively. The width of the peak evidenced a narrow range of temperatures, during which the maximum loss/degradation took place. Additionally, the peak temperature for functionalized nanofibers shifted up compared to the reference samples (from 418 to 423°C).

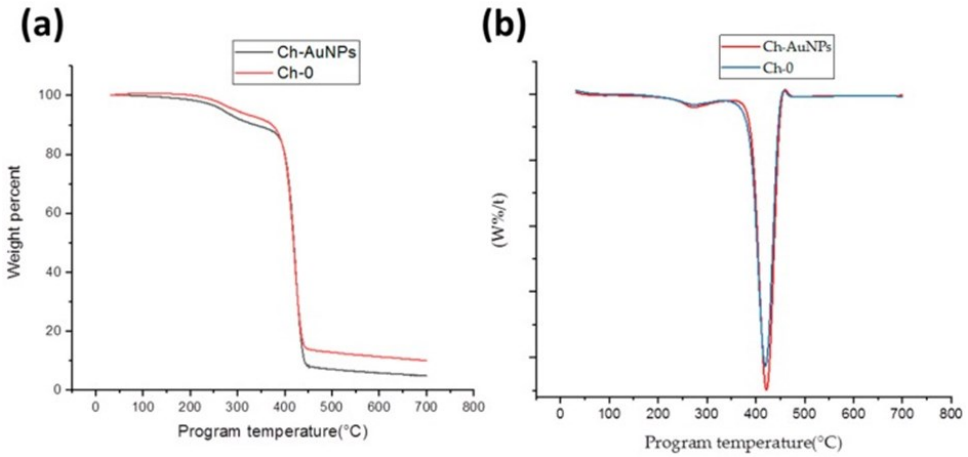

Figure 3.4: Thermogravimetric analysis (TGA) thermograms (a) with corresponding derivative thermogravimetric DTG curves (b) of chitosan/PEO nanofibers functionalized with bare laser synthesized AuNPs.

Subsequently, DSC was carried out to record phase transition changes, which took place e.g., at nanofiber melting points after their functionalization with gold nanoparticles. Here, both types of nanofibers displayed classical DSC curves. As shown in Figure 3.5, an endothermic peak could be observed for the reference nanofibers (Ch-0) at 59.10°C, corresponding to the melting transition of PEO, while for Ch-AuNPs nanofibers similar peak was observed at 57.86°C. Additionally, the normalized peak heat required to enable those transitions was 5.78 mW mg^{-1} and 6.81 mW mg^{-1} for Ch-0 and Ch-AuNPs, respectively. The enthalpy calculated from the area under the curves were 19.21 J g^{-1} and 16.96 J g^{-1} for Ch-AuNPs and Ch-0 samples, respectively. The nanoparticles used for the functionalization absorbed additional heat and, therefore, more heat was required to enable a similar transition in functionalized nanofibers. Additionally, a second event was observed after the melting transition of nanofibers for both Ch-AuNPs and Ch-0. At 147.52°C an exothermic peak could be observed for the reference sample and at 134.90°C for the functionalized nanofibers, which could be attributed to the Tg of the chitosan present in both samples. Therefore, it could be presumed that the heat provided while doing the analysis was not only limited to the nanofibers but absorbed by nanoparticles. Both TGA and DSC showed that the functionalization of nanofibers using bare laser AuNPs provided extra thermal stability in terms of absorbed heat and degradation rate. It should be noted that TGA and DSC data were highly reproducible based on the analysis of many samples.

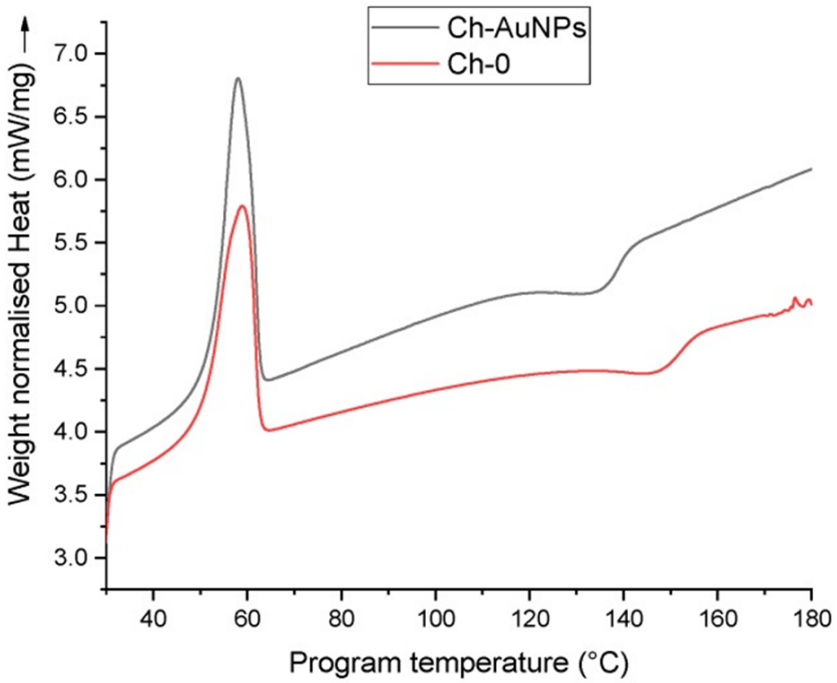

Figure 3.5: Differential scanning calorimetry (DSC) thermogram curve of chitosan/PEO reference (Ch-0) nanofibers and nanofibers functionalized with bare laser AuNPs (Ch-AuNPs).

The chemical composition of nanofibers was analysed using FTIR, before and after the functionalization. As shown in Figure 3.6, characteristic peaks were observed for both constituent polymers (chitosan and PEO). The functionalization of nanofibers with bare laser synthesized AuNPs had no effect on absorption spectra. Both the reference and the functionalized nanofibers displayed a broad band of NH_2 and OH, stretching from 3500–3000 cm^{-1}. A peak for amide absorption could also be observed at 1570 cm^{-1} for both functionalized and reference nanofibers [160–162]. A sharp and strong absorption peak attributed to CH_2 stretching in PEO could also be observed at 2885 cm^{-1}. The spectra beyond 1500 cm^{-1} seem to be dominated with intense PEO bands at 1145, 1095, and 1059 cm^{-1}, complimentary to C-O-C stretching vibrations [162,163]. The functionalization of nanofibers using bare laser AuNPs seems to have no impact on the absorption signature of nanofibers, as observed by FTIR.

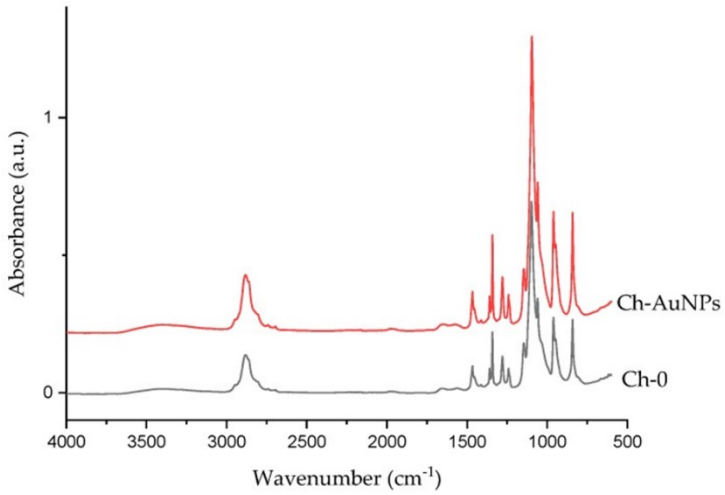

Figure 3.6: FTIR chitosan/PEO nanofibers functionalized with bare laser AuNPs.

3.4.1 Post-processing of Chitosan/PEO Nanofibers

As mentioned earlier, stability of chitosan in aqueous media is a crucial issue. High reactivity of the $-NH_3^+$ group could lead to a rapid dissolution of chitosan/PEO complexes, making them hardly useful for applications in biological systems [28]. Hence, an additional neutralization step is needed to ensure mechanical stability of the fibrous structure and prevent dissolution in biological media. Two methods were tested to transform the $-NH_3^+$ group into the $-NH_2$ insoluble form: (i) 1M K_2CO_3 dissolved in ethanol (70%) and (ii) 5M NaOH in methanol (70%). After the treatment, the samples were washed in distilled water and immersed in phosphate-buffered saline (PBS) for 24 h to test the neutralization efficacy. For the first method employing 1M K_2CO_3, the overall structure of the treated nanofibers had a non-woven mat-like morphology (Figure 3.7a).

However, SEM examination of samples after their immersion in PBS solution for 24 h revealed the loss of the original fibrous structure, as individual nanofibers were not resolvable (Figure 3.7b), suggesting ineffective neutralization of NH_3^+. In contrast, when 5M NaOH solution in 70% methanol was used for the neutralization, the overall nanofibers morphology was conserved at nano- and macro-scale, as indicated by the yellow arrows (Figure 3.7c). SEM analyses clearly showed that most of the fibers were present, while the presence of AuNPs could still be resolved by EDX analysis (Figure 3.7d). Moreover, we found the possibility for conserving the structural integrity of nanofibers suspended over six months in PBS, after neutralization with 5M NaOH. As shown in a macroscopic photo of nanofibers (Figure 3.8a, b), the immersion of nanofiber structures in biological PBS fluid did not lead to the dissolution of nanofibers or a dramatic change of their morphology. It was visible that some swelling and shrinkage effects took place, but these structural changes did not look critical for projected applications, such as biomaterial matrices.

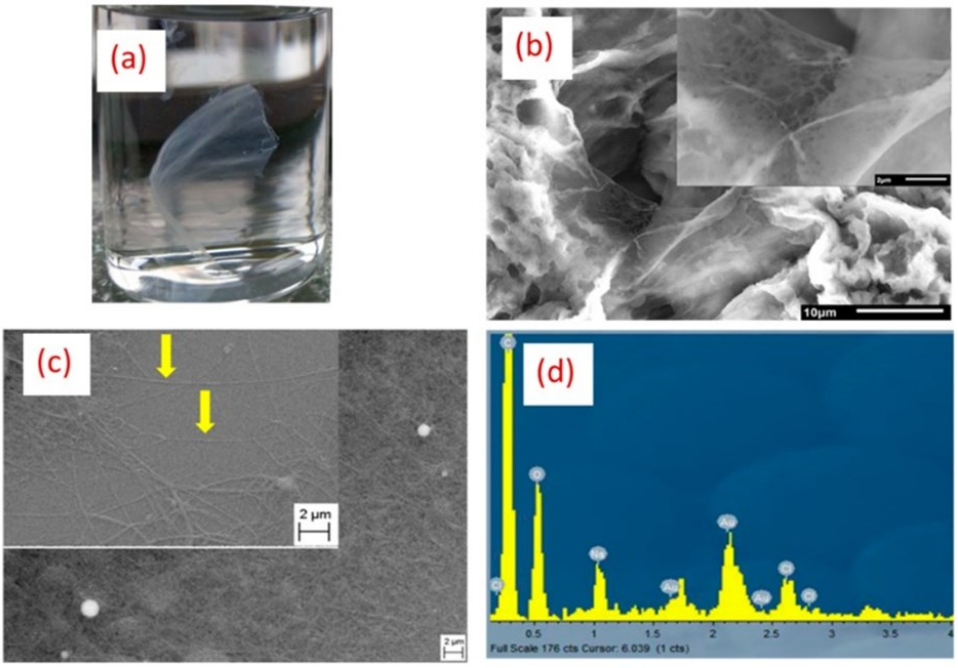

Figure 3.7: Macroscopic photo of chitosan/PEO functionalized with bare laser AuNPs neutralized with 1M of K_2CO_3 immersed in phosphate-buffered saline (PBS) for 24 h (a) with corresponding SEM micrograph (b) (The inner image is given as illustration at higher magnification). SEM micrograph of functionalized chitosan/PEO nanofibers with bare laser AuNPs neutralized with 5M NaOH (indicated by yellow arrows) in two different areas (c) with the corresponding EDX spectrum (d).

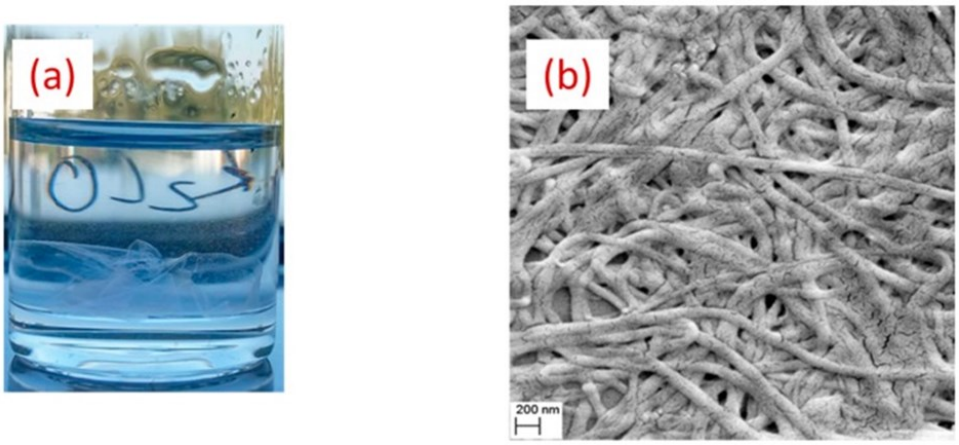

Figure 3.8: Macroscopic photo of functionalized chitosan/PEO with bare laser AuNPs immersed in PBS over six months (a) with the corresponding SEM image (b).

To confirm the conservation of chemical composition of chitosan/PEO nanofibers after their treatment by 1M of K_2CO_3 and 5M of NaOH, additional FTIR was carried out (Figure 3.9). Our analysis revealed that a large part of the PEO was removed, which was especially visible when 5M of NaOH was applied. In fact, main bands of pure PEO including 1467 cm^{-1}, 1277 cm^{-1}, 1343 cm^{-1}, and 1283 cm^{-1} were not resolvable after such a treatment by NaOH, while a characteristic peak of chitosan amine at 3500 cm^{-1} became dominant. A secondary amine peak at 1680 cm^{-1} was also resolvable after both treatments, although

this peak is often overshadowed by peaks from PEO [5,41]. Based on the first morphological assessment and FTIR studies, it was concluded that the neutralization of secondary amine in chitosan/PEO with 5M NaOH was successful.

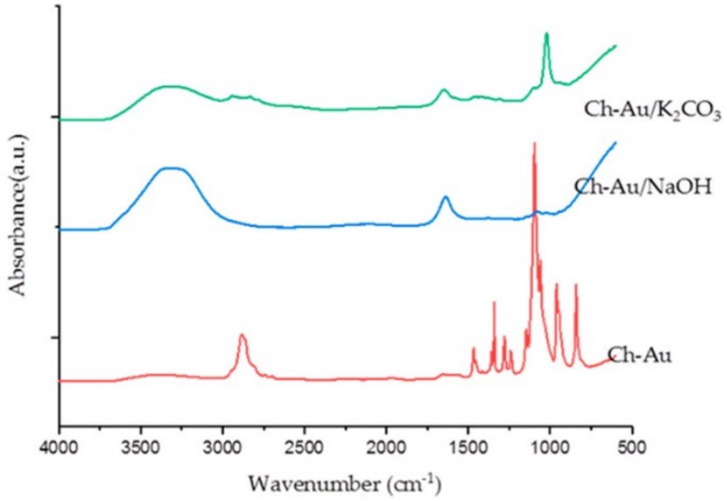

Figure 3.9: FTIR spectra of chitosan/PEO nanofibers functionalized with AuNPs before neutralization (Ch-Au) and after neutralization with K2CO3 (Ch-Au/K2CO3) or NaOH (Ch-Au/NaOH).

3.5 Conclusions

This chapter reports the electrospinning of innovative formulation of chitosan (PEO) functionalised with bare laser-ablated AuNPs.

For the preparation of AuNPs functionalised hybrid nanofibers, 3% (w/v) medium molecular eight chitosan was successfully dissolved in 10% (v/v) aqueous acetic acid, having a volume ratio of chitosan solution to co-spinning agent (PEO) at 1:3, which is higher compared to previously reported concentration of 1% (w/v) chitosan at volume ratio of 1:4 [76,145]. Systematic physicochemical analysis demonstrated improvements of the structural characteristics of the fibers. Microscopic measurements revealed that electrospun nanofibers were deposited on the collector as cylindrical non-woven homogenous network with AuNPs dispersed in the matrix. Additionally, statistical measurements showed an average diameter of 189 ± 86 nm. Functionalised hybrid nanofibers were shown to possess improved thermal stability in TGA and DSC analysis.

Spectroscopic (FTIR) analysis was done to reveal the changes in absorption spectra after functionalisation with AuNPs and neutralisation of $-NH_3^+$ on the nanofibers' surface. Further microscopic and spectroscopic measurements revealed the immersion in 5M NaOH to be a more effective naturalisation strategy.

The work presented in this chapter provided the possibility of development multifunctional hybrid nanofibers for techniques such as tissue-engineering. The proposed approach looked promising for template electrospinning of unprocessable but useful biodegradable polymer chitosan by post processing of nanofibers. This approach gave optimised electrospinning parameters and possibility of including the selection of polymers, functionalisation agents, for obtaining uniform nanofibers.

CHAPTER 4

Template nanofiber fabrication blending organic (matrix) and inorganic polymer

Contents

4.1 Introduction

In this chapter, unique templated nanofibers were electrospun based on the methodology and platform established in previous chapter. In contrast to previous chapter, smart inorganic polymer was templated into nanofibers using homopolymer as co-spinning agent to induce multifunctionality. Template fabrication of one-dimensional material via electrospinning into 2-d nonstructured materials has been demonstrated. Smart inorganic polymers poly (ferrocenylphosphinoboranes) **Fe A** [{Fe(C_5H_5)($C_5H_4CH_2PH$-BH_2)}n] and **Fe B** [{Fe (C_5H_5)($C_5H_4PHBH_2$)}n], synthesised by the research group of prof. Evamarie Hey-Hawkins in Institute for Inorganic Chemistry, Leipzig, were template electrospun as functionalisation agents in PEO and PS matrix. With the objective of utilising main-group elements and a ferrocene moiety as pendent group in inorganic polymer. Specifically, for efficient catalysing agents with electron rich moieties. Here, the focus was on utility of nanofibers rather than their bio-degradability. The work has been published in **LoP-2**.

4.2 Context

Hybrid 2D structures or bio-hybrid technologies are emerging platforms in materials science for developing advanced structural and multifunctional materials, supporting several technological applications [164,165]. Hybrid 2D nanostructures can be developed using various techniques and typically comprise a wide range of traditionally noncompatible constituents. They can be fabricated by either using combinations of inorganic–inorganic or organic–inorganic, which again have different structures ranging from simply bare nanoparticles to complex arrangement of multi-layered nanofibers. There are various strategies, which are applied for producing such advanced structures and multifunctional materials. They are categorized as top-down and bottom-up approach [166,167]. For instance, synthesis of nanoparticles from a homogeneous solution and further growth of nanoparticles to develop 2D structures such as nanowires or nanoflowers, can be one example of a bottom-up approach [168,169]. Electrospinning for fabrication of nanofibers has emerged as a leading alternative top-down approach to develop nanostructures using bulk materials and to incorporate multifunctionality [170–172]. The emergence of electrospinning could be attributed to its compatibility with various natural or synthetic polymers [173–175]. Thus, electrospinning can bring together a variety of materials including proteins and other macromolecules, polymer hybrids, ceramics, and metal oxides, consequently leading to applications such as tissue engineering, wound dressing, transport and release of drugs, catalysis, filter, and surface modifications among many others [15,176–179]. For instance, there have been multiple studies showing the improvement of antibacterial characteristics of nanofibers by the inclusion of silver nanoparticles or copper nanoparticles [57]. Similarly, various ligands could also be introduced to remove unwanted substances from a solution, using their physical adsorption properties [180]. Moreover, the secondary structure of nanofibers can be manipulated by tuning simple yet intertwined parameters. This has led to

formation of pores on the nanofibers, parallel arrangement in two-dimensional space, formation of arrays and other hierarchical structure such as folding and stacking [129,170,181].

Significant efforts have been made to incorporate entities which cannot be directly used for electrospinning, such as chitosan [76,159], or inorganic polymers such as poly(ferrocenylphosphinoboranes) **Fe A** [{Fe(C_5H_5)($C_5H_4CH_2PHBH_2$)}n] and **Fe B** [{Fe(C_5H_5)- ($C_5H_4PHBH_2$)}n] [39,182], shown in Figure 4.1. In recent years, poly(phosphinoboranes) have gained attention as the P– B polymer backbone is valence-isoelectronic with a C-C backbone of most polymers used in daily life. Moreover, the P–B backbone of poly(phosphinoboranes) is polar due to the electronegativity difference and might introduce conductivity throughout the chain, which is an added advantage compared to polymers having a C-C backbone. Due to their inherent polar nature, the polymers can organize in a systematic way, which might be beneficial to construct optoelectronic devices. **Fe A** and **Fe B** are thermally very stable and soluble in a wide range of solvents, which helped blending them with other polymers. Co-spinning agents such as poly(ethylene oxide) (PEO) and polystyrene (PS) were used to facilitate electrospinning. These polymers provided the matrix for co-spinning of **Fe A** and **Fe B**. Additionally, the lone pair of electrons at oxygen in PEO and the electron cloud present in polystyrene might be involved in weak interactions with the polar P–B backbone of **Fe A** and **Fe B** [183].

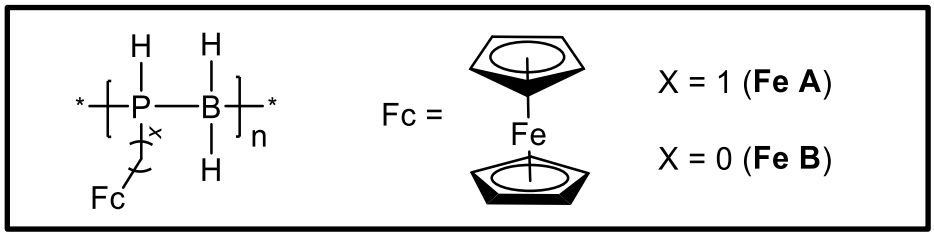

Figure 4.1: Structure of poly(ferrocenylphosphinoboranes) **Fe A** [{Fe(C5H5)(C5H4CH2PHBH2)}n] and **Fe B** [{Fe(C5H5) (C5H4PHBH2)}n].

This chapter presents unique combinations of a polymer matrix and ferrocene-based polymers **Fe A** and **Fe B**, providing unique collective physical properties toward higher surface reactivity and conductivity of the resulting hybrid nanofibers. Moreover, we demonstrate possibility for the enhanced processability of smart inorganic polymers based on ferrocene by introducing them as functional components of generated hybrid nanofibers. This could further be optimized by adding higher quantities of the functional inorganic polymers to the electrospinning solution hence, increasing their effectivity or influence on the collective properties of the nanofibers.

4.3 Materials and Methods

4.3.1 Materials

PEO powder (Mw = 300 kD) and polystyrene (PS) beads (Mw = 250 kD), obtained from Sigma Aldrich, Darmstadt, Germany and Carl Roth, Karlsruhe, Germany, respectively, were used as template for co-spinning with **Fe A** [{Fe(C_5H_5)($C_5H_4CH_2PHBH_2$)}n] (Mw = 14–17 kD) and **Fe B** [{Fe(C_5H_5)($C_5H_4PHBH_2$)}n] (Mw = 12–15 kD). **Fe A** and **Fe B** were prepared according to the literature [24,25]. Tetrahydrofuran and chloroform ($CHCl_3$) from Carl Roth, Karlsruhe, Germany were the best choices for electrospinning due to their ability to dissolve both, the inorganic and organic polymers.

4.3.2 Preparation of electrospun nanofibers

Electrospinning was performed using four different solutions. Each of the solutions contained one of the poly(phosphinoboranes) and the polymer for co-spinning. **Fe A**/PS and **Fe B**/PS solutions were prepared by mixing the polymers in a ratio of 1:4 (wt./wt.) in THF. Similarly, **Fe A**/PEO and **Fe B**/PEO solutions were prepared in a ratio of 5:16 in chloroform. Both poly(phosphinoboranes) dissolved rapidly in their respective solvents giving a distinctive shade of rust brown colour which was also noticed in the electrospun nanofibers. The solutions were stirred at room temperature for a couple of hours followed by ultrasonication for an hour for homogeneity. All the solutions were used within a week of preparation. The electrospinning was started by preparing four formulations with fixed concentrations of **Fe A** and **Fe B** added to respective concentrations of PEO and PS. Table 4.1 displays the composition and used terminology.

	Polymer concentrations % (w/v)			
	Fe A	**Fe B**	PS	PEO

Fe A/PEO	2.5	-	-	8
Fe B/PEO	-	2.5	-	8
Fe A/PS	2.5	-	10	-
Fe B/PS	-	2.5	10	-

Table 4.1: Polymer composition of hybrid nanofibers and their concentrations.

4.3.3 Electrospinning of hybrid polymer (PEO/PS) nanofibers

An electrospinning platform with options to control various parameters was used for producing nanofibers. The machine was developed by IME medical electrospinning technologies (Netherlands) and consisted of a closed chamber to prevent accidental interaction with high voltage, separating the electrospinning process from outside interference, such as temperature and humidity. The setup was used in horizontal configuration with a rotating negatively charged cylinder covered with aluminium foil as collector. The prepared solutions were transferred to 3 ml syringes attached to a PTFE-tube via Leur-Lock with blunt ended needles (internal diameter 0.8 mm). The syringes were placed on a programmable pump to control the flow rate while electrospinning. For all solutions, the flow rate was fixed at 0.3 ml h^{-1}. The collector was rotating at 2300 rpm. Additionally, voltages applied to the spinneret and the collector were fixed at 14 kV and -2 kV. Electrospinning was conducted at 25°C and 28% relative humidity.

4.3.4 Preparation of polymers Fe A and Fe B

A dehydrocoupling reaction was employed to obtain the ferrocene-based poly(phosphinoboranes) from their respective monomers [39,182] namely, the ferrocenyl phosphine-borane and ferrocenyl methylphosphineborane adducts. Dehydrocoupling of phosphineboranes is a well-established process and can be performed with [{Rh(μ-Cl)(cod)}$_2$] (cod = 1,5-cyclooctadiene) as catalyst. The polymerization process can be monitored through ^{31}P NMR spectroscopy. The monomer contains a PH_2 group, the polymer a PH group. This fact can be detected in the proton-coupled ^{31}P NMR spectrum. The monomer exhibits a triplet, the polymer a doublet [182].

4.3.5 Analysis of Fabricated Nanofibers

Scanning electron microscopy (using a JSM-IT 100 InTouchScope instrument) was used to analyse the surface morphology of co-spun nanofibers at accelerating voltage of 20 kV. The fibers were removed from the aluminium foil by scratching and were fixed on the stage using carbon tape. ImageJ [184] was used for measuring diameter and statistical analysis of the generated nanofibers.

Multinuclear NMR spectroscopy was employed to check the purity of the electrospun polymers. NMR spectra were recorded in $CDCl_3$ with a Bruker AVANCE DRX 400 spectrometers. The chemical shifts of ^{1}H, ^{11}B, and ^{31}P NMR spectra are reported in parts

per million (ppm) at 400.1, 128.4, and 161.9 MHz, respectively. Tetramethylsilane (TMS) was used as an internal standard for ^{1}H NMR spectroscopy and for referencing the ^{11}B and ^{31}P NMR spectra to the unified scale [185]. The hybrid nanofibers were also compared with pristine polymers (PEO or PS). FTIR spectra were recorded with a PerkinElmer Spectrum 2000 spectrometer. IR spectra of the electrospun polymers exhibited the distinctive vibrations of both pristine polymers (PEO or PS) and poly(ferrocenylphosphinoboranes) (**Fe A** and **Fe B**) without significant changes (see Figures A.7 and A.8 in appendix).

Differential scanning calorimetry (DSC) (PerkinElmer, Waltham, MA) was performed under nitrogen atmosphere to analyse the change in thermal properties in the hybrid nanofibers as compared to the reference sample. 3.5 mg of each type of nanofiber was sealed in an aluminium pan for measurements. The samples were subjected to multiple heating and cooling cycles at a rate of 10°C min^{-1} from −70 to 350°C, depending on the type of polymer used for co-spinning. Thermogravimetric analysis (TGA) (Perkin Elmer) was performed to check the thermal stability and degradation of the co-spun polymers. 7.5 mg of nanofibers was placed in a ceramic cuvette under nitrogen atmosphere (flow rate - 20 ml min^{-1}). The samples were heated at 10°C min^{-1} from 30 to 700°.

4.4 Results and discussion

Nanofibers were prepared from optimized concentrations of co-spinning polymers, which was obtained by analysing various weight ratio and eliminating the concentration, which gave no fibers (checked with SEM). Moreover, the selected solvents had to dissolve **Fe A**, **Fe B**, PEO and PS, and form stable solutions for the electrospinning process. The polymers, PEO and PS, have very high molecular weights and long chains, which were ideal for electrospinning [135]. Moreover, they interact with the **Fe A**, **Fe B** polymers via hydrogen bonds and dispersion forces, therefore stabilizing the solution. The spinning solution was loaded into the syringe and voltage was applied. Once the polymer was charged enough to overcome the surface tension, a fine jet emerged from the spinneret and deposited at the other end on the aluminium foil. The presence of **Fe A** or **Fe B** in their respective resulting nanofibers could easily be identified due to the distinctive colour of the fibers as shown in Figure 4.2. Additionally, the presence of **Fe A** or **Fe B** in the nanofibers was also proven by NMR and IR spectroscopy.

Figure 4.2: Example of nonwoven fibers scratched from Al foil after co-spinning PEO and **Fe A**. PEO fibers are white or semitranslucent; the distinctive colour is due to the presence of polymer **Fe A**.

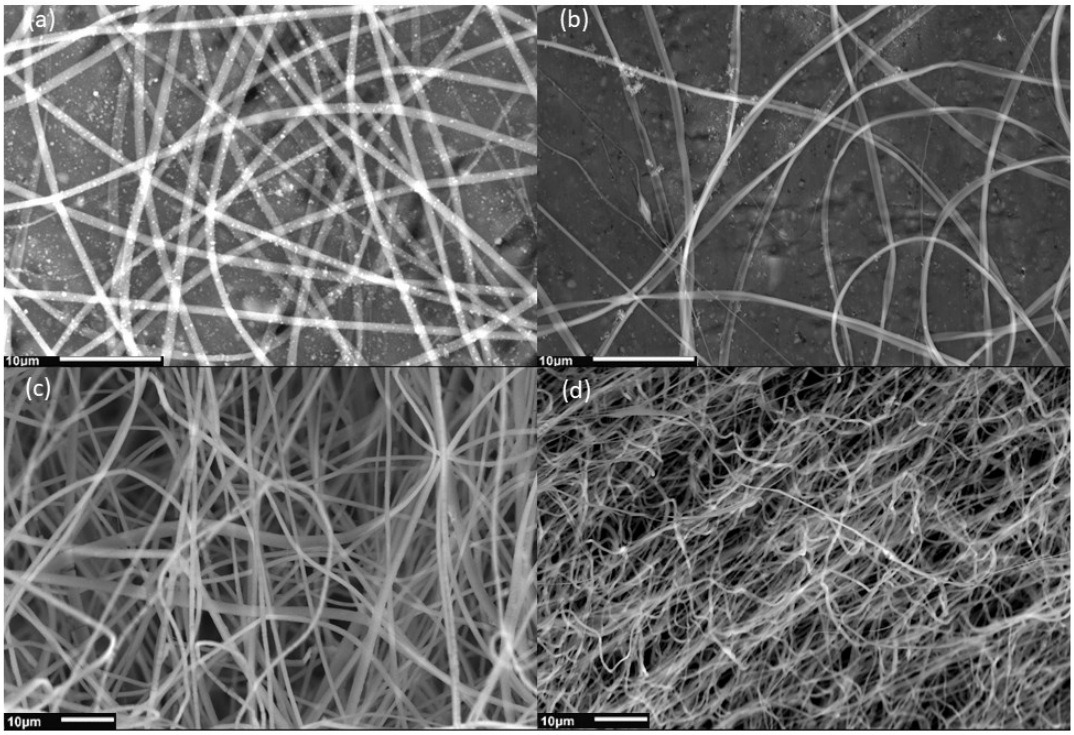

Figure 4.3: SEM of blended ferrocene-based polymers Fe A and Fe B with corresponding copolymers revealing various morphologies: (a) **Fe A**/PS, (b) **Fe B**/PS, (c) **Fe A**/PEO, and (d) **Fe B**/PEO.

The analysis revealed that the nanofibers obtained by co-spinning **Fe A**/PS fibers had a mean diameter of 623 nm with a standard deviation of 491 nm and **Fe B**/PS fibers 478 nm with a standard deviation of 325 nm. Similar sized fibers were also obtained when **Fe A** and **Fe B** were co-spun with PEO (mean diameter 525 nm with standard deviation 252 nm, and 491 nm with standard deviation 271 nm, respectively) (Figure 4.4).

Multinuclear NMR studies confirmed that the respective polymers were present in their resulting nanofibers. ^{1}H NMR spectroscopy showed the distinctive broad signals of the ferrocenyl protons in **Fe A** and **Fe B** around 4 ppm and indicated that the poly(phosphinoboranes) were present in very small amount compared to the co-spinning organic polymers (see Figures A.1–A.6, appendix). The broad signals of P–H and B–H protons were not detected due to the inherent broadness of the peaks of the polymers. $^{31}P\{^{1}H\}$ NMR spectra of the electrospun polymers showed broad signals at around −60 ppm, which is a characteristic peak of **Fe A** and **Fe B**. The change in their chemical shifts in the ^{1}H and $^{31}P\{^{1}H\}$ NMR spectra was, however, insignificant. The $^{11}B\{^{1}H\}$ NMR spectra of the electrospun polymers exhibited a very broad peak around 0 ppm along with distinctive peaks for **Fe A** or **Fe B** at around −40 ppm for tetracoordinated boron bonded to phosphorus (see Figures A.5 and A.6, appendix) [186–188]. Interaction of the B–H protons with the organic polymer could be the reason for these changes.

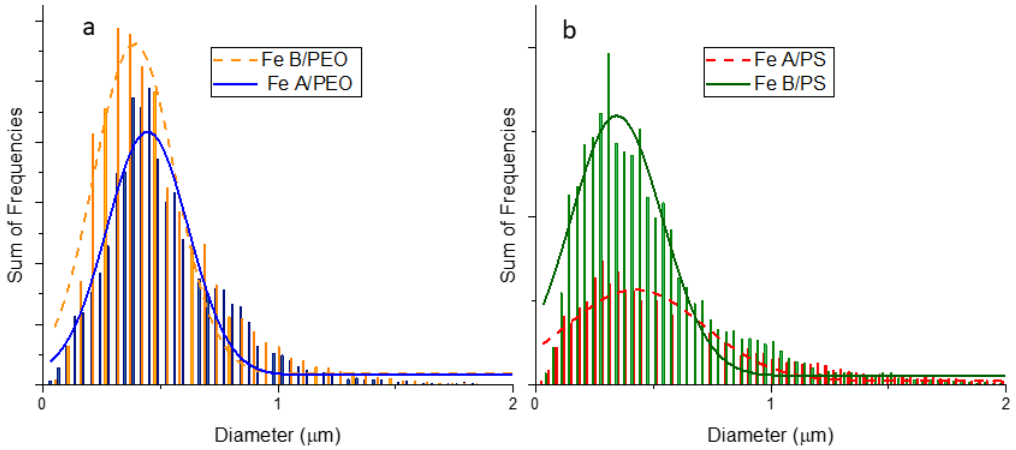

Figure 4.4: Distribution of diameter of nanofibers prepared by co-spinning of polymers Fe A or Fe B with: (a) PEO and (b) PS.

In the IR spectra, νP–H and νB–H of the respective poly(phosphinoboranes) were observed at ca. 2,400 cm^{-1} (see Figures S7 and S8, ESI) [189,190].

Thermal characteristics of co-spun nanofibers were studied by TGA (Figure 4.6). The initiation for major weight loss occurred at lower temperature for **Fe B** (219°C) as compared to 246°C for polymer **Fe A** and can be attributed to degradation [39]. However, both polymers retain 60–67% of their initial weight even at 700°C. There was a marked difference in the initial temperature for degradation compared to the reference fibers.

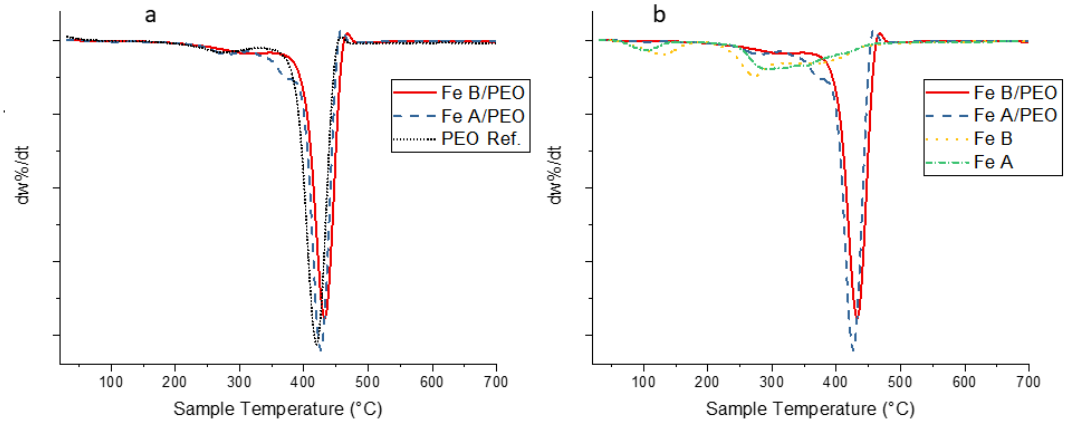

Figure 4.5: DTG graph comparing the degradation of (a) co-spun **Fe A** and **Fe B** nanofibers to respective polymers **Fe A** and **Fe B**, (b) graph comparing the degradation of co-spun **Fe A** and **Fe B** nanofibers to PEO reference nanofibers.

Degradation of the reference fiber containing only PEO occurred at 420°C, whereas degradation of **Fe A**/PEO and **Fe B**/PEO was observed at 426 and 432°C, respectively (Figure 4.6). More significant differences were found when comparing the thermal degradation for **Fe A**/PS and **Fe B**/PS with the corresponding reference sample. The difference between peaks in the thermogram for nanofibers samples blended with PS was more distinguishable as compared to that observed from PEO blended nanofibers. The degradation of the reference sample started at 418°C. As shown in Figure 4.7, the same peak for hybrid fibers containing **Fe A** or **Fe B** had shifted to higher temperatures, 449 and 444°C, respectively.

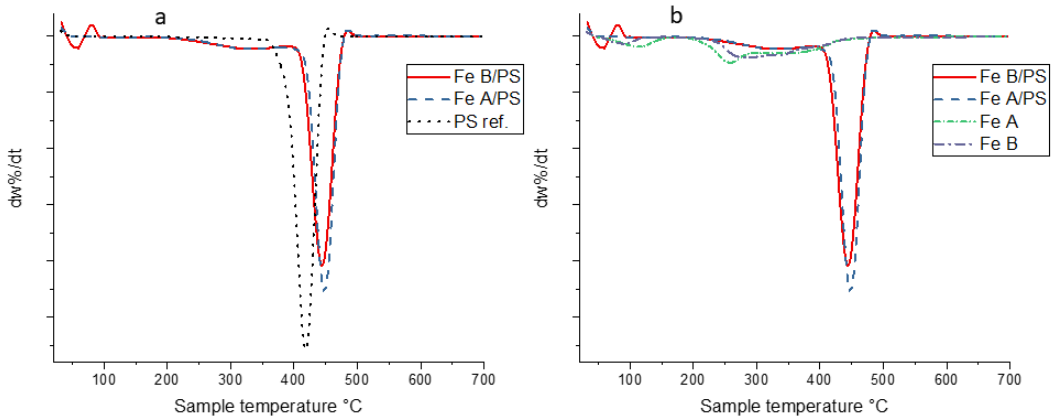

Figure 4.6: DTG graph comparing the degradation of (a) co-spun PS/**Fe A** or PS/**Fe B** nanofibers to the respective polymer **Fe A** and **Fe B**, (b) graph comparing the degradation of co-spun PS/**Fe A** or PS/**Fe B** nanofibers to PS reference nanofibers.

Differential scanning calorimetry (DSC) was performed on the nanofibers (Figure 4.8a, b). Hybrid nanofibers were compared with either PEO nanofibers or PS nanofibers as reference. While analysing **Fe A**/PEO and **Fe B**/PEO in comparison to pristine nanofibers, a typical DSC curve was obtained with one significant event. As the hybrid nanofibers and pristine nanofibers were heated from −50 to 200°C, a dominant peak was observed. The peak in positive y-axis represents an endothermic process and can also be interpreted as the melting point of the respective sample. The peak shifted toward the positive x-axis for hybrid nanofibers **Fe A**/PEO (63°C) and **Fe B**/PEO (6°C) as compared to 62°C for pristine PEO nanofibers. Additionally, by calculating the area under the curve the heat required to enable the phase transition observed through DSC is 15.2 mW mg^{-1} for pristine PEO nanofibers, whereas it is 16.4 and 15.3 mW mg^{-1} for PEO **Fe A** and PEO **Fe B** nanofibers, respectively. Hence, in conjugation with similar results obtained by TGA, it was concluded that blending of polymers **Fe A** or **Fe B** with PEO for co-spinning, provided added functionality and thermal stability of the corresponding hybrid nanofibers.

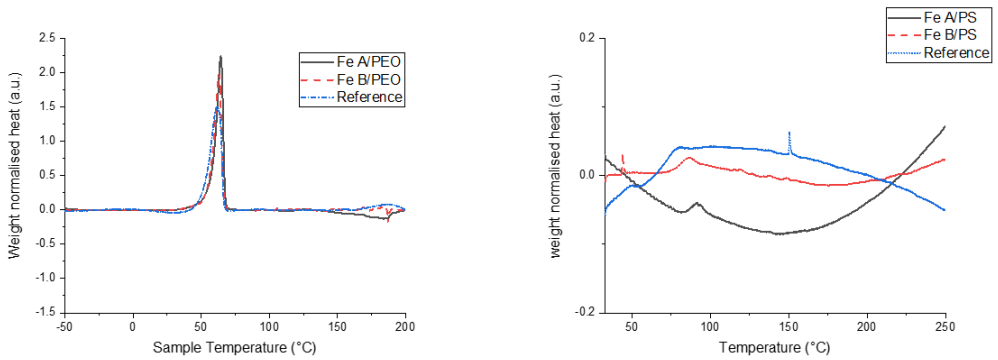

Figure 4.7: DSC graphs highlighting changes in pristine nanofibers and hybrid nanofibers: (a) co-spinning PEO, and (b) co-spinning P

In contrast, for **Fe A**/PS or **Fe B**/PS no significant change was observed. A typical DSC curve was observed in each sample containing PS and functionalized nanofibers, with Tg of polystyrene in case of functionalized nanofibers moving a few degrees higher to around 86°C as compared to 79°C for pristine PS polymer. Both samples functionalized with polymer **Fe A** and **Fe B** exhibited a similar curve at higher temperature. When pristine **Fe A** and **Fe B** were subjected a to similar program, they showed a typical DSC curve reflecting their glass transition temperature.

4.5 **Conclusions**

In this chapter, a method for template fabricating nanofibers containing functional inorganic polymers blended with organic polymer as matrix was established. Advanced hybrid multifunctional nanofiber mats were obtained with high surface reactivity and electron-rich domains for varieties of interaction with macromolecules and redox chemistry.

Template nanofibers were obtained from 2% (w/v) of inorganic polymer blended with homopolymers PS and PEO, providing the electrospinnable solution. Resulting elongated continuous uniform nanofibers had average diameter between 475 and 625 nm. The interaction between the inorganic and organic polymers was confirmed by NMR and FTIR spectroscopy. Furthermore, the templated nanofibers showed higher thermal stability. Poly(ferrocenylphosphinoboranes) containing domains namely, ferrocenylphosphineborane and ferrocenylmethylphosphineborane were used taking advantage of valence-isoelectronic P–B polymer backbone. Inorganic polymers possessed polarity due to electronegativity differences therefore, had the potential to induce conductivity in nanofiber structure.Co-spinning of polymer resulted in improved collective properties of generated nanofibers.

CHAPTER 5

Fabrication of PCL and plasmonic TiN NPs based smart nanofibers

Contents

5.1 Introduction

This chapter report the first fabrication and testing of formulation of polycaprolactone (PCL)-based nanofibers functionalized with bare (ligand-free) titanium nitride (TiN) nanoparticles (NPs). Laser ablation was used for the synthesis of bare nanoparticles which were then dispersed in to provide a platform for tissue engineering applications. The possibility to functionalize the nanofibers with plasmonic TiN NPs, without affecting their biological compatibility was demonstrated. The nanofibers were electrospun at the facility in Rhine-Waal University, Germany while the nanoparticles were synthesised in LP3, Marseille, France. The nanofibers were subjected to i*n vitro* viability tests using the incubation of 3T3 fibroblast cells at research department in Institute of Experimental Medicine of the Czech Academy of Sciences, Czech Republic. Results discussed in this chapter are now in press (**LoP-1**).

5.2 Context

The development of novel platforms for regenerative medicine forms one of the attractive applications of nanotechnologies and newly synthesized inorganic nanomaterials, which can be used in combination with organic matrices for tissue engineering [57,59,191]. Here, hybrid nanofibers fabricated via electrospinning can provide numerous advantages over counterparts prepared by conventional techniques, including the possibility of using bio-degradable natural or synthetic polymers [55,56], or conductive polymers such as poly(ferrocenylphosphinoboranes) (when blended with traditional synthetic polymer such as polystyrene) [172], good control of nanofiber dimensions, capability of incorporating multiple drugs (even if they are hydrophobic) [172,192,193]. These attractive properties stimulate the development of novel nanofiber formulations and their functionalization for a variety of applications ranging from antimicrobial action to biosensing and tissue grafting [43,194–197].

Various polymers with varying molecular weights, bio-degradability and hydrophilicity have been successfully electrospun in the form of homogenous nanofiber structures. Such nanofibers can have unique properties such as high surface area and pore size, but their functional domain remained limited. To enable new functionalities, one can decorate the nanofibers with functional agents such as inorganic nanoparticles (NPs) or biomolecules [132,164,180]. As an example, nanofibers functionalized by silver (Ag) and copper (Cu) NPs were shown to exhibit antibacterial activity and used as extracellular matrix (ECM) to promote wound healing and tissue engineering [198], while gold (Au) NPs are often used as additives to improve mechanical properties of nanofibers, promote protein adsorption and cell adhesion, and finally to reduce bacterial colonization [58,60,199]. However, since most inorganic nanomaterials are fabricated by chemical methods implying the use of various reagents and stabilizing agents, they are often contaminated by hazardous by-products complicating their applications in biological systems [200].

Pulsed laser ablation presents a “physical” alternative to fabricate nanomaterials, which are free from stabilizing agents and impurities [68,69]. This technique is based on natural production of nanoclusters under the action of laser radiation on a solid target [201], followed by their release into a gaseous or liquid medium to form a nanostructured film [153,202] or a nanoparticle solution [68,69], respectively. In this case, solutions of NPs can be stable even in bare (ligand-free) state and contamination-free, which opens avenues for their successful use in biological systems *in vitro* and *in vivo* [157,203]. As an example, we recently elaborated the technique of femtosecond (fs) laser ablation in water and organic media, which makes efficient control over size characteristics of NPs from a variety of materials possible, including Au and Si NPs [155,156,204]. As demonstrated in previous chapters, the inclusion of such ligand-free Au and Si NPs into chitosan nanofibers via electrospinning provided a very promising platform for tissue engineering applications [10,54,76,205]. Here, the functionalized nanofibers were shown to be stable, with uniform thickness for given electrospinning parameters, while the presence of NPs could lead to the decrease of their mean diameter. It was also important that such NPs-blended nanofibers did not cause any negative effect on cell viability. However, the employment of chitosan for the fabrication of nanofibers imposes some limitations on the electrospinning process due to its poor solubility and swelling behaviour [206]. In addition, post processing based on the neutralization of NH_3^+ is typically required to stabilize the nanofibers and adapt them for the utilization in biological systems.

It was inferred from research done in previous chapters, the properties of nanoparticle-decorated hybrid nanofiber matrices must be further improved, by the choice of appropriate materials as building-blocks. Here, polycaprolactone (PCL) looked as a promising material for the formation of nanofiber matrix, as a result of the combination of biocompatibility and biodegradability options [122,207,208], as well as easy-solubility in acetone and dichloromethane (DCM) for making electrospinning solutions. In addition, PCL has been approved for use in human body for controlled drug delivery, implants, etc. On the other hand, having strong and broad plasmonic peak around 640–700 nm with a significant tail over 800 nm even for small NPs sizes (<7 nm) [53], bare laser-synthesized titanium nitride (TiN) nanoparticles seemed as extremely promising functional element for such hybrid nanofiber platforms. Several studies had already shown, TiN NPs possessed low toxicity *in vitro* and *in vivo*, as well as can initiate strong photothermal therapeutic effect under near-infrared laser irradiation in the region of relative tissue transparency [207–209]. Furthermore, processability of PCL in acetone, while synthesis of stable solutions of TiN NPs in acetone by femtosecond laser ablation, simplified their co-dissolution for electrospinning.

This chapter reports a successful electrospinning of PCL together with laser-synthesized TiN NPs at various ratios, providing an advanced hierarchical hybrid nanofiber platform for tissue engineering. The obtained nanofibers are characterized by a panel materials analysis technique such as scanning electron microscopy (SEM), Fourier Transform Infrared Spectroscopy (FTIR) and thermal analysis (TGA and DSC). The nanofibers containing various concentrations of TiN NPs were further studied to compare

their influence on cell growth behaviour and overall cytotoxicity of the functionalized nanofibers.

5.3 Materials and methods

5.3.1 Materials

Commercial, Polycaprolactone (PCL) powder (M_w = 80 kD) from Purasorb®, Corbion, Netherlands. Dichloromethane (DCM), acetone (analytical reagent grade) and ethanol from Carl Roth, Karlsruhe, Germany were used as solvents. A TiN (99.99%) pellet from GoodFellow, Cambridge, United Kingdom was used as the target for the synthesis of TiN NPs.

5.3.2 Laser-Ablative Synthesis of Bare AuNPs

Bare TiN NPs were synthesized using methods of femtosecond (fs) laser ablation of bulk TiN target in acetone, as it was earlier described in [53]. Briefly, a 2.3mm diameter beam from a Yb:KGW laser (Amplitude Systems, France, 1025 nm, 480 fs, 10 kHz) was focused via a 75mm lens on the surface of the hot-pressed TiN target placed at the bottom of a glass cuvette filled with acetone. The thickness of the liquid above the target was kept constant at 1cm. Concentration of the nanoparticles in the solution was calculated at 0.15 mgL^{-1}, as determined from target weight loss during laser ablation.

5.3.3 Preparation of electrospun solutions

Electrospinning was performed using 7 different solutions, increasing the concentration of PCL until homogenous fibers were not identified in SEM micrographs. Two solutions were prepared using PCL starting with the concentration of 8% (w/v) in DCM (3 mL) and acetone/ethanol (2 mL). 5 mL solution was prepared for each concentration for electrospinning, as described in Table 5.1. Based on micrographs from SEM, 20% (w/v) PCL was chosen as optimised concentration for the functionalization with TiN NPs. Solutions of the polymer with TiN NPs at various concentrations were solubilized in DCM and acetone having the ratio of 3:2 (v/v).

5.3.4 Electrospinning of PCL and functionalized PCL nanofibers

An electrospinning system from IME Technologies, Netherlands having a climate control among many other parameters was used for the fabrication of nanofibers. The system consisted of a closed chamber enabling a controlled temperature and humidity, as well as excluding the contact of users with high voltages. The setup had a horizontal configuration and included a rotating negatively charged cylinder as the collector. Prepared solutions were transferred to 5 mL syringes attached to a PTFE tube via a Leur-Lock with blunt ended needles (internal diameter 0.8 mm), which were inserted into a spinneret. The syringes were placed on a programmable pump to control the flow rate

during the electrospinning. The flow rate for all the solutions was fixed at 0.2 or 0.3 mL hr^{-1}. The collector was covered in aluminium foil and rotated at 2500 rpm. The voltages applied to the spinneret and the collector were fixed at 10 kV and -2 kV, respectively. The electrospinning process was conducted at 18°C and 80% relative humidity.

Sample name	PCL concen-trations (w/v)	Solvents (mL)		TiN NPs	Morphology	Voltage (kV)	Flow rate (mL hr^{-1})
		DCM	Acetone				
T8_0	8%	3	0 (2 mL ethanol)	-	Fibers/Beads	10	0.3
T8_2	8%	3	2	-	Fibers/Beads	10	0.3
T10_2	10%	3	2	-	Fibers/Beads	10	0.2
T12_2	12%	3	2	-	Fibers/Beads	10	0.2
T15_2	15%	3	2	-	Fibers/Beads	10	0.2
T20_2	20%	3	2	-	Fibers	10	0.2
T25_2	25%	3	2	-	Fibers	10	0.2
T20_1N1	20%	3	1	1 mL (0.15 mg L^{-1})	Fibers	10	0.2
T20_0N2	20%	3	0	2 mL (0.15 mg L^{-1})	Fibers	10	0.2
T20_0N6	20%	3	0	2 mL (0.45 mg L^{-1})	Fibers	10	0.2

Table 5.1: Summary of used solutions and electrospinning parameter for successful fabrication of functionalized PCL TiN nanofibers.

5.3.5 Morphological and physicochemical analysis

To characterize the size and surface morphology of electrospun nanofibers, a scanning electron microscope (JSM-IT 100 InTouchScope™, Germany) was used at the accelerating voltage of 20 kV. The observation was done after scratching the fibers from the aluminium foil and fixing them on the stub using a carbon tape, which was attached to the stage. A DSM 982 Gemini Zeiss, Germany system at the accelerating voltage of 20 kV was used to provide higher magnification micrographs after the functionalization process. ImageJ® and OriginLab software were used for the analysis and graphical representation of obtained nanofibers images.

A differential scanning calorimetry (DSC) (Perkin Elmer, USA) was used to characterize thermal properties of formed nanofibers. The samples were subjected to multiple heating cycles at the rate of 10°C min^{-1} from -70°C to 200°C. Briefly, 7 mg of each fiber type was sealed in an aluminium pan, while an empty pan of similar dimension was used as a reference. The heating cycle was carried out in nitrogen atmosphere. The degradation profile of functional nanofibers was studied using Thermogravimetric analysis (TGA) (Perkin Elmer, USA). For each sample, 7.5 mg of scratched nanofibers from aluminium foil

were placed in a ceramic cuvette at nitrogen flow rate of 20 mL min^{-1}. The samples were heated at 10°C min^{-1} from 30°C to 700°C.

Infrared spectroscopy was applied for nanofibers and polymers in their solid state to distinguish specific vibrational frequency of pristine nanofibers and its changes due to functionalization. FTIR spectra were recorded using a PerkinElmer Spectrum 2000 spectrometer.

5.3.6 *In vitro* testing

Basic cytotoxicity tests that are commonly used in in vitro studies, including metabolic activity, cell proliferation, cell adhesion and live/dead staining assays were performed. Mouse 3T3 fibroblasts, clone A31, which are used as a standard cell line were used for cytotoxicity testing.

Nanofibers were cut to circles with the diameter of 6 mm and sterilized in 70% ethanol for 30 min, washed twice with phosphate buffered saline (PBS) and seeded with mouse 3T3 fibroblasts at a density 25.8 x 10^3 cells cm^{-2} and cultured in Dulbecco´s Modified Eagle´s Medium (high glucose, Sigma Aldrich, USA), supplemented with 10% fetal bovine serum (Cat. No. 10270, Gibco, Brazil) and 100 I. U. mL^{-1} penicillin and 100 ug mL^{-1} streptomycin (Gibco, USA). Four samples were seeded for each item for MTS/DNA testing, three samples for live/dead test and three samples for DiOC6(3)/propidium iodide staining.

Metabolic activity was evaluated using CellTiter 96® AQueous One Solution Cell Proliferation Assay (MTS, Promega Corporation, USA) after 1, 3, 7, 10 and 15 days. Scaffolds were put into new wells with 100 µL medium and 20 µL MTS solution and incubated in CO_2 incubator for 2 hours. Then, absorbance of 100 µL solution was measured using a spectrophotometer Infinite M200 Pro (Tecan, USA). Scaffolds without cells were used as negative controls.

DNA amount was measured using a Quant-iT tm dsDNA assay (High sensitivity KIT Q33120, Invitrogen, USA). Fluorescence was measured using a spectrophotometer (Infinite M200 Pro, Tecan, USA) and dsDNA amount was counted from calibration curve of standards.

1µg mL^{-1} DiOC6(3) staining (Cat. No. D273, Invitrogen™), was used for cells visualization on day 1. After 45 min incubation with DiOC6(3), the cells were incubated with 5 µg mL^{-1} propidium iodide for 8 min, washed with PBS and visualized using a confocal Zeiss LSM 880 Airyscan microscope at λ_{exc} = 488 nm and λ_{em} = 505-515 nm for DiOC6(3) and λ_{exc} = 561 nm and λ_{em} > 576 nm for propidium iodide.

Live/dead staining was performed using 1 µg mL^{-1} 2′,7′-Bis(2-carboxyethyl)-5(6)-carboxyfluorescein acetoxymethyl ester (BCECF-AM Cat. No. B8806, Sigma-Aldrich), which was dissolved in serum-free medium and incubated with the scaffolds for 45 min. The scaffolds were then incubated with 5 µg mL^{1} propidium iodide (in PBS) for 8 min. Cells were visualized using a confocal microscope Olympus FV10i at λ_{exc} = 488 nm and λ_{em} = 505-515 nm for BCECF-AM (living cells) and λ_{exc} = 561 nm and λ_{em} > 576 nm for propidium iodide (dead cells).

5.3.7 Statistical analysis

Statistical analysis was performed using SigmaStat 3.5 software (Systat Software, Inc., USA). One Way ANOVA of Variance and Student-Newman-Keuls Method were used for data analysis. The level of significance was set at 0.05.

5.4 Results and Discussion

Several nanofiber formulations based on PCL solutions were prepared by electrospinning and then examined using SEM to optimize parameters of nanofibers before their functionalisation with TiN NPs. Then, the nanofibers were fabricated using various concentrations of TiN NPs. Table 5.1 summarizes parameters of all used formulations, while Figure 5.1 presents SEM images of the nanofibers prepared under increasing concentrations of PCL. One can see that at low concentrations of 8% (w/v) the polymer matrix presented a combination of fibers disrupted by beads, while the increase of PCL concentration led to the minimization of number of beads. On the other hand, at highest concentration of 25% (w/v) the fibers merged and formed structures of a non-uniform thickness. In addition, the electrospinning process at high concentrations was not stable due to high concentration of polymer blocking the flow of polymer through spinneret. Therefore, after careful analysis of morphologies of obtained structures, 20% (w/v) concentration was selected as the optimal one. This concentration was later used in co-electrospinning of PCL and TiN NPs.

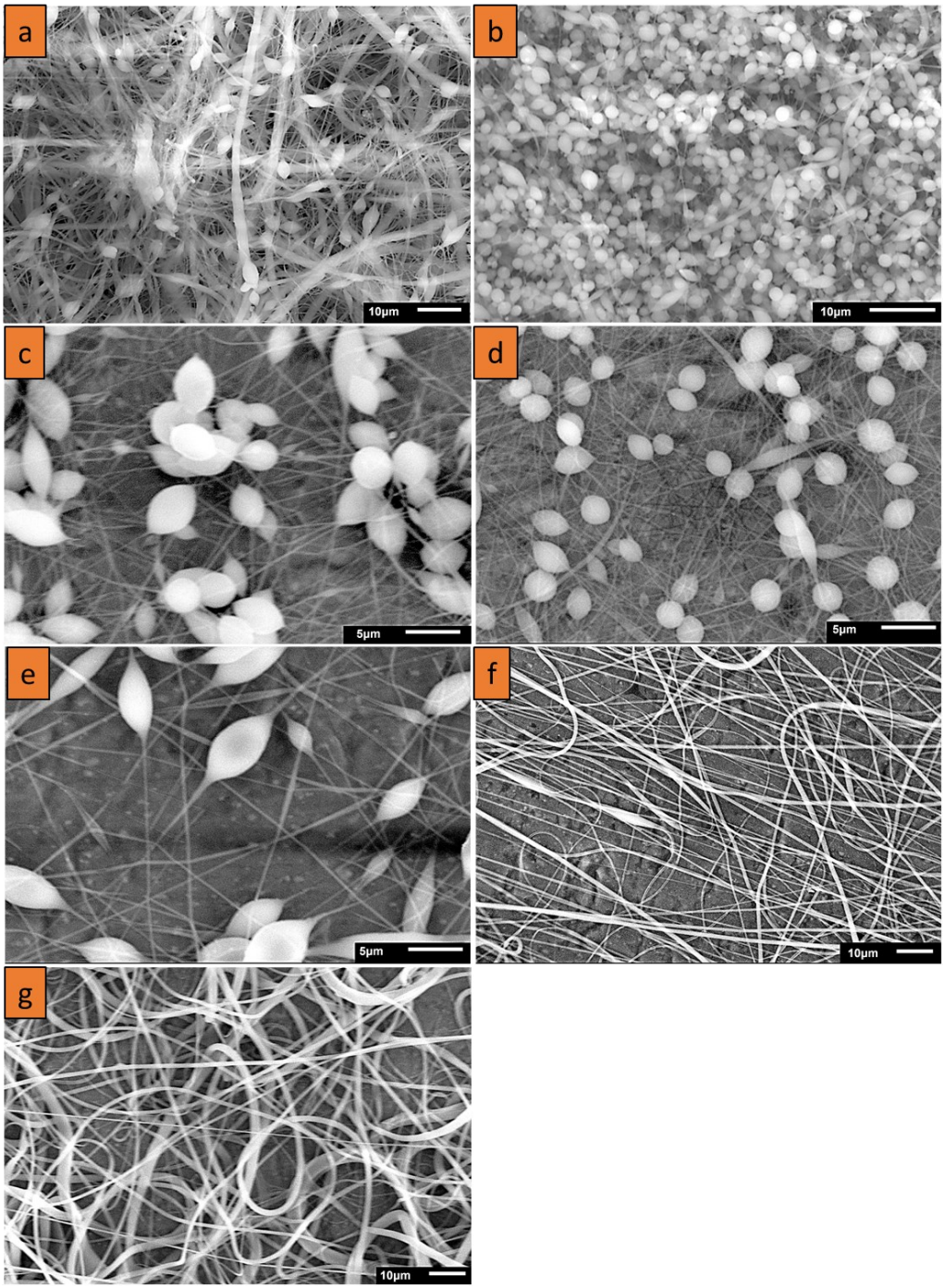

Figure 5.1: SEM micrographs of nanofibers obtained at different concentrations of PCL in nanofibers: (a) 8%, sample T8_0 solvent ethanol instead of acetone; (b) 8%, sample T8_2; (c) 10%, sample T10_2; (d) 12%, sample T12_2; (e) 15%, sample T15_2; (f) 20%, sample T20_2; (g) 25%, sample T25_2.

Based on optimized parameters of PCL solutions, we then performed electrospinning of PCL together with TiN NPs at different concentrations. Typical SEM images of hybrid nanofibers prepared under different nanoparticle concentrations are shown in Figure 5.2. One can see that the nanofibers were decorated by the nanoparticles, while their mean diameter was larger as compared to non-functionalized nanofibers. ImageJ® software [184] was used to measure the diameter of nanofibers. These tests showed that there was

an increase of the mean diameter from 400 nm ± 210 nm to 1.1 µm ± 192 nm under the co-electrospinning of PCL together with the NPs, while the diameters of formed nanofibers did not depend on concentration of TiN NPs (Figure 5.3 and Table 5.2). However, the standard deviation for diameters of functionalized nanofibers was lower compared to the reference sample, suggesting that the nanofibers were more uniform when TiN NPs were co-electrospun with PCL, as shown in Table 5.2. It should be noted that the increase of the nanofiber diameter under the addition of NPs could be compensated by increasing the voltage applied to the spinneret, as the increase of potential up to the threshold voltage results in reduced diameter of obtained nanofibers [138].

Sample name	PCL Concentrations (w/v)	TiN NPs	Mean diameter	Standard deviation
T20_2	20%	0	400 nm	230 nm
T20_1N1	20%	1 mL (0.15 mg L^{-1})	1.03 µm	0.19 µm
T20_0N2	20%	2 mL (0.15 mg L^{-1})	1.05 µm	0.06 µm
T20_0N6	20%	2 mL (0.45 mg L^{-1})	1.03 µm	0.15 µm

Table 5.2: Summary of diameter statistics for pristine and functionalized nanofibers (Figure 5.3).

The presence of TiN NPs on the surface PCL nanofibers can be clearly identified on SEM images, as shown in Figure 5.2. At high 150k resolution, single strands of nanofibers showing bunches of nanoparticles attached to the nanofiber surface could be observed (Figure 5.2a, b, c).

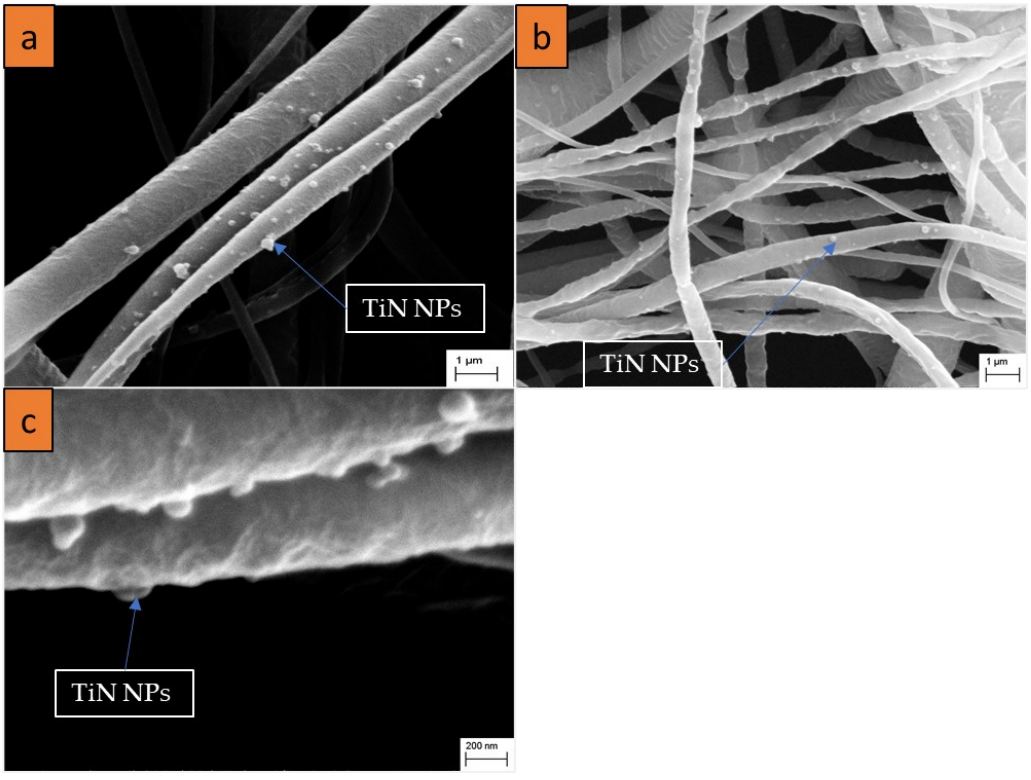

Figure 5.2: SEM micrographs of functionalized nanofibers obtained under different concentrations of TiN solubilized in solutions: (a) 1 mL (0.15 mg L-1) TiN NPs, 20% PCL

(T20_1N1); (b) 2 mL (0.15 mg L-1) TiN NPs, 20% PCL (T20_0N2); (c) 2 mL (0.45 mg L-1) TiN NPs, 20% PCL (T20_0N6).

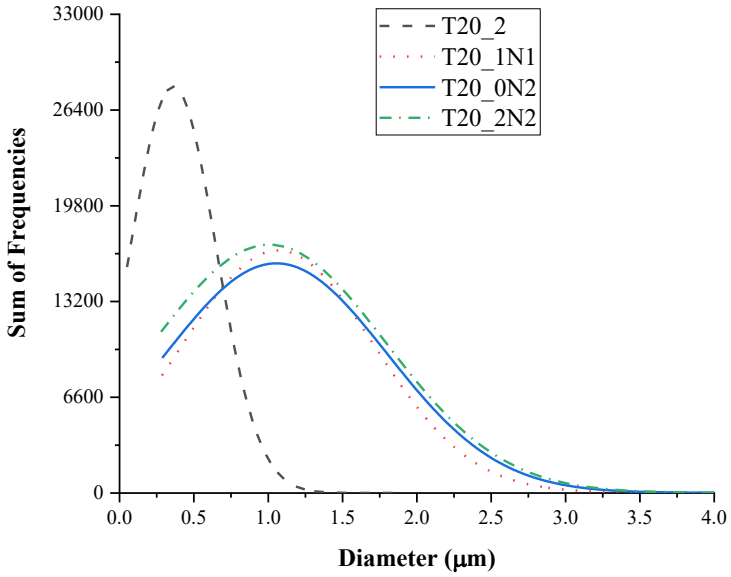

Figure 5.3: Normal diameter distribution of non-functionalized and functionalized nanofibers with various concentrations of laser ablated TiN NPs.

5.4.1 Thermal analysis

The thermal analysis was done using TGA. Our tests did not reveal any major difference in maximal degradation temperatures and degradation initiation temperatures, when the pristine nanofibers and the nanofibers functionalized with TiN NPs were used. All samples followed an identical trend with a single step degradation and similar degrading temperatures. The degradation initiation temperature was calculated with a minimum 5% mass loss for the samples (Figure 5.4). Pristine nanofibers displayed a classical PCL degrading behaviour with mass loss initiation at 329°C, while the functionalized nanofibers had lower initiation temperatures (328, 214 and 271°C for T20_1N1, T20_0N2 and T20_0N6, respectively). The degradation initiation temperature for pristine nanofibers was almost identical to the one observed for functionalised nanofibers with lowest concentration of TiN NPs (T20_1N1). However, when the temperature was further increased, both curves disassociated, while the functionalized nanofibers started to degrade faster. This trend was especially clear in the end of temperature cycle (441 and 439°C for pristine and functionalised nanofibers (T20_1N1), respectively) in which only 5% of initial mass was present. For comparison, the end temperature for samples T20_0N2 and T20_0N6 was observed at 429 and 441°C, respectively.

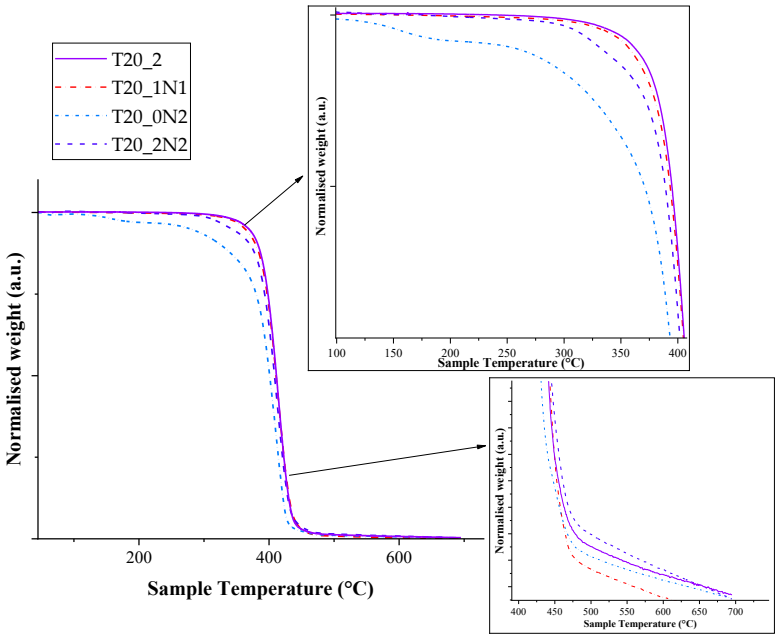

Figure 5.4: TGA graph depicting thermal degradation behaviour of TiN NPs-functionalized and pristine PCL nanofibers, inset zoomed view. (Table 5.1)

Sample T20_0N2 prepared under relatively low concentration of TiN NPs (2ml at 0.15mg mL-^{1}) started to degrade at lower temperature of about 100°C, which could be attributed to insufficient number of NPs within fibers matrix to dissipate heat. The increase of concentration of TiN NPs improved the stability of nanofibers at low temperatures due to the increase of heat capacity. Here, sample T20_0N6 with highest concentration of TiN NPs (2 mL at 0.45 mg L^{-1}) demonstrated similar degradation behaviour to pristine nanofibers. It should be also noted that most of the organic part degraded at the end of the program cycle. Indeed, about 0.1% of the initial mass was available in the cycle end for pristine nanofibers, while the relevant values for functionalized nanofibers were in the range of 0.2-0.35%.

As one can see from derivative thermogram (DTG) curve of hybridized nanofibers (Figure 5.5), the presence of NPs at lower concentrations in the nanofibers (T20_1N1) did not affect the temperature at the which the maximum mass loss event takes place, but the increase of NPs amount led to the decrease of this temperature by several degrees. The latter fact can be explained by the increase of heat transfer over the nanofibers due to the presence of inorganic TiN NPs in the matrix. As shown in the figure 5.5, the maximal mass loss event occurred at 412°C for pristine and nanofiber sample T20_1N1, while for T20_0N2 and T20_0N6 it took place at 406 and 409°C, respectively

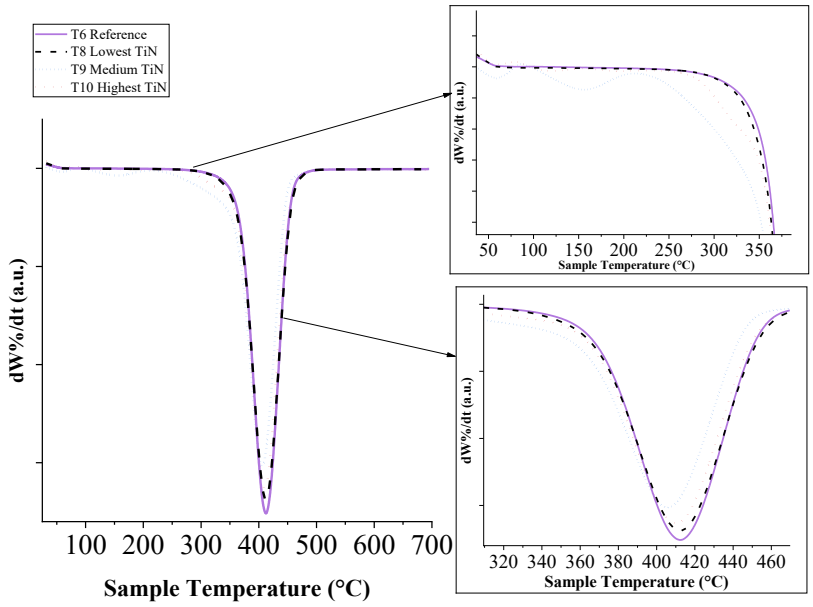

Figure 5.5: Derivative thermogram depicting influence of TiN NPs-based functionalisation on degradation rate of PCL nanofibers, inset zoomed scale x-y.

Differential scanning calorimetry (DSC) tests were then undertaken to further examine changes in thermal behaviour of the functionalised nanofibers. The samples were analysed through two heating cycles. There were no comprehensible differences between the 2 heating cycles used for DSC analysis. First heating cycle has been shown in Figure 5.6. Typical DSC curves for all examined samples are shown in Figure 5.6. Here, one can see that the peaks were endothermic without mass loss for pristine and functionalised nanofibers samples indicating melting phase of PCL. We observed slight differences between the peaks for pristine and functionalised nanofibers. Here, phase change (melting temperature, T_m) for pristine nanofibers and sample T20_1N1 was observed at 57.5 and 59°C, respectively. The area under the peak showing the enthalpy change (ΔH) was measured at 9.5 $mWmg^{-1}$ for pristine nanofibers, while the nanofibers functionalised with lowest concentration of TiN NPs (T20_1N1) demonstrated a very slight increase in enthalpy up to 11.4 $mWmg^{-1}$ (Figure 5.6). The nanofibers functionalized with TiN NPs at higher concentrations (T20_0N2 and T20_0N6) demonstrated similar behaviour, while the T_m decreased slightly from 57.8°C to 57°C under highest concentration of TiN NPs. The respective change of enthalpy ΔH was 8.9 $mWmg^{-1}$ and 8.3 $mWmg^{-1}$ for samplesT20_0N2 and T20_0N6, respectively.

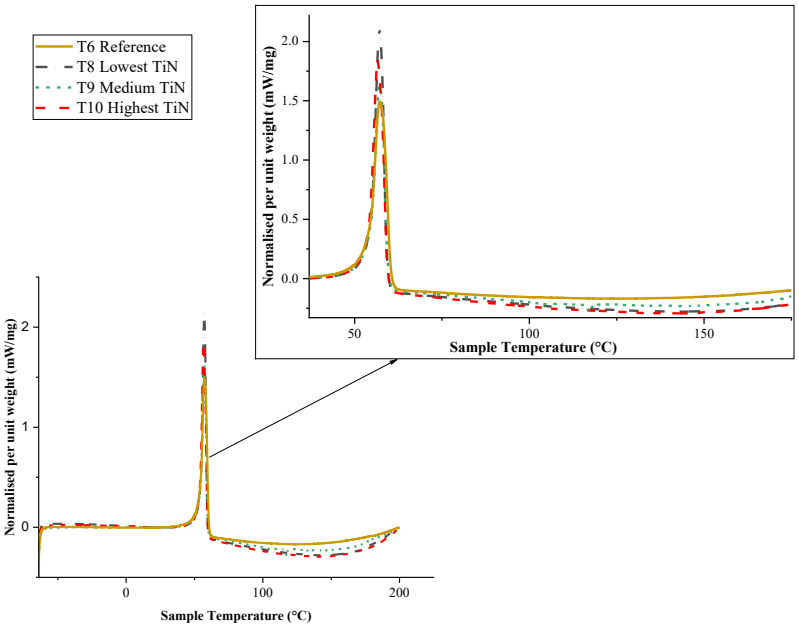

Figure 5.6: Differential scanning calorimetry graph depicting the different phase changes with in functionalized and non-functionalized PCL nanofibers, inset zoomed scale x-y. (Table 5.1).

Such a trend was consistent with results of TGA/DTG analysis. It should be noted that there was a slight dip in curves observed for all the samples as the heating program goes above 120°C, which could be attributed a change in samples' weight due to volatilization. No other phase change behaviour was observed until the end of the program at 200°C.

5.4.2 FTIR spectroscopy

The functionalized and non-functionalized nanofibers were then studied by FTIR spectroscopy to analyse changes in infrared absorption peaks. Results of FTIR examination are demonstrated in Figure 5.7. As shown in the graph, the peak characterizing the presence of a nitride group could be observed at 3324 cm^{-1}, which is consistent with the literature [210,211]. One can also find that absorption spectra of the functionalized nanofibers are similar to that of the non-functionalized nanofibers. A signature peak for C=C stretching mode can be resolved at around 1650 cm^{-1}, while a weak peak at 1600 cm^{-1} related to acetone is resolvable in the case of the pure nanoparticle solution. C-O stretched bonds from 1200 to 1160 cm^{-1} are also resolvable for all samples containing PCL [212]. It is also visible that the addition of TiN NPs to the polymer matrix did not lead to the interference with absorbance peaks of PCL

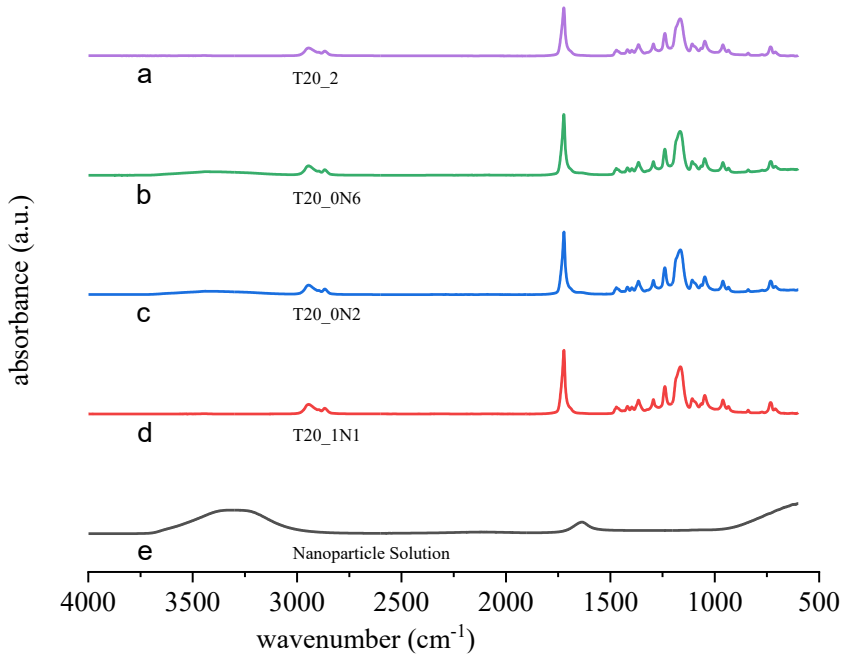

Figure 5.7: FTIR graphs of nanofiber samples prepared at different concentrations of TiN NPs. a) reference fibers T20_2, b) fibers prepared under 2 mL of 0.45 mg L^{-1} of TiN NPs, sample T20_0N6; c) fibers prepared under 2 mL of 0.15 mg L^{-1} of TiN, sample T20_0N2; d) fibers prepared under 1 mL of 0.15 mg L^{-1} of TiN NPs, T20_1N1; e) nanoparticle solution (Table 5.1).

5.4.3 *In vitro* testing

In MTS assays, absorbance increased every experimental day from day 1 till day 15 for all scaffolds. As shown in Figure 5.8a, there were no significant changes in metabolic activity of mouse 3T3 fibroblasts immobilized on the scaffolds from day 1 till day 10. On day 15, higher absorbance was observed for the sample prepared at higher concentration of TiN NPs (T10). Moreover, higher absorbance compared to that of the other samples was observed for tissue culture polystyrene (TCP), which is often used to improve cell culture viability.

As shown in Figure 5.8b, no significant differences were observed in dsDNA assay during the whole experiment. The amount of dsDNA increased significantly after day 10 for the all the samples. On day 15, maximum amount of the dsDNA was observed for both pristine and functionalised scaffolds. There is slight difference between the pristine scaffold and the scaffold functionalised with higher concentration of TiN NPs. However, the significance is not relevant to conclude the role of the TiN NPs, leading to an increase in the amount of dsDNA. On day 1, 3T3 fibroblasts were homogeneously adhered and spread over all scaffolds, while during next days the cell number significantly increased (Figure 5.9). Cell viability (live/dead assay) was evaluated from live/dead staining and microscopy analysis. Here, one could observe areas with living cells and other areas with dead cells on samples of nanofibers with TiN NPs and TCP. No statistical differences were observed for different scaffolds (Figure 5.8c and Figure 5.9).

Inorganic nanomaterials have already been explored in various clinical applications. As an example, silver NPs were found to improve wound healing in both acute burn wounds and in chronic wounds [213], while zinc peroxide NPs showed both antimicrobial and anti-inflammatory effects in burn wounds [214]. The toxicity of NPs is typically influenced by chemical composition, physical characteristics, such as their size, crystalline structure, and photo-activation. In addition, the toxicity is often enhanced by the production of the reactive oxygen species (ROS) and leads to oxidative stress, inflammation, genotoxicity or carcinogenesis [215].

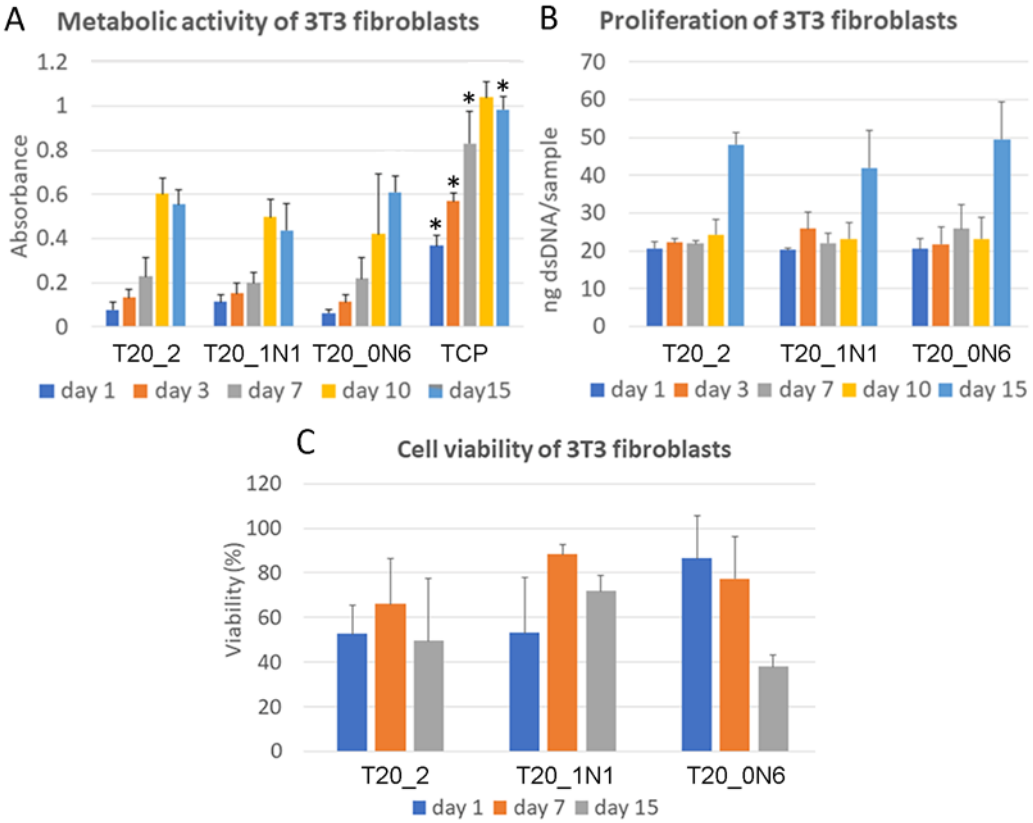

Figure 5.8: Metabolic activity measured using the MTS assay (A), proliferation using dsDNA assay (B) and viability using live/dead assay (C) for 3T3 fibroblasts immobilized of nanofibers with different concentrations of TiN NPs. Tissue culture plastic (TCP) was chosen as a reference to provide the highest absorbance in MTS test. * means statistical difference related to all other samples. No significant differences were observed in both cell proliferation and cell viability tests. All assays show results as a mean and standard deviation.

TiO2 nanofibers and TiO2 NPs in a dose range 2.5–80 μg cm-2 were tested for the viability of Raw 264.7 (macrophages) and adenocarcinoma epithelial cells A549 [216]. At the highest dose, the macrophages showed decreased viability by 22%, but no affect was seen using A549 cells. Interestingly, NPs did not show changes in cell viability of both cell types. Both TiO2 nanofibers and NPs induced low production of ROS species. TiO2 nanofibers changed the normal round morphology of macrophages to spindle shaped [216]. On the other hand, anatase TiO_2 nanospheres of longer fibre structures over 15 μm initiated

inflammatory response by alveolar macrophages and the production of inflammatory cytokines similarly to silica or asbestos [217].

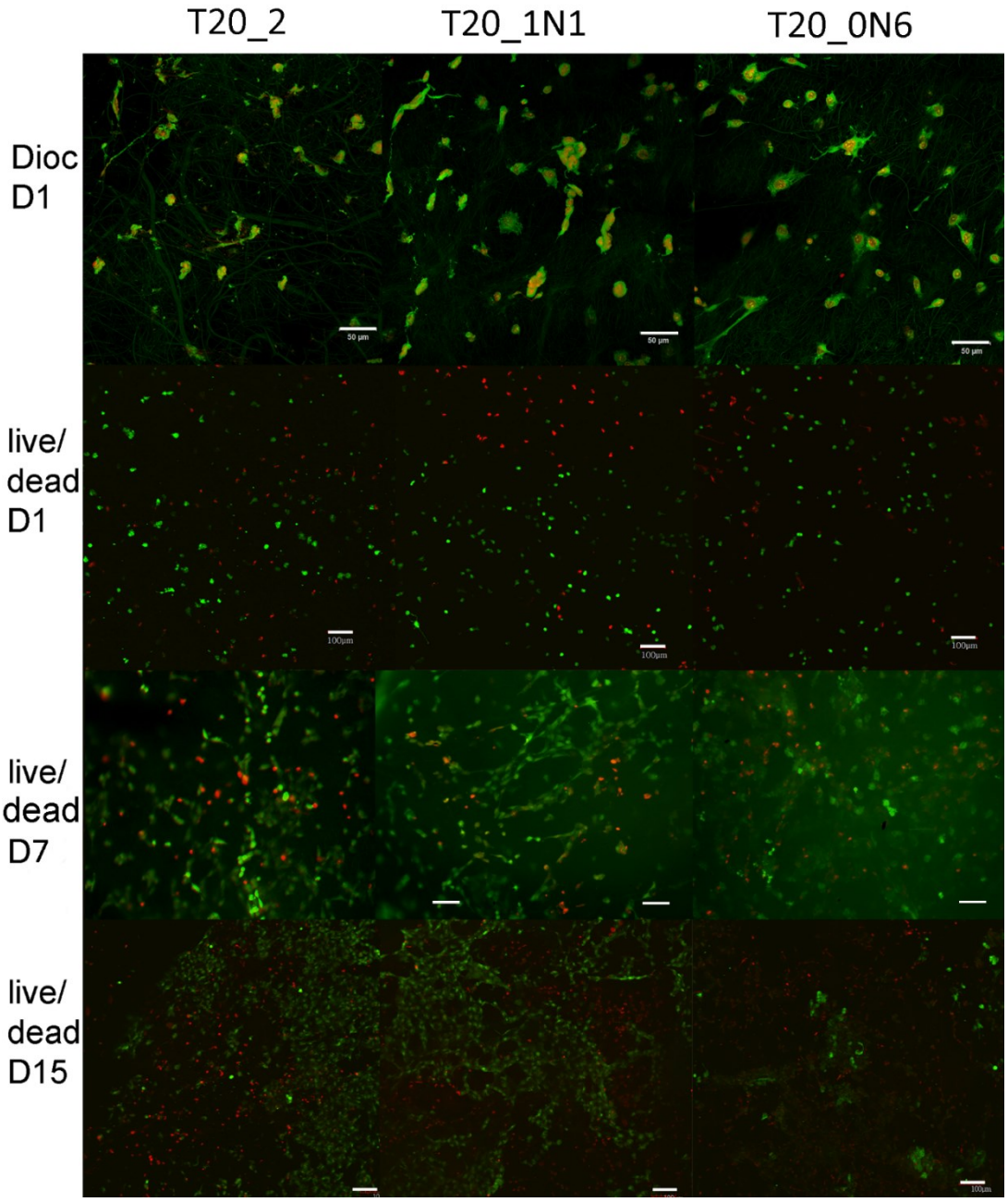

Figure 5.9: Adhesion and viability of 3T3 cells. On day 1, cell adhesion was labelled using DiOC6(3) staining (green) for plasma membranes visualization and propidium iodide staining (red) for cell nuclei (Dioc D1). As shown in images, 3T3 cell well adhered and spread on all scaffolds. On day 1 and 15, live/dead staining was done using BCECF-AM staining (green viable cells) and propidium iodide (red nuclei of dead cells). Cells were visualized using confocal microscope Zeiss LSM 880 Airyscan. Obj. 20x, bar = 50 µm for Dioc D1 staining and Obj. 10x, bar = 100 µm for live/dead staining.

Owing to high wear-resistance, high hardness, high scratch resistance, low friction coefficient and high wettability, TiN-based materials had a wide spectrum of applications

as coatings of articulating surfaces of implants. This material is approved by FDA and considered as physiologically inert and non-carcinogenic. A prolonged exposure of biological objects and tissues to TiN does not cause any toxic effects [218]. Titanium oxynitride coating ($TiNO_x$) thin layers prepared by atomic layer deposition on cellulose fibers demonstrated layer depth-depending adhesion of human adipose-derived adult stem cells with the highest adhesion for samples with 20 Å coating [219].

Polished discs of pure titanium ASTM F67, titanium alloy (Ti-6Al-4V) ASTM F136 (10), stainless steel ASTM F138, and cobalt alloy (Co-Cr-Mo) ASTM F75 were explored in corrosion tests in condition of bare and TiN layer-coated surface. 2.2 μm- height TiN coating of stainless steel increased its corrosion resistance, but no positive effect was seen on pure Ti or Ti-6Al-4V. Interestingly, TiN coatings of these materials exhibited no cytotoxicity, intradermal irritation, or acute systemic toxicity response (measured by intraperitoneal administration of 50 mL kg^{-1} solution) [220].

In this investigation, TiN NPs were incorporated in PCL, a biocompatible polymer, which excludes a direct exposition of cells to potentially toxic TiN NPs. Biological tests showed good biocompatibility of all tested materials with increased metabolic activity on day 10 and highest increase of dsDNA content on day 15. Here, T20_0N6 samples with highest concentration of TiN NPs (4 mL) demonstrated the best metabolic activity. However, in both TiN NPs samples and PCL some areas with dead cells were observed on day 1 and 15. As the presented in vitro tests did not show fully biocompatible material, further long-term in vitro tests over at least 5 weeks must be performed. It is important that the fabricated hybrid organic-inorganic nanofiber structures can combine good biocompatibility of PCL and specific physical properties of inorganic TiN NPs. In particular, plasmonic and catalytic properties of TiN NPs can be used e.g. for the phototherapy of cancer and its combination with chemotherapy and radiotherapy, which are especially effective during G2 phase of cell cycle and can be enhanced by optimizations of pH, microcirculation, metabolism, and the presence of sensitizers [221].

5.5 Conclusions

This chapter concludes with a primary demonstration of simple methodology to fabricate functional hybrid nanofibers based on co-electrospinning of polycaprolactone solutions and bare laser-synthesized TiN NPs. A unique combination was formulated and standardised to achieve PCL TiN NPs nanofibers through electrospinning. PCL at concentration of 20% (w/v) dissolved in dichloromethane and acetone at 3:2 (v/v) ratio, was found to be optimal for functionalization with TiN NPs. Nanofibers were electrospun from solutions possessing several concentrations of TiN NPs.

Electrospun hybrid nanofibers demonstrated an uniform morphology. The presence of TiN NPs in the system was confirmed by high-resolution scanning electron microscopy, where NPs could be observed being attached to the polymer matrix or partially embedded. Thermal analysis by DSC and TGA revealed an improved thermal distribution character of functionalised nanofibers as compared to pristine PCL nanofibers. Further, biological assessment of hybrid nanofibers showed that NPs-decorated nanofibers

demonstrated good biocompatibility *in vitro* identical to pristine PCL nanofiber samples. Overall, observed results are indications of multifunctional hybrid PCL (TiN NPs) nanofibers as excellent platform for tissue engineering and cancer theranostics.

CONCLUSIONS

This thesis was aimed at the development of multifunctional nanofibers platform and their physicochemical characterizations for potential applications such as tissue engineering scaffolds, theranostics, controlled drug delivery, catalytic activity, filtration. Various systems were designed with several polymers acting as matrix, for immobilizing metallic nanoparticles and inorganic polymers as functional agents. Electrospinning is used for fabrication of non-woven hybrid nanofiber mats.

Organic matrix/matrices and inorganic functional agents used for electrospinning offered unique combination. While organic materials provided the structure and matrix for the nanofibers having very high surface area to volume ratio, inorganic functional agents provided improved functionality. Mainly, two types of functional agents were used in the research, metallic nanoparticles, and inorganic polymers. The nanoparticles were synthesised via wet-chemistry methods and pulsed laser ablation in liquids (PLAL). However, PLAL was preferred for the synthesis of nanoparticles due to the advantage of possessing a bare ligand-free surface with lower bio-toxic potential. Therefore, the focus was to immobilize this class of nanoparticles within nanofiber matrix along with inorganic polymers.

1. Here, the differences in properties were analysed after functionalizing the nanofibers with laser ablation synthesized and wet-chemistry synthesised nanoparticles. The nanofibers were fabricated using chitosan blended in poly(ethylene oxide) with AuNPs. It was found that chemically synthesised AuNPs prepared by Turkevich's method affected the thermal degradation of the nanofibers and the peak degradation temperature quite similar to nanofibers functionalised with laser ablated NPs. Further, the morphology analysis of nanofibers showed near identical diameter distributions. However, laser ablated nanoparticles provided an advantage to nanofibers while offering similar properties to chemistry synthesized particles, due to absence of surface ligands. Hence, functionalisation of nanofibers with such agents potentially offers much better bio-compatibility for use in biological system. Further analyses were proposed with some modifications for increasing the amount of AuNPs and chitosan.
2. From observations in previous chapter, necessary modifications and optimizations were done to fabricate nanofibers with significantly higher concentrations of chitosan and AuNPs in poly (ethylene oxide) (PEO) blended nanofibers. Chitosan is a highly bio-degradable and biocompatible polymer but has very low processability. However, it was successfully electrospun by PEO blending, and functionalised by bare laser-ablated AuNPs. Nanofibers

mimicking the microscopic structural network of extracellular matrix (ECM) were obtained. Statistical analysis showed that nanofibers possessed an average diameter of 190 ± 86 nm. Furthermore, functionalised nanofibers had better thermal stability as compared to pristine nanofibers. FTIR analysis did not reveal any difference in the absorption spectra of functionalised and pristine nanofibers. However, the nanofibers solubilised quite effectively in PBS saline. Therefore, post-processing of nanofibers was done to obtain chitosan AuNPs nanofibers by immersing fibers in neutralising solutions which also lead to removal of PEO. This step transformed the $-NH_3^+$ group into the $-NH_2$ insoluble form, stabilising the nanofibers in aqueous medium. The nanofibers were stable and possessed fibril structure even after keeping in saline solution for considerable amount of time. The nanofibers possessed significant properties for their potential use as tissue engineering scaffolds.

3. In this chapter, advanced nanofibers were fabricated and functionalised from unusual combinations of organic and inorganic (poly(ferrocenylphosphinoboranes)) polymers. Poly(ferrocenylphosphinoboranes) are a group of inorganic polymers denoted as **Fe A** and **Fe B**. The polymers had a slight difference in their monomer structure where **Fe A** monomer contains additional methane group attached to the phosphine. These polymers are polycationic and have high thermal stability. However, they possessed low molecular weight, thus it had to be co-spun in blend of higher molecular weight homopolymers such as PEO and PS. At least, 2% (w/v) inorganic polymers were blended with the homopolymers and electrospun resulting in uniform nanofibers with colour similar to that of inorganic polymers. Hybrid nanofibers possessed an average diameter between 475 to 625 nm. Further analyses such as NMR and FTIR, confirmed the presence of the inorganic polymer within the organic matrix. DSC and TGA showed that functionalized nanofibers were thermally stable. As a result, hybrid nanofiber structures were obtained, possessing high surface reactivity, and positively charged surface due to presence in polycationic domains which can provide attachment sites for macromolecules and nanocatalysis.
4. Finally, a distinctive formulation was electrospun from widely used and biocompatible polycaprolactone (PCL) and bare laser-ablated titanium nitride nanoparticles (TiN NPs). Initial fabrication of pristine nanofibers required extensive optimization of PCL concentration in electrospinning solution and electrospinning parameters. Thereafter, various concentrations of bare laser-ablated TiN NPs were suspended in PCL solutions and electrospun into nanofibers. SEM was used to study the morphology of fabricated pristine and functionalised nanofibers which showed that bead-free smooth nanofibers were obtained. TiN NPs functionalised nanofibers were uniform and possessed higher average diameter. DSC and TGA showed that functionalised nanofibers had a better thermal dissipation. Their average weight normal heat capacity and maximum thermal degradation temperature were lower, as compared to

pristine nanofibers. Further, biological characterizations were done for analysing bio-compatibility of the functionalised nanofibers. MTS assay showed highest metabolic activity of 3T3 fibroblasts on day 10, for all the samples, except nanofibers functionalised with highest concentration of TiN NPS. While on day 15, highest amount of dsDNA could be observed for all samples. Correspondingly, no statistical insignificant differences were observed in cell-viability. Some areas with dead cells were observed which requires further investigations. It was evident that hybrid multifunctional nanofibers were bio-compatible even when TiN NPs were present in the matrix which also provided plasmonic resonance and catalytic activity, useful for theranostics of cancer, in combination with chemo- and radiotherapy. Moreover, providing a platform for tissue-engineering, offering an extracellular-matrix like scaffold network.

This research provided multiple strategies for the fabrication of multifunctional hybrid nanofibers using electrospinning. Inclusion of functional agents such as laser-ablated nanoparticles offered a clean alternative with minimal bio-compatibility issues. Nanofibers have shown enormous potential owing to their unique properties. However, a major effort is required to establish nanofibers, by means of optimization and standardisation while offering reliability, reproducibility, and bio-compatibility. As the yield of nanofiber from electrospinning was relatively low and producing large amount of fibers required multiple hours of operation. However, multiple strategies have been implemented recently, utilising various spinnerets and collector mechanisms for improving the yield. Consequently, making the nanofibers a commercially viable and widely-accepted solution in future for existing and emerging technologies.

List of abbreviations

AC	Alternating Current
AFM	Atomic Force Microscopy
ASTM	American Society for Testing and Materials
ATR	Attenuated Total Reflection
AuNPs	Gold Nanoparticles
Cit.	Citrate
DC	Direct Current
DCM	Dichloromethane
DioC6(3)	3,3'-Dihexyloxacarbocyanine Iodide
DNA	Deoxyribonucleic Acid
DLS	Dynamic Light Scattering
DSC	Differential Scanning Calorimetry
ds DNA	Double Stranded Deoxyribonucleic Acid
DTG	Derivative Thermogravimetry
ECM	Extracellular Matrix
EDX	Energy-Dispersive X-ray (spectroscopy)
Fe A	Poly(ferrocenylmethylphosphinoborane)
Fe B	Poly(ferrocenylphosphinoborane)
Fs	Femtosecond
FTIR	Fourier transform infrared spectroscopy
HAp	Hydroxyapatite nanoparticles
HR-TEM	High-Resolution Transmission Electron Microscopy
IR	InfraRed
K_2CO_3	Potassium Carbonate
MTS	Tetrazolium Salt

NaOH	Sodium Hydroxide
Nm	Nanometers
NMR	Nuclear Magnetic Resonance
NPs	Nanoparticles
Ns	Nanosecond
PBS	Phosphate-Buffered Saline
PCL	Polycaprolactone
PEG	Poly(ethylene glycol)
PEO	Poly(ethylene oxide)
PLAL	Pulsed Laser Ablation in Liquid
PS	Polystyrene
PTFE	Polytetrafluoroethylene
ROS	Reactive Oxygen Species
SERS	Surface Enhanced Raman Spectroscopy
SEM	Scanning Electron Microscope
SiNPs	Silicon Oxide Nanoparticles
TCP	Tissue Culture Polystyrene
TEM	Transmission Electron Microscopy
TFA	Trifluoroacetic acid
TGA	Thermogravimetric Analysis
T_g	Glass Transition
T_m	Melting Temperature
TM	Trademark
THF	Tetrahydrofuran
TiN NPs	Titanium Nitride Nanoparticles
TMS	Tetramethylsilane
UV	Ultraviolet
UV-Vis	Ultraviolet-visible

APPENDIX A

Supplementary Data

The NMR and IR spectra of the individual polymers before and after electrospinning were obtained and are presented here. The spectra gave insight about the interactions of these polymers with each other.

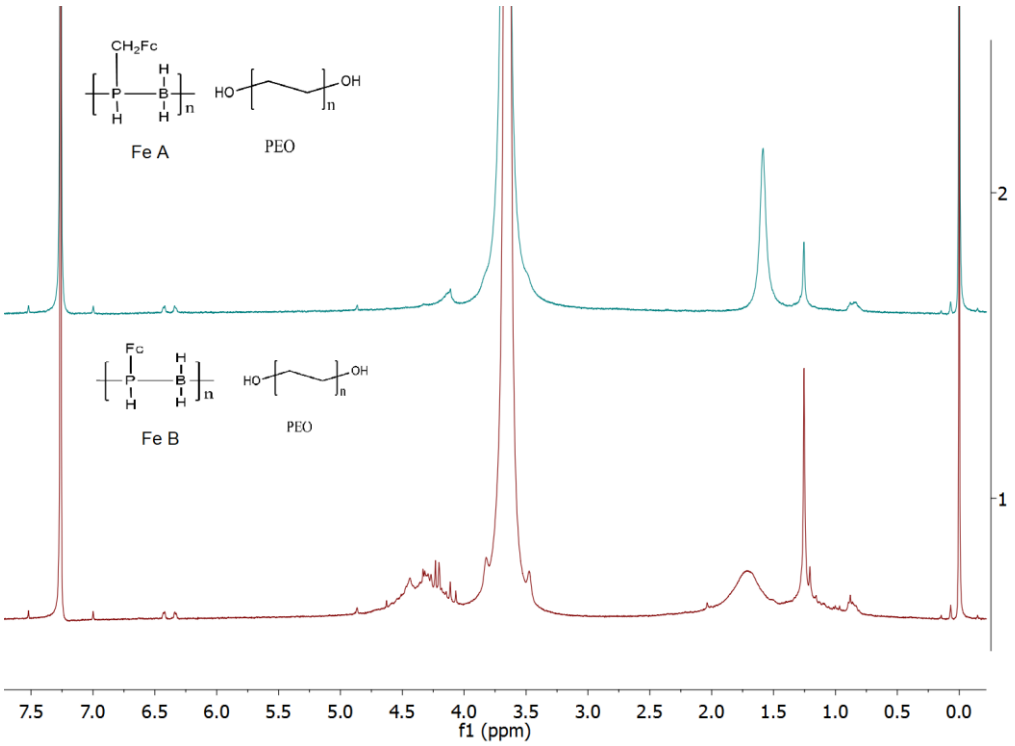

Figure A.1: ^{1}H NMR spectra of electrospun polymer **Fe A/PEO** and **Fe B/PEO**.

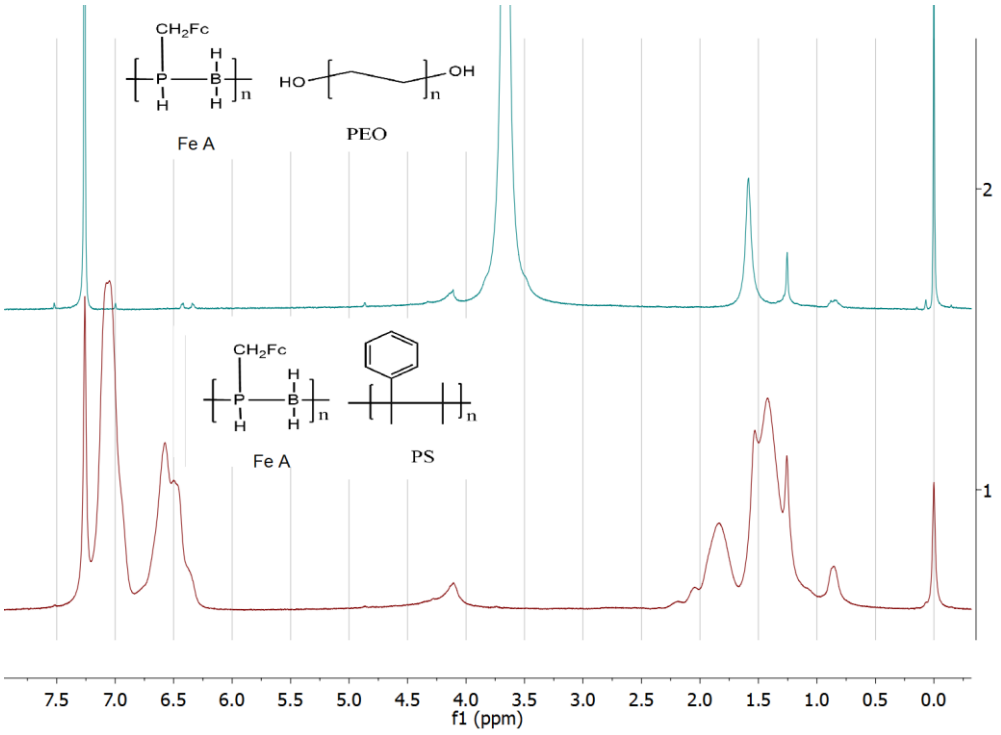

Figure A.2: ^{1}H NMR spectra of electrospun polymer **Fe A/PEO** and **Fe A/PS**.

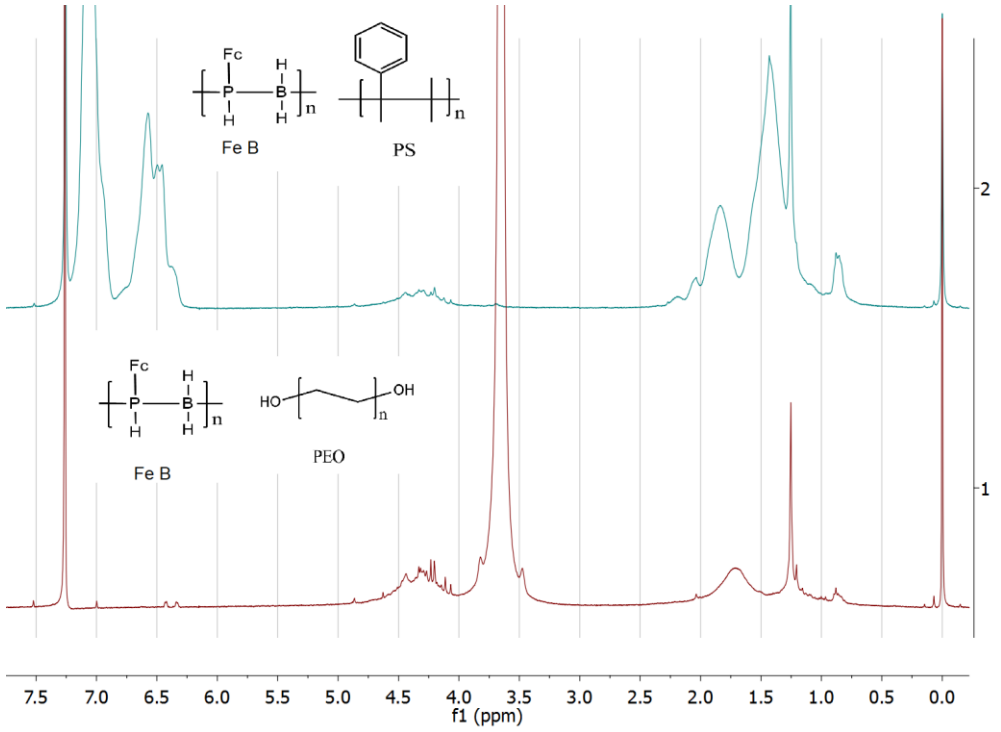

Figure A.3: ^{1}H NMR spectra of electrospun polymer **Fe B/PS** and **Fe B/PEO**.

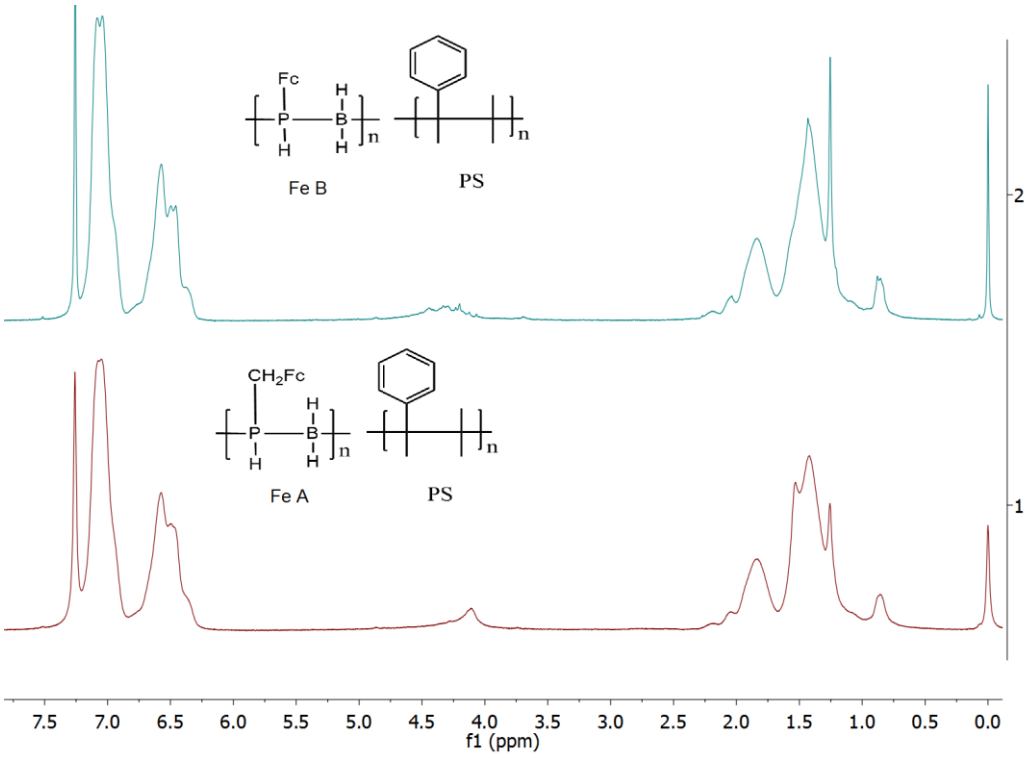

Figure A.4: ^{1}H NMR spectra of electrospun polymer **Fe A/PS** and **Fe B/PS**.

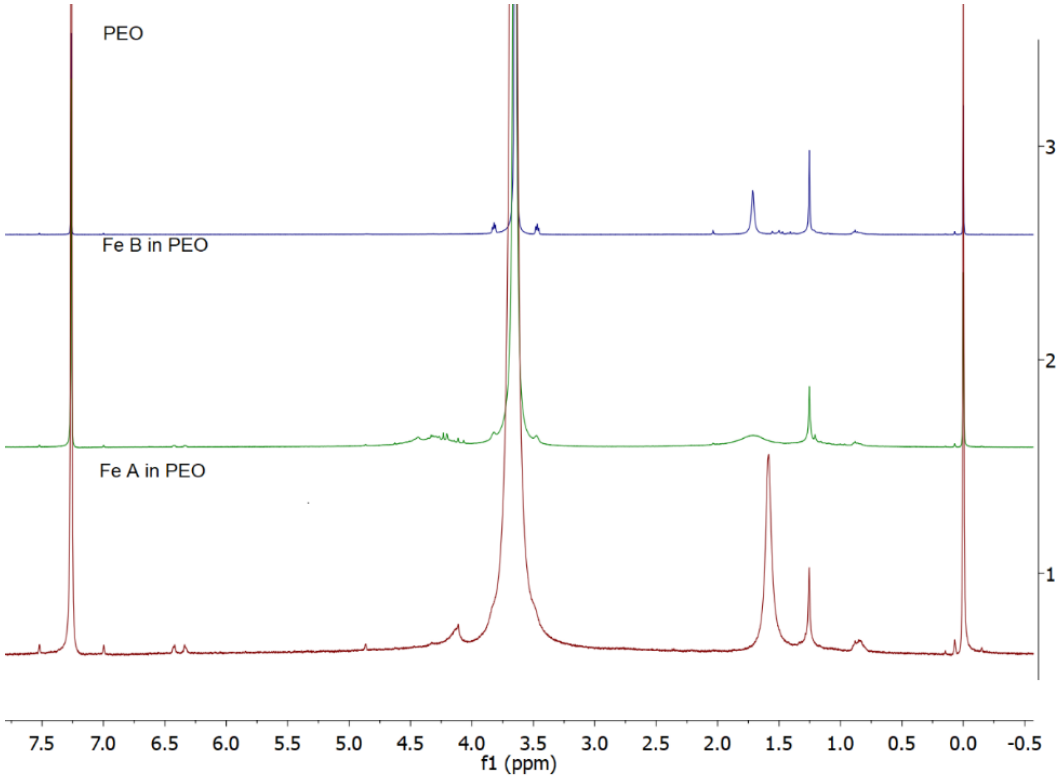

Figure A.5: ^{1}H NMR spectra of electrospun polymer **Fe A/PEO** and **Fe B/PEO**.

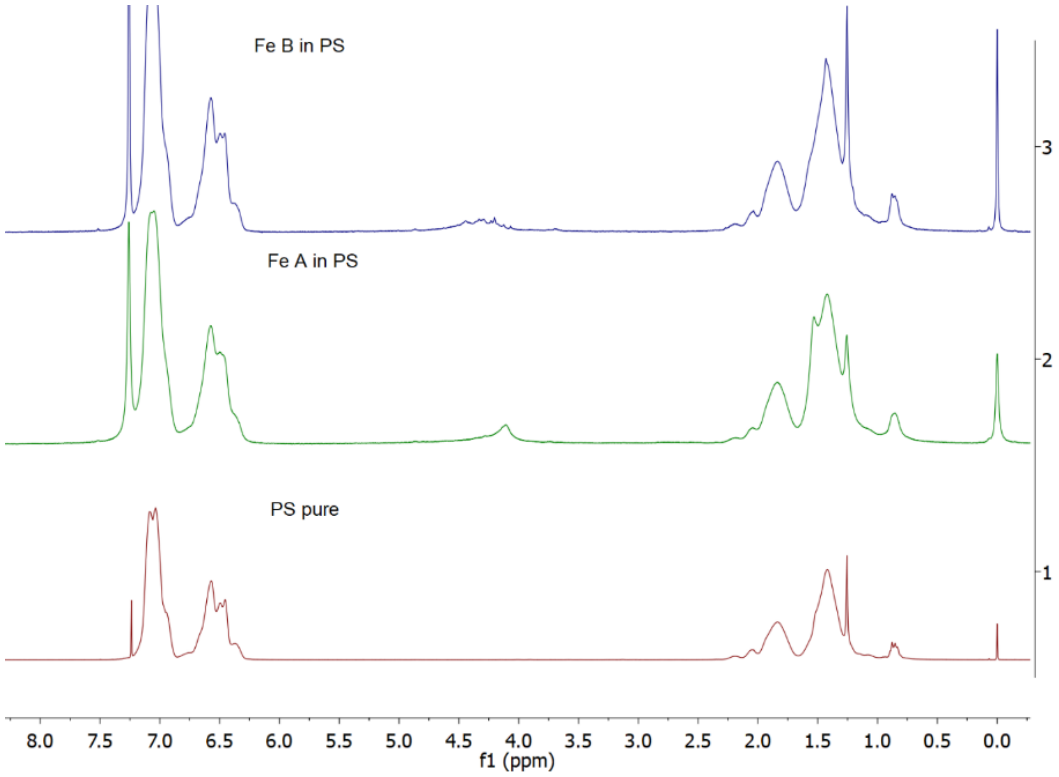

Figure A.6: ^{1}H NMR spectra of electrospun polymer **Fe A/PS**, **Fe B/PS** with pure PS.

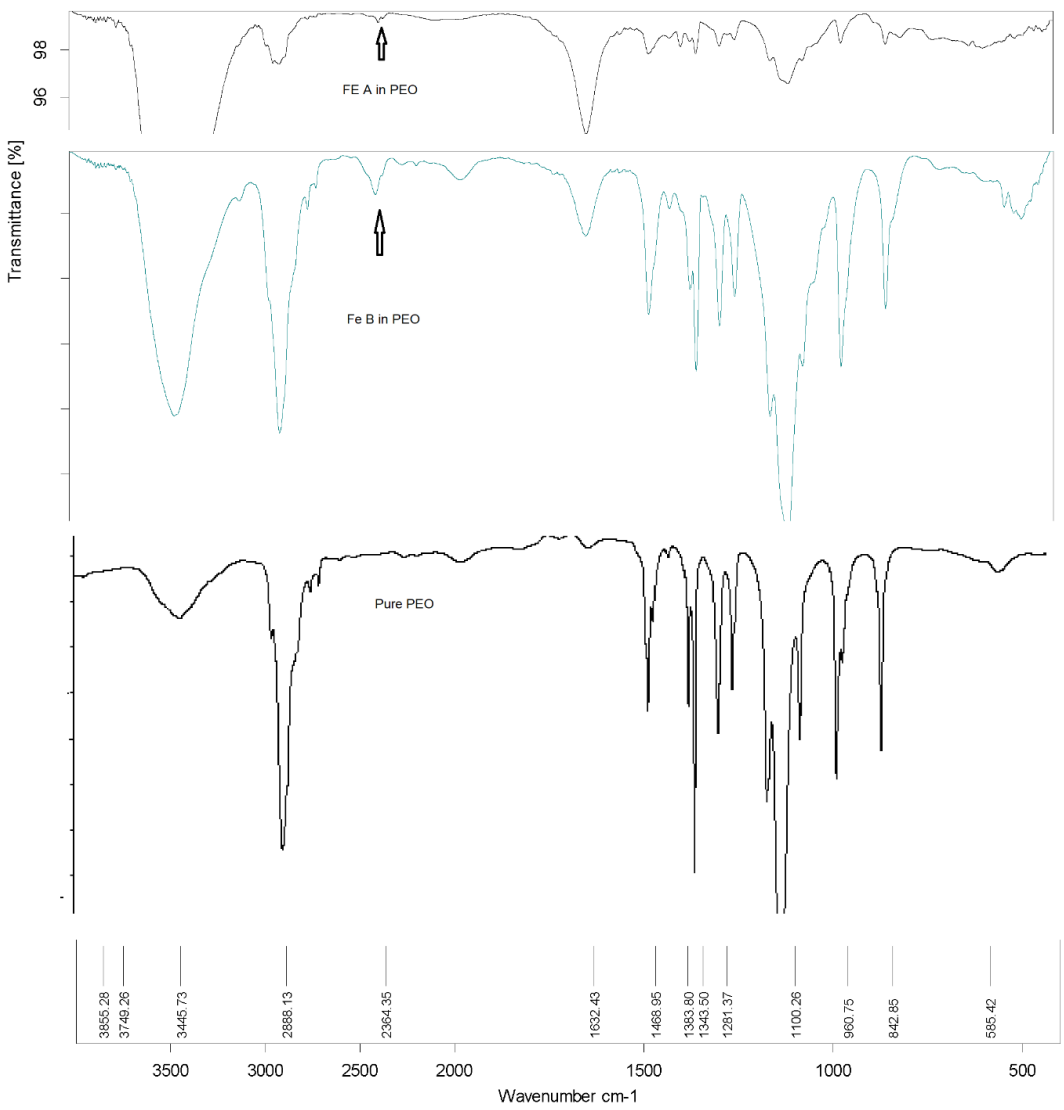

Figure A.7: IR spectra of electrospun **Fe A** and **Fe B** in PEO and compared with pure **PEO**.

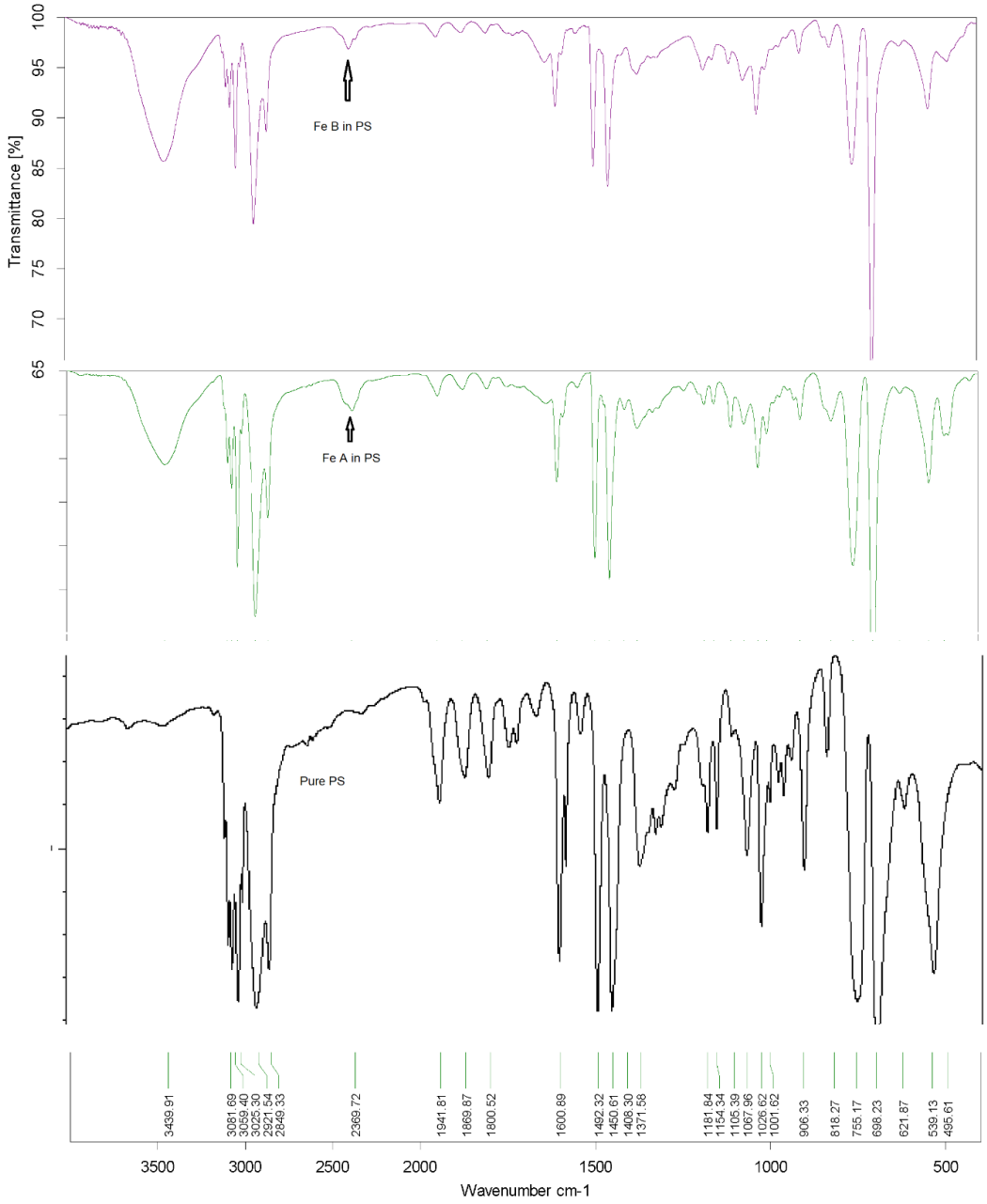

Figure A.8: IR spectra of electrospun **Fe A** and **Fe B** in **PS** and compared with pure **PS.**

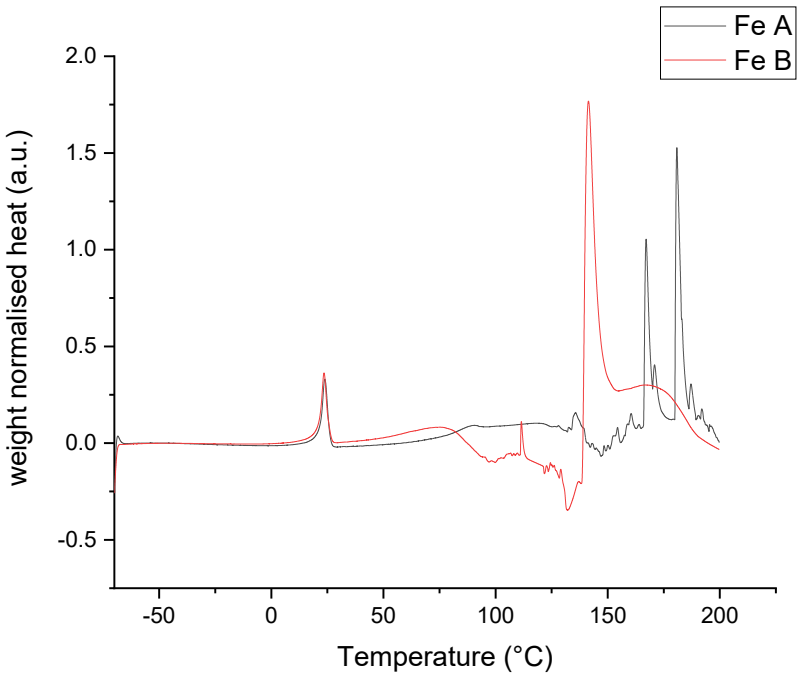

Figure A.9: DSC curve for Pristine Fe A and Fe B polymers.

Name of the sample	Temperature (°C)
Pristine **Fe A**	237
Pristine **Fe B**	130
Fe A/PEO	272
Fe B/PEO	283
Fe A/PS	292
Fe B/PS	285
PEO reference	275
PS reference	376

Table A.1: Degradation Initiation temperature of polymers based on minimum 5% loss of mass.

List of Publications

LoP-1. Nirwan, V.P.; Filova, E.; Al-Kattan, A.; Kabashin, A. V; Fahmi, A. Smart Electrospun Hybrid Nanofibers Functionalized with Ligand-Free Titanium Nitride (TiN) Nanoparticles for Tissue Engineering. Nanomaterials **2021**, 11, 519.

LoP-2. Nirwan, V.P.; Pandey, S.; Hey-Hawkins, E.; Fahmi, A. Hybrid 2D nanofibers based on poly(ethylene oxide)/polystyrene matrix and poly(ferrocenylphosphinoboranes) as functional agents. *J. Appl. Polym. Sci.* **2020**, *137*, 49091.

LoP-3. Shammas, M.; Zinicovscaia, I.; Humelnicu, D.; Cepoi, L.; Nirwan, V.; Demčák, Š.; Fahmi, A. Bioinspired electrospun hybrid nanofibers based on biomass templated within polymeric matrix for metal removal from wastewater. *Polym. Bull.* **2020**, *77*, 3207–3222.

LoP-4. Nirwan, V.P.; Al-Kattan, A.; Fahmi, A.; Kabashin, A. V. Fabrication of Stable Nanofiber Matrices for Tissue Engineering via Electrospinning of Bare Laser-Synthesized Au Nanoparticles in Solutions of High Molecular Weight Chitosan. *Nanomaterials* **2019**, *9*, 1058.

LoP-5. Al-Kattan, A.; Nirwan, V.; Popov, A.; Ryabchikov, Y.; Tselikov, G.; Sentis, M.; Fahmi, A.; Kabashin, A. Recent Advances in Laser-Ablative Synthesis of Bare Au and Si Nanoparticles and Assessment of Their Prospects for Tissue Engineering Applications. *Int. J. Mol. Sci.* **2018**, *19*, 1563.

LoP-6. Al-kattan, A.; Nirwan, V.P.; Munnier, E.; Chourpa, I.; Popov, A.A.; Munnier, E.; Tselikov, G.; Ryabchikov, Y.V.; et al. Bare laser-synthesized Si nanoparticles as functional elements for chitosan nanofiber-based tissue. Proc. SPIE. Synth. Photonics Nanoscale Mater. XV **2018**, 9, 10521.

LoP-7. Nirwan, V.P.; Al-Kattan, A.; Kabashin, A.; Fahmia, A. Electrospun PEO/Chitosan Nanofibers Templated with Gold Nanoparticles Prepared with Laser and Wet Synthesis. In Proceedings of the 2018 IEEE 8th International Conference Nanomaterials: Application & Properties (NAP); IEEE, **2018**; pp. 1–4.

Bibliography

1. Faustini, M.; Nicole, L.; Ruiz-Hitzky, E.; Sanchez, C. History of organic–inorganic hybrid materials: prehistory, art, science, and advanced applications. *Adv. Funct. Mater.* **2018**, *28*, 1704158.
2. Kokarneswaran, M.; Selvaraj, P.; Ashokan, T.; Perumal, S.; Sellappan, P.; Murugan, K.D.; Ramalingam, S.; Mohan, N.; Chandrasekaran, V. Discovery of carbon nanotubes in sixth century BC potteries from Keeladi, India. *Sci. Rep.* **2020**, *10*, 19786.
3. Livage, J.; Henry, M.; Sanchez, C. Sol-gel chemistry of transition metal oxides. *Prog. Solid State Chem.* **1988**, *18*, 259–341.
4. Fahmi, A.; Pietsch, T.; Mendoza, C.; Cheval, N. Functional hybrid materials. *Mater. Today* **2009**, *12*, 44–50.
5. Brinker, C.J.; Scherer, G.W. *Sol-gel science: the physics and chemistry of sol-gel processing*; Academic press, 2013; ISBN 0080571034.
6. Gao, C.; Che, S. Organically functionalized mesoporous silica by co-structure-directing route. *Adv. Funct. Mater.* **2010**, *20*, 2750–2768.
7. Heinz, H.; Pramanik, C.; Heinz, O.; Ding, Y.; Mishra, R.K.; Marchon, D.; Flatt, R.J.; Estrela-Lopis, I.; Llop, J.; Moya, S. Nanoparticle decoration with surfactants: molecular interactions, assembly, and applications. *Surf. Sci. Rep.* **2017**, *72*, 1–58.
8. Sajti, C.L.; Sattari, R.; Chichkov, B.N.; Barcikowski, S. Gram scale synthesis of pure ceramic nanoparticles by laser ablation in liquid. *J. Phys. Chem. C* **2010**, *114*, 2421–2427.
9. Leonés, A.; Mujica-Garcia, A.; Arrieta, M.P.; Salaris, V.; Lopez, D.; Kenny, J.M.; Peponi, L. Organic and Inorganic PCL-Based Electrospun Fibers. *Polymers (Basel).* **2020**, *12*, 1325.
10. Nirwan, V.P.; Al-Kattan, A.; Fahmi, A.; Kabashin, A. V. Fabrication of Stable Nanofiber Matrices for Tissue Engineering via Electrospinning of Bare Laser-Synthesized Au Nanoparticles in Solutions of High Molecular Weight Chitosan. *Nanomaterials* **2019**, *9*, 1058.
11. Lei, F.; Yang, J.; Wu, B.; Chen, L.; Sun, H.; Zhang, H.; Sun, D. Facile design and fabrication of highly transparent and hydrophobic coatings on glass with anti-scratch property via surface dewetting. *Prog. Org. Coatings* **2018**, *120*, 28–35.
12. Pardo, R.; Zayat, M.; Levy, D. Photochromic organic–inorganic hybrid materials. *Chem. Soc. Rev.* **2011**, *40*, 672.
13. Yan, C.; Zhu, P.; Jia, H.; Zhu, J.; Selvan, R.K.; Li, Y.; Dong, X.; Du, Z.; Angunawela, I.; Wu, N.; et al. High-Performance 3-D Fiber Network Composite Electrolyte Enabled with Li-Ion Conducting Nanofibers and Amorphous PEO-Based Cross-Linked Polymer for Ambient All-Solid-State Lithium-Metal Batteries. *Adv. Fiber Mater.* **2019**, *1*, 46–60.

14. Pastore, C.; Kiekens, P. *Surface Characteristics of Fibers and Textiles, Part 1.*; CRC Press, 2000; Vol. 94; ISBN 0824700023.
15. Schreuder-Gibson, H.L.H.; Gibson, P.; Senecal, K.; Sennett, M.; WALKER, J.; Yeomans, W.; Ziegler, D.; P. Tsai, P.; Tsai, P.P. Protective Textile Materials Based on Electrospun Nanofibers. *J. Adv. Mater.* **2002**, *34*, 44–55.
16. John, M.J.; Thomas, S. Biofibres and biocomposites. *Carbohydr. Polym.* **2008**, *71*, 343–364.
17. Ovesen, L. Clothes make the man. *Eur. J. Cancer Prev.* 2001, *10*, 385–386.
18. Agarwal, S.; Burgard, M.F.; Greiner, A.; Wendorff Joachim *Electrospinning A Practical Guide to Nanofibers*; Walter de Gruyter GmbH & Co KG, 2016; ISBN 978-3-11-033351-0.
19. Cho, J.; Joshi, M.S.; Sun, C.T. Effect of inclusion size on mechanical properties of polymeric composites with micro and nano particles. *Compos. Sci. Technol.* **2006**, *66*, 1941–1952.
20. Sun, Y.; Chen, Q. Diameter dependent strength of carbon nanotube reinforced composite. *Appl. Phys. Lett.* **2009**, *95*, 21901.
21. Lutz, P.J.; Peruch, F. Graft Copolymers and Comb-Shaped Homopolymers. In *Polymer Science: A Comprehensive Reference*; Elsevier, 2012; Vol. 6, pp. 511–542 ISBN 9780080878621.
22. Reed, A.M.; Gilding, D.K. Biodegradable polymers for use in surgery — poly(glycolic)/poly(Iactic acid) homo and copolymers: 2. In vitro degradation. *Polymer (Guildf).* **1981**, *22*, 494–498.
23. Angulakshmi, N.; Prem Kumar, T.; Thomas, S.; Manuel Stephan, A. Ionic conductivity and interfacial properties of nanochitin-incorporated polyethylene oxide-LiN(C2F5SO2)2 polymer electrolytes. *Electrochim. Acta* **2010**, *55*, 1401–1406.
24. Abbas, Q.; Mirzaeian, M.; Olabi, A.-G.; Gibson, D. Solid State Electrolytes. In *Reference Module in Materials Science and Materials Engineering*; Elsevier BV, 2020.
25. Gooday, G.W. Physiology of microbial degradation of chitin and chitosan. *Biodegradation* **1990**, *1*, 177–190.
26. Islam, N.; Dmour, I.; Taha, M.O. Degradability of chitosan micro/nanoparticles for pulmonary drug delivery. *Heliyon* **2019**, *5*, e01684.
27. Kaliva, M.; Georgopoulou, A.; Dragatogiannis, D.A.; Charitidis, C.A.; Chatzinikolaidou, M.; Vamvakaki, M. Biodegradable chitosan-graft-poly(l-lactide) copolymers for bone tissue engineering. *Polymers (Basel).* **2020**, *12*, 316.
28. Shafqat, A.; Tahir, A.; Mahmood, A.; Tabinda, A.B.; Yasar, A.; Pugazhendhi, A. A review on environmental significance carbon foot prints of starch based bio-plastic: A substitute of conventional plastics. *Biocatal. Agric. Biotechnol.* **2020**, *27*, 101540.
29. Hamed, I.; Özogul, F.; Regenstein, J.M. Industrial applications of crustacean by-products (chitin, chitosan, and chitooligosaccharides): A review. *Trends Food Sci. Technol.* **2016**, *48*, 40–50.
30. Huang, R.; Lei, Y.; Zhang, D.; Xie, H.; Liu, X.; Wang, H. Solvent-Free Assembled Fe-Chitosan Chelates Derived N-Doped Carbon Layer-Encapsulated Fe/Fe 3 C for ORR and OER . *Nano* **2020**, 2050070.

31. Lima, K.; Caballero, M.L.; Alemán, A. Biological activity of hydrolysates from industrial by-products encapsulated in chitosan nanoparticles. **2019**.
32. Hamedi, H.; Moradi, S.; Hudson, S.M.; Tonelli, A.E. Chitosan based hydrogels and their applications for drug delivery in wound dressings: A review. *Carbohydr. Polym.* **2018**, *199*, 445–460.
33. Wünsch, J.R. *Polystyrene: Synthesis, production and applications*; iSmithers Rapra Publishing, 2000; Vol. 112; ISBN 1859571913.
34. Cottrell, D.J. Food container 1980.
35. Ho, B.T.; Roberts, T.K.; Lucas, S. An overview on biodegradation of polystyrene and modified polystyrene: the microbial approach. *Crit. Rev. Biotechnol.* **2018**, *38*, 308–320.
36. Uddin, M.N.; Desai, F.J.; Asmatulu, E. Biomimetic electrospun nanocomposite fibers from recycled polystyrene foams exhibiting superhydrophobicity. *Energy, Ecol. Environ.* **2020**, *5*, 1–11.
37. Lambert, S.; Wagner, M. Characterisation of nanoplastics during the degradation of polystyrene. *Chemosphere* **2016**, *145*, 265–268.
38. Vo, C. V.; Fox, R.T. Assessment of hydrofluoropropenes as insulating blowing agents for extruded polystyrene foams. *J. Cell. Plast.* **2013**, *49*, 423–438.
39. Pandey, S.; Lönnecke, P.; Hey-Hawkins, E. Phosphorus-boron-based polymers obtained by dehydrocoupling of ferrocenylphosphine-borane adducts. *Eur. J. Inorg. Chem.* **2014**, 2456–2465.
40. Pietschnig, R. Polymers with pendant ferrocenes. *Chem. Soc. Rev.* **2016**, *45*, 5216–5231.
41. Ibrahim, M.; Wei, M.M.; Deydier, E.; Manoury, E.; Poli, R.; Lecante, P.; Philippot, K. Rhodium nanoparticles stabilized by ferrocenyl-phosphine ligands: Synthesis and catalytic styrene hydrogenation. *Dalt. Trans.* **2019**, *48*, 6777–6786.
42. Turrin, C.O.; Manoury, E.; Caminade, A.M. Ferrocenyl phosphorhydrazone dendrimers synthesis, and electrochemical and catalytic properties. *Molecules* **2020**, *25*, 447.
43. Nirwan, V.P.; Pandey, S.; Hey-Hawkins, E.; Fahmi, A. Hybrid 2D nanofibers based on poly(ethylene oxide)/polystyrene matrix and poly(ferrocenylphosphinoboranes) as functional agents. *J. Appl. Polym. Sci.* **2020**, *137*, 49091.
44. Labet, M.; Thielemans, W. Synthesis of polycaprolactone: A review. *Chem. Soc. Rev.* **2009**, *38*, 3484–3504.
45. Manakhov, A.; Kedroňová, E.; Medalová, J.; Černochová, P.; Obrusník, A.; Michlíček, M.; Shtansky, D. V.; Zajíčková, L. Carboxyl-anhydride and amine plasma coating of PCL nanofibers to improve their bioactivity. *Mater. Des.* **2017**, *132*, 257–265.
46. Ghosal, K.; Manakhov, A.; Zajíčková, L.; Thomas, S. Structural and Surface Compatibility Study of Modified Electrospun Poly(ε-caprolactone) (PCL) Composites for Skin Tissue Engineering. *AAPS PharmSciTech* **2017**, *18*, 72–81.
47. Canbolat, M.F.; Savas, H.B.; Gultekin, F. Enzymatic behavior of laccase following interaction with γ-CD and immobilization into PCL nanofibers. *Anal. Biochem.* **2017**, *528*, 13–18.

48. Dhiman, V.; Seth, N.; Hari Kumar, S.L. NANOTECHNOLOGY IN CANCER THERAPY. *J. Drug Deliv. Ther.* **2013**, *3*, 137–142.
49. Biju, V.; Itoh, T.; Anas, A.; Sujith, A.; Ishikawa, M. Semiconductor quantum dots and metal nanoparticles: Syntheses, optical properties, and biological applications. *Anal. Bioanal. Chem.* **2008**, *391*, 2469–2495.
50. Cadusch, J.J.; Panchenko, E.; Kirkwood, N.; James, T.D.; Gibson, B.C.; Webb, K.J.; Mulvaney, P.; Roberts, A. Emission enhancement and polarization of semiconductor quantum dots with nanoimprinted plasmonic cavities: Towards scalable fabrication of plasmon-exciton displays. *Nanoscale* **2015**, *7*, 13816–13821.
51. Rane, A.V.; Kanny, K.; Abitha, V.K.; Thomas, S. Methods for synthesis of nanoparticles and fabrication of nanocomposites. In *Synthesis of inorganic nanomaterials*; Elsevier, 2018; pp. 121–139.
52. Hosseinzadeh, S.; Behboudnia, M.; Jamilpanah, L.; Sheikhi, M.H.; Mohajerani, E.; Tian, K.; Tiwari, A.; Elahi, P.; Mohseni, S.M. High saturation magnetization, low coercivity and fine YIG nanoparticles prepared by modifying co-precipitation method. *J. Magn. Magn. Mater.* **2019**, *476*, 355–360.
53. Popov, A.A.; Tselikov, G.; Dumas, N.; Berard, C.; Metwally, K.; Jones, N.; Al-Kattan, A.; Larrat, B.; Braguer, D.; Mensah, S.; et al. Laser- synthesized TiN nanoparticles as promising plasmonic alternative for biomedical applications. *Sci. Rep.* **2019**, *9*, 1194.
54. Al-Kattan, A.; Nirwan, V.P.P.; Popov, A.; Ryabchikov, Y.V. V.; Tselikov, G.; Sentis, M.; Fahmi, A.; Kabashin, A.V. V. Recent Advances in Laser-Ablative Synthesis of Bare Au and Si Nanoparticles and Assessment of Their Prospects for Tissue Engineering Applications. *Int. J. Mol. Sci.* **2018**, *19*, 1563.
55. Bizarria, M.T.M.; D'Ávila, M.A.; Mei, L.H.I. Non-woven nanofiber chitosan/PEO membranes obtained by electrospinning. *Brazilian J. Chem. Eng.* **2014**, *31*, 57–68.
56. Gu, B.K.; Park, S.J.; Kim, M.S.; Kang, C.M.; Kim, J. Il; Kim, C.H. Fabrication of sonicated chitosan nanofiber mat with enlarged porosity for use as hemostatic materials. *Carbohydr. Polym.* **2013**, *97*, 65–73.
57. Singh, S.; Ashfaq, M.; Singh, R.K.; Joshi, H.C.; Srivastava, A.; Sharma, A.; Verma, N. Preparation of surfactant-mediated silver and copper nanoparticles dispersed in hierarchical carbon micro-nanofibers for antibacterial applications. *N. Biotechnol.* **2013**, *30*, 656–665.
58. Xiang, J.; Li, X.; Ma, Y.; Zhao, Q.; Ho, C.-L.; Wong, W.-Y. Efficient flash memory devices based on non-conjugated ferrocene-containing copolymers. *J. Mater. Chem. C* **2018**, *6*, 11348–11355.
59. Alismail, H.; Du, Y.; Zhou, J.; Ryan Tian, Z. A cell-sensory bioscaffold of biocompatible titanate nanofiber. In Proceedings of the TechConnect Briefs 2018 - Advanced Materials; TechConnect, 2018; Vol. 3, pp. 42–45.
60. Lyu, J.; Wang, X.; Liu, L.; Kim, Y.; Tanyi, E.K.; Chi, H.; Feng, W.; Xu, L.; Li, T.; Noginov, M.A.; et al. High Strength Conductive Composites with Plasmonic Nanoparticles Aligned on Aramid Nanofibers. *Adv. Funct. Mater.* **2016**, *26*, 8435–8445.
61. Cooley, J.F. Apparatus for electrically dispersing fluids. 1902.

62. Hohman, M.M.; Shin, M.; Rutledge, G.; Brenner, M.P. Electrospinning and electrically forced jets. I. Stability theory. *Phys. fluids* **2001**, *13*, 2201–2220.
63. Taylor, G.I. Disintegration of water drops in an electric field. *Proc. R. Soc. London. Ser. A. Math. Phys. Sci.* **1964**, *280*, 383–397.
64. Tian, J.; Shao, Q.; Dong, X.; Zheng, J.; Pan, D.; Zhang, X.; Cao, H.; Hao, L.; Liu, J.; Mai, X.; et al. Bio-template synthesized NiO/C hollow microspheres with enhanced Li-ion battery electrochemical performance. *Electrochim. Acta* **2018**, *261*, 236–245.
65. Wang, X.-X.; Yu, G.-F.; Zhang, J.; Yu, M.; Ramakrishna, S.; Long, Y.-Z. Conductive polymer ultrafine fibers via electrospinning: Preparation, physical properties and applications. *Prog. Mater. Sci.* **2021**, *115*, 100704.
66. Nangare, S.; Jadhav, N.; Ghagare, P.; Muthane, T. Pharmaceutical applications of electrospinning. *Ann. Pharm. Fr.* **2020**, *78*, 1–11.
67. Joshi, V.; Srivastava, C.M.; Gupta, A.P.; Vats, M. Electrospun Nano-architectures for Tissue Engineering and Regenerative Medicine. In *Nanoscience in Medicine Vol. 1*; Springer, 2020; pp. 213–248.
68. Kabashin, A. V; Delaporte, P.; Pereira, A.; Grojo, D.; Torres, R.; Sarnet, T.; Sentis, M. Nanofabrication with pulsed lasers. *Nanoscale Res. Lett.* **2010**, *5*, 454.
69. Zhang, D.; Gökce, B.; Barcikowski, S. Laser Synthesis and Processing of Colloids: Fundamentals and Applications. *Chem. Rev.* **2017**, *117*, 3990–4103.
70. Kabashin, A. V.; Meunier, M. Synthesis of colloidal nanoparticles during femtosecond laser ablation of gold in water. *J. Appl. Phys.* **2003**, *94*, 7941–7943.
71. Hebié, S.; Holade, Y.; Maximova, K.; Sentis, M.; Delaporte, P.; Kokoh, K.B.; Napporn, T.W.; Kabashin, A. V. Advanced Electrocatalysts on the Basis of Bare Au Nanomaterials for Biofuel Cell Applications. *ACS Catal.* **2015**, *5*, 6489–6496.
72. Kabashin, A. V; Meunier, M.; Kingston, C.; Luong, J.H.T. Fabrication and characterization of gold nanoparticles by femtosecond laser ablation in an aqueous solution of cyclodextrins. *J. Phys. Chem. B* **2003**, *107*, 4527–4531.
73. Sylvestre, J.-P.; Kabashin, A. V; Sacher, E.; Meunier, M.; Luong, J.H.T. Stabilization and size control of gold nanoparticles during laser ablation in aqueous cyclodextrins. *J. Am. Chem. Soc.* **2004**, *126*, 7176–7177.
74. Sylvestre, J.-P.; Poulin, S.; Kabashin, A. V; Sacher, E.; Meunier, M.; Luong, J.H.T. Surface chemistry of gold nanoparticles produced by laser ablation in aqueous media. *J. Phys. Chem. B* **2004**, *108*, 16864–16869.
75. Correard, F.; Maximova, K.; Estève, M.A.; Villard, C.; Roy, M.; Al-Kattan, A.; Sentis, M.; Gingras, M.; Kabashin, A. V.; Braguer, D. Gold nanoparticles prepared by laser ablation in aqueous biocompatible solutions: Assessment of safety and biological identity for nanomedicine applications. *Int. J. Nanomedicine* **2014**, *9*, 5415–5430.
76. Al-Kattan, A.; Nirwan, V.P.; Munnier, E.; Chourpa, I.; Fahmi, A.; Kabashin, A. V. Toward multifunctional hybrid platforms for tissue engineering based on chitosan(PEO) nanofibers functionalized by bare laser-synthesized Au and Si nanoparticles. *RSC Adv.* **2017**, *7*, 31759–31766.
77. Dell'Aglio, M.; Gaudiuso, R.; De Pascale, O.; De Giacomo, A. Mechanisms and processes of pulsed laser ablation in liquids during nanoparticle production. *Appl.*

Surf. Sci. **2015**, *348*, 4–9.

78. Itina, T.E.; Gouriet, K.; Zhigilei, L. V; Noël, S.; Hermann, J.; Sentis, M. Mechanisms of small clusters production by short and ultra-short laser ablation. *Appl. Surf. Sci.* **2007**, *253*, 7656–7661.
79. Povarnitsyn, M.E.; Itina, T.E.; Levashov, P.R.; Khishchenko, K. V Mechanisms of nanoparticle formation by ultra-short laser ablation of metals in liquid environment. *Phys. Chem. Chem. Phys.* **2013**, *15*, 3108–3114.
80. Zhigilei, L. V; Lin, Z.; Ivanov, D.S. Atomistic modeling of short pulse laser ablation of metals: connections between melting, spallation, and phase explosion. *J. Phys. Chem. C* **2009**, *113*, 11892–11906.
81. Shih, C.-Y.; Shugaev, M. V; Wu, C.; Zhigilei, L. V The effect of pulse duration on nanoparticle generation in pulsed laser ablation in liquids: Insights from large-scale atomistic simulations. *Phys. Chem. Chem. Phys.* **2020**, *22*, 7077–7099.
82. Blandin, P.; Maximova, K.A.; Gongalsky, M.B.; Sanchez-Royo, J.F.; Chirvony, V.S.; Sentis, M.; Timoshenko, V.Y.; Kabashin, A. V. Femtosecond laser fragmentation from water-dispersed microcolloids: Toward fast controllable growth of ultrapure Si-based nanomaterials for biological applications. *J. Mater. Chem. B* **2013**, *1*, 2489–2495.
83. Maximova, K.; Aristov, A.; Sentis, M.; Kabashin, A. V. Size-controllable synthesis of bare gold nanoparticles by femtosecond laser fragmentation in water. *Nanotechnology* **2015**, *26*, 65601.
84. Thomas, S.; Thomas, R.; Zachariah, A.K.; Kumar, R. *Microscopy methods in nanomaterials characterization*; Elsevier, 2017; Vol. 1; ISBN 0323461476.
85. Abd Mutalib, M.; Rahman, M.A.; Othman, M.H.D.; Ismail, A.F.; Jaafar, J. Scanning electron microscopy (SEM) and energy-dispersive X-ray (EDX) spectroscopy. In *Membrane characterization*; Elsevier, 2017; pp. 161–179.
86. Šesták, J.; Hubík, P.; Mareš, J.J. *Thermal Physics and Thermal Analysis: From Macro to Micro, Highlighting Thermodynamics, Kinetics and Nanomaterials*; Springer, 2017; Vol. 11; ISBN 331945899X.
87. Höhne, G.; Hemminger, W.F.; Flammersheim, H.-J. *Differential scanning calorimetry*; Springer Science & Business Media, 2013; ISBN 3662067102.
88. Sommer, L. *Analytical absorption spectrophotometry in the visible and ultraviolet: the principles*; Elsevier, 2012; ISBN 044459745X.
89. Penner, M.H. Basic Principles of Spectroscopy. In *Food analysis*; Springer, 2017; pp. 79–88.
90. Baravkar, A.A.; Kale, R.N.; Sawant, S.D. FTIR Spectroscopy: principle, technique and mathematics. *Int. J. Pharma Bio Sci.* **2011**, *2*, 513–519.
91. Smith, D.R.; Morgan, R.L.; Loewenstein, E. V. Comparison of the Radiance of Far-Infrared Sources. *J. Opt. Soc. Am.* **1968**, *58*, 433.
92. SCoEaNIHR, E.C.S. Risk assessment of products of nanotechnologies. *Eur. Comm. Sci. Comm. Emerg. New. Identified Heal. Risks* **2009**.
93. Feynman, R. There's plenty of room at the bottom. *Feynman Comput.* **2018**, *23*, 63–76.

94. Risks, S.C. on E. and N.I.H. Modified Opinion (after Public Consultation) on the Appropriateness of Existing Methodologies to Assess the Potential Risks Associated with Engineered and Adventitious Products of Nanotechnologies. **2006**.
95. Hayashi, H.; Aratani, N.; Yamada, H. Semiconducting Self-Assembled Nanofibers Prepared from Photostable Octafluorinated Bisanthene Derivatives. **2017**.
96. Liang, C.; Ye, Z.; Xue, B.; Zeng, L.; Wu, W.; Zhong, C.; Cao, Y.; Hu, B.; Messersmith, P.B. Self-assembled nanofibers for strong underwater adhesion: the trick of barnacles. *ACS Appl. Mater. Interfaces* **2018**, *10*, 25017–25025.
97. Guo, Y.; Jiang, S.; Grena, B.J.B.; Kimbrough, I.F.; Thompson, E.G.; Fink, Y.; Sontheimer, H.; Yoshinobu, T.; Jia, X. Polymer composite with carbon nanofibers aligned during thermal drawing as a microelectrode for chronic neural interfaces. *ACS Nano* **2017**, *11*, 6574–6585.
98. Brennan, D.A.; Jao, D.; Siracusa, M.C.; Wilkinson, A.R.; Hu, X.; Beachley, V.Z. Concurrent collection and post-drawing of individual electrospun polymer nanofibers to enhance macromolecular alignment and mechanical properties. *Polymer (Guildf).* **2016**, *103*, 243–250.
99. Chawla, S.; Cai, J.; Naraghi, M. Mechanical tests on individual carbon nanofibers reveals the strong effect of graphitic alignment achieved via precursor hot-drawing. *Carbon N. Y.* **2017**, *117*, 208–219.
100. Yu, Q.; Lv, J.; Liu, Z.; Xu, M.; Yang, W.; Owusu, K.A.; Mai, L.; Zhao, D.; Zhou, L. Macroscopic synthesis of ultrafine N–doped carbon nanofibers for superior capacitive energy storage. *Sci. Bull.* **2019**, *64*, 1617–1624.
101. Grande, R.; Trovatti, E.; Carvalho, A.J.F.; Gandini, A. Continuous microfiber drawing by interfacial charge complexation between anionic cellulose nanofibers and cationic chitosan. *J. Mater. Chem. A* **2017**, *5*, 13098–13103.
102. Costa, L.; Al-Hashimi, M.; Heeney, M.; Terekhov, A.; Rajput, D.; Hofmeister, W.; Verma, A. Template-synthesis of conjugated poly (3-hexylselenophene)(P3HS) nanofibers using femtosecond laser machined fused silica templates. *MRS Adv.* **2017**, *2*, 2957–2960.
103. Yan, J.; Han, Y.; Xia, S.; Wang, X.; Zhang, Y.; Yu, J.; Ding, B. Polymer template synthesis of flexible BaTiO3 crystal nanofibers. *Adv. Funct. Mater.* **2019**, *29*, 1907919.
104. Liu, S.; Shan, H.; Xia, S.; Yan, J.; Yu, J.; Ding, B. Polymer Template Synthesis of Flexible SiO2 Nanofibers to Upgrade Composite Electrolytes. *ACS Appl. Mater. Interfaces* **2020**, *12*, 31439–31447.
105. Zhou, C.-J.; Chen, C.; Zhou, H.; He, J.-H. Fabrication of Latex-based Nanofibers by Electrospinning. *Recent Pat. Nanotechnol.* **2019**, *13*, 202–205.
106. Zhang, W.; Ronca, S.; Mele, E. Electrospun nanofibres containing antimicrobial plant extracts. *Nanomaterials* **2017**, *7*, 42.
107. Aydogdu, A.; Yildiz, E.; Ayhan, Z.; Aydogdu, Y.; Sumnu, G.; Sahin, S. Nanostructured Poly (lactic acid)/Soy Protein/HPMC films by electrospinning for potential applications in food industry. *Eur. Polym. J.* **2019**, *112*, 477–486.
108. Mirjalili, M.; Zohoori, S. Review for application of electrospinning and electrospun nanofibers technology in textile industry. *J. Nanostructure Chem.* **2016**, *6*, 207–213.

109. Mendes, A.C.; Strohmenger, T.; Goycoolea, F.; Chronakis, I.S. Electrostatic self-assembly of polysaccharides into nanofibers. *Colloids Surfaces A Physicochem. Eng. Asp.* **2017**, *531*, 182–188.
110. Zhao, X.; Li, L.; Zhao, Y.; An, H.; Cai, Q.; Lang, J.; Han, X.; Peng, B.; Fei, Y.; Liu, H. In Situ Self-Assembled Nanofibers Precisely Target Cancer-Associated Fibroblasts for Improved Tumor Imaging. *Angew. Chemie* **2019**, *131*, 15431–15438.
111. Formhals, A. Process and apparatus for preparing artificial threads. US Patent: 1975504. *vol* **1934**, *1*, 7.
112. Motamedi, A.S.; Mirzadeh, H.; Hajiesmaeilbaigi, F.; Bagheri-Khoulenjani, S.; Shokrgozar, M. Effect of electrospinning parameters on morphological properties of PVDF nanofibrous scaffolds. *Prog. Biomater.* **2017**, *6*, 113–123.
113. Ray, S.S.; Chen, S.-S.; Li, C.-W.; Nguyen, N.C.; Nguyen, H.T. A comprehensive review: electrospinning technique for fabrication and surface modification of membranes for water treatment application. *RSC Adv.* **2016**, *6*, 85495–85514.
114. SalehHudin, H.S.; Mohamad, E.N.; Mahadi, W.N.L.; Muhammad Afifi, A. Multiple-jet electrospinning methods for nanofiber processing: A review. *Mater. Manuf. Process.* **2018**, *33*, 479–498.
115. Nagle, A.R.; Fay, C.D.; Wallace, G.G.; Xie, Z.; Wang, X.; Higgins, M.J. Patterning and process parameter effects in 3D suspension near-field electrospinning of nanoarrays. *Nanotechnology* **2019**, *30*, 495301.
116. Liu, Z.; Zhou, L.; Ruan, F.; Wei, A.; Zhao, J.; Feng, Q. Needle-disk Electrospinning: Mechanism Elucidation, Parameter Optimization and Productivity Improvement. *Recent Pat. Nanotechnol.* **2020**, *14*, 46–55.
117. Ghosal, K.; Agatemor, C.; Tucker, N.; Kny, E.; Thomas, S. CHAPTER 1. Electrical Spinning to Electrospinning: a Brief History. In; Royal Society of Chemistry, 2018; pp. 1–23.
118. Homayoni, H.; Ravandi, S.A.H.; Valizadeh, M. Electrospinning of chitosan nanofibers: Processing optimization. *Carbohydr. Polym.* **2009**, *77*, 656–661.
119. Pakravan, M.; Heuzey, M.C.; Ajji, A. A fundamental study of chitosan/PEO electrospinning. *Polymer (Guildf).* **2011**, *52*, 4813–4824.
120. Qasim, S.B.; Zafar, M.S.; Najeeb, S.; Khurshid, Z.; Shah, A.H.; Husain, S.; Rehman, I.U. Electrospinning of chitosan-based solutions for tissue engineering and regenerative medicine. *Int. J. Mol. Sci.* **2018**, *19*, 407.
121. Younes, I.; Rinaudo, M. Chitin and chitosan preparation from marine sources. Structure, properties and applications. *Mar. Drugs* **2015**, *13*, 1133–1174.
122. Yahia, S.; Khalil, I.A.; El-Sherbiny, I.M. Sandwich-Like Nanofibrous Scaffolds for Bone Tissue Regeneration. *ACS Appl. Mater. Interfaces* **2019**, *11*, 28610–28620.
123. Shalihah, H.; Kusumaatmaja, A.; Nugraheni, A.D.; Triyana, K. Optimization of chitosan/pva concentration in fabricating nanofibers membrane and its prospect as air filtration. *Mater. Sci. Forum* **2017**, *901 MSF*, 20–25.
124. Turkevich, J.; Stevenson, P.C.; Hillier, J. A study of the nucleation and growth processes in the synthesis of colloidal gold. *Discuss. Faraday Soc.* **1951**, *11*, 55–75.
125. Popov, A.A.; Tselikov, G.; Al-Kattan, A.; Kabashin, A. V. Femtosecond laser-ablative

synthesis of plasmonic Au and TiN nanoparticles for biomedical applications. In Proceedings of the Synthesis and Photonics of Nanoscale Materials XVI; Kabashin, A. V., Dubowski, J.J., Geohegan, D.B., Eds.; SPIE, 2019; Vol. 10907, p. 7.

126. Dykman, L.; Khlebtsov, N. *Gold nanoparticles in biomedical applications*; CRC Press: Boca Raton : Taylor & Francis, 2017., 2017; Vol. 41; ISBN 9781351360487.
127. Cui, Q.; Yashchenok, A.; Zhang, L.; Li, L.; Masic, A.; Wienskol, G.; Möhwald, H.; Bargheer, M. Fabrication of bifunctional gold/gelatin hybrid nanocomposites and their application. *ACS Appl. Mater. Interfaces* **2014**, *6*, 1999–2002.
128. Kabashin, A.V.; Sarnet, T.; Grojo, D.; Delaporte, P.; Charmasson, L.; Blandin, P.; Torres, R.; Derrien, T.. Y.; Sentis, M. Laser-ablative nanostructuring of surfaces. *Int. J. Nanotechnol.* **2012**, *9*, 230.
129. Kai, D.; Jin, G.; Prabhakaran, M.P.; Ramakrishna, S. Electrospun synthetic and natural nanofibers for regenerative medicine and stem cells. *Biotechnol. J.* **2013**, *8*, 59–72.
130. Sridhar, R.; Sundarrajan, S.; Venugopal, J.R.; Ravichandran, R.; Ramakrishna, S. Electrospun inorganic and polymer composite nanofibers for biomedical applications. *J. Biomater. Sci. Polym. Ed.* 2013, *24*, 365–385.
131. Stumpf, T.R.; Yang, X.; Zhang, J.; Cao, X. In situ and ex situ modifications of bacterial cellulose for applications in tissue engineering. *Mater. Sci. Eng. C* 2018, *82*, 372–383.
132. Patel, H.; Bonde, M.; Srinivasan, G. Biodegradable polymer scaffold for tissue engineering. *Trends Biomater. Artif. Organs* **2011**, *25*, 20–29.
133. Wu, J.; Xie, L.; Lin, W.Z.Y.; Chen, Q. Biomimetic nanofibrous scaffolds for neural tissue engineering and drug development. *Drug Discov. Today* 2017, *22*, 1375–1384.
134. Pierini, F.; Nakielski, P.; Urbanek, O.; Pawlowska, S.; Lanzi, M.; De Sio, L.; Kowalewski, T.A. Polymer-Based Nanomaterials for Photothermal Therapy: From Light-Responsive to Multifunctional Nanoplatforms for Synergistically Combined Technologies. *Biomacromolecules* **2018**, *19*, 4147–4167.
135. Huang, Z.M.; Zhang, Y.Z.; Kotaki, M.; Ramakrishna, S. A review on polymer nanofibers by electrospinning and their applications in nanocomposites. *Compos. Sci. Technol.* **2003**, *63*, 2223–2253.
136. Sachlos, E.; Czernuszka, J.T.; Gogolewski, S.; Dalby, M. Making tissue engineering scaffolds work. Review on the application ofsolid freeform fabrication technology to the production of tissue engineeringscaffolds. *Eur. Cells Mater.* 2003, *5*, 29–40.
137. Abidian, M.R.; Martin, D.C. Multifunctional nanobiomaterials for neural interfaces. *Adv. Funct. Mater.* **2009**, *19*, 573–585.
138. Agarwal, S.; Greiner, A.; Wendorff, J.H. Functional materials by electrospinning of polymers. *Prog. Polym. Sci.* **2013**, *38*, 963–991.
139. Klein, K.L.; Melechko, A. V.; McKnight, T.E.; Retterer, S.T.; Rack, P.D.; Fowlkes, J.D.; Joy, D.C.; Simpson, M.L. Surface characterization and functionalization of carbon nanofibers. *J. Appl. Phys.* **2008**, *103*.
140. Ahmed, S.; Ikram, S. Chitosan Based Scaffolds and Their Applications in Wound Healing. *Achiev. Life Sci.* **2016**, *10*, 27–37.
141. Zhao, L.M.; Shi, L.E.; Zhang, Z.L.; Chen, J.M.; Shi, D.D.; Yang, J.; Tang, Z.X. Preparation

and application of chitosan nanoparticles and nanofibers. *Brazilian J. Chem. Eng.* 2011, *28*, 353–362.

142. Muxika, A.; Etxabide, A.; Uranga, J.; Guerrero, P.; de la Caba, K. Chitosan as a bioactive polymer: Processing, properties and applications. *Int. J. Biol. Macromol.* 2017, *105*, 1358–1368.
143. Dash, M.; Chiellini, F.; Ottenbrite, R.M.; Chiellini, E. Chitosan - A versatile semi-synthetic polymer in biomedical applications. *Prog. Polym. Sci.* 2011, *36*, 981–1014.
144. Elsabee, M.Z.; Naguib, H.F.; Morsi, R.E. Chitosan based nanofibers, review. *Mater. Sci. Eng. C* 2012, *32*, 1711–1726.
145. Tselikov, G.; Ryabchikov, Y. V.; Popov, A.A.; Chourpa, I.; Fahmi, A.W.; Munnier, E.; Nirwan, V.P. Bare laser-synthesized Si nanoparticles as functional elements for chitosan nanofiber-based tissue engineering platforms. In Proceedings of the Synthesis and Photonics of Nanoscale Materials XV; Kabashin, A. V., Dubowski, J.J., Geohegan, D.B., Cao, L., Eds.; SPIE, 2018; Vol. 10521, p. 9.
146. Jayakumar, R.; Menon, D.; Manzoor, K.; Nair, S. V.; Tamura, H. Biomedical applications of chitin and chitosan based nanomaterials - A short review. *Carbohydr. Polym.* 2010, *82*, 227–232.
147. Torres-Giner, S.; Ocio, M.J.; Lagaron, J.M. Development of active antimicrobial fiber based chitosan polysaccharide nanostructures using electrospinning. *Eng. Life Sci.* **2008**, *8*, 303–314.
148. Adrienne, H.; Nanofibers, E.C. The emergence of a temporally extended self and factors that contribute to its development: from theoretical and empirical perspectives. *Monogr. Soc. Res. Child Dev.* **2013**, *78*, vii, 1–120.
149. Lemma, S.M.; Bossard, F.; Rinaudo, M. Preparation of pure and stable chitosan nanofibers by electrospinning in the presence of poly(ethylene oxide). *Int. J. Mol. Sci.* **2016**, *17*.
150. Wendorff, J.H.; Agarwal, S.; Greiner, A. *Electrospinning: Materials, Processing, and Applications*; 2012; ISBN 9783527320806.
151. Ohkawa, K.; Cha, D.; Kim, H.; Nishida, A.; Yamamoto, H. Electrospinning of chitosan. *Macromol. Rapid Commun.* **2004**, *25*, 1600–1605.
152. de Vasconcelos, C.L.; Bezerril, P.M.; dos Santos, D.E.S.; Dantas, T.N.C.; Pereira, M.R.; Fonseca, J.L.C. Effect of molecular weight and ionic strength on the formation of polyelectrolyte complexes based on poly(methacrylic acid) and chitosan. *Biomacromolecules* **2006**, *7*, 1245–1252.
153. Kabashin, A.V. V.; Meunier, M. Laser-induced treatment of silicon in air and formation of Si/SiO x photoluminescent nanostructured layers. *Mater. Sci. Eng. B Solid-State Mater. Adv. Technol.* **2003**, *101*, 60–64.
154. Gongalsky, M.B.; Osminkina, L.A.; Pereira, A.; Manankov, A.A.; Fedorenko, A.A.; Vasiliev, A.N.; Solovyev, V. V.; Kudryavtsev, A.A.; Sentis, M.; Kabashin, A. V.; et al. Laser-synthesized oxide-passivated bright Si quantum dots for bioimaging. *Sci. Rep.* **2016**, *6*, 24732.
155. Al-Kattan, A.; Ryabchikov, Y. V.; Baati, T.; Chirvony, V.; Sánchez-Royo, J.F.; Sentis, M.; Braguer, D.; Timoshenko, V.Y.; Estève, M.A.; Kabashin, A. V. Ultrapure laser-

synthesized Si nanoparticles with variable oxidation states for biomedical applications. *J. Mater. Chem. B* **2016**, *4*, 7852–7858.

156. Baati, T.; Al-Kattan, A.; Esteve, M.A.; Njim, L.; Ryabchikov, Y.; Chaspoul, F.; Hammami, M.; Sentis, M.; Kabashin, A. V.; Braguer, D. Ultrapure laser-synthesized Si-based nanomaterials for biomedical applications: In vivo assessment of safety and biodistribution. *Sci. Rep.* **2016**, *6*, 1–13.
157. Kabashin, A. V.; Timoshenko, V.Y. What theranostic applications could ultrapure laser-synthesized Si nanoparticles have in cancer? *Nanomedicine* **2016**, *11*, 2247–2250.
158. Kögler, M.; Ryabchikov, Y. V.; Uusitalo, S.; Popov, A.; Popov, A.; Tselikov, G.; Välimaa, A.L.; Al-Kattan, A.; Hiltunen, J.; Laitinen, R.; et al. Bare laser-synthesized Au-based nanoparticles as nondisturbing surface-enhanced Raman scattering probes for bacteria identification. *J. Biophotonics* **2018**, *11*, e201700225.
159. Sangsanoh, P.; Supaphol, P. Stability improvement of electrospun chitosan nanofibrous membranes in neutral or weak basic aqueous solutions. *Biomacromolecules* **2006**, *7*, 2710–2714.
160. Pawlak, A.; Mucha, M. Thermogravimetric and FTIR studies of chitosan blends. In Proceedings of the Thermochimica Acta; 2003; Vol. 396, pp. 153–166.
161. Osman, Z.; Arof, A.K. FTIR studies of chitosan acetate based polymer electrolytes. *Electrochim. Acta* **2003**, *48*, 993–999.
162. Zivanovic, S.; Li, J.; Davidson, P.M.; Kit, K. Physical, mechanical, and antibacterial properties of chitosan/PEO blend films. *Biomacromolecules* **2007**, *8*, 1505–1510.
163. Pucić, I.; Jurkin, T. FTIR assessment of poly(ethylene oxide) irradiated in solid state, melt and aqeuous solution. *Radiat. Phys. Chem.* **2012**, *81*, 1426–1429.
164. Cui, Y.; Li, B.; He, H.; Zhou, W.; Chen, B.; Qian, G. Metal–Organic Frameworks as Platforms for Functional Materials. *Acc. Chem. Res.* **2016**, *49*, 483–493.
165. Mao, L.; Ke, W.; Pedesseau, L.; Wu, Y.; Katan, C.; Even, J.; Wasielewski, M.R.; Stoumpos, C.C.; Kanatzidis, M.G. Hybrid Dion-Jacobson 2D Lead Iodide Perovskites. *J. Am. Chem. Soc.* **2018**, *140*, 3775–3783.
166. Ribeiro, T.; Baleizão, C.; Farinha, J.P.S. Functional films from silica/polymer nanoparticles. *Materials (Basel).* **2014**, *7*, 3881–3900.
167. Boissiere, C.; Grosso, D.; Chaumonnot, A.; Nicole, L.; Sanchez, C. Aerosol route to functional nanostructured inorganic and hybrid porous materials. *Adv. Mater.* **2011**, *23*, 599–623.
168. Liebig, F.; Henning, R.; Sarhan, R.M.; Prietzel, C.; Bargheer, M.; Koetz, J. A new route to gold nanoflowers. *Nanotechnology* **2018**, *29*, 185603.
169. Niu, Z.; Cui, F.; Kuttner, E.; Xie, C.; Chen, H.; Sun, Y.; Dehestani, A.; Schierle-Arndt, K.; Yang, P. Synthesis of Silver Nanowires with Reduced Diameters Using Benzoin-Derived Radicals to Make Transparent Conductors with High Transparency and Low Haze. *Nano Lett.* **2018**, *18*, 5329–5334.
170. Massaglia, G.; Quaglio, M. Semiconducting Electrospun Nanofibers for Energy Conversion. In *Semiconductors - Growth and Characterization*; Inguanta, R., Sunseri, C., Eds.; InTech: Rijeka, 2018; pp. 159–175.

171. Pant, H.R.; Bajgai, M.P.; Nam, K.T.; Seo, Y.A.; Pandeya, D.R.; Hong, S.T.; Kim, H.Y. Electrospun nylon-6 spider-net like nanofiber mat containing TiO2 nanoparticles: A multifunctional nanocomposite textile material. *J. Hazard. Mater.* **2011**, *185*, 124–130.
172. Lim, H.S.; Baek, J.H.; Park, K.; Shin, H.S.; Kim, J.; Cho, J.H. Multifunctional hybrid fabrics with thermally stable superhydrophobicity. *Adv. Mater.* **2010**, *22*, 2138–2141.
173. Shankar, A.; Seyam, A.F.M.; Hudson, S.M. Electrospinning of soy protein fibers and their compatibility with synthetic polymers. *J. Text. Apparel, Technol. Manag.* **2013**, *8*, 1–14.
174. Dan Li; Younan Xia Electrospinning of Nanofibers: Reinventing the Wheel? *Adv. Mater.* **2004**, *16*, 1151–1170.
175. Repanas, A.; Andriopoulou, S.; Glasmacher, B. The significance of electrospinning as a method to create fibrous scaffolds for biomedical engineering and drug delivery applications. *J. Drug Deliv. Sci. Technol.* **2016**, *31*, 137–146.
176. Maze, B.; Vahedi Tafreshi, H.; Wang, Q.; Pourdeyhimi, B. A simulation of unsteady-state filtration via nanofiber media at reduced operating pressures. *J. Aerosol Sci.* **2007**, *38*, 550–571.
177. Formo, E.; Lee, E.; Campbell, D.; Xia, Y. Functionalization of electrospun TiO 2 nanofibers with Pt nanoparticles and nanowires for catalytic applications. *Nano Lett.* **2008**, *8*, 668–672.
178. Hellmann, C.; Greiner, A.; Wendorff, J.H. Design of pheromone releasing nanofibers for plant protection. *Polym. Adv. Technol.* **2011**, *22*, 407–413.
179. Liu, D.; Liu, S.; Jing, X.; Li, X.; Li, W.; Huang, Y. Necrosis of cervical carcinoma by dichloroacetate released from electrospun polylactide mats. *Biomaterials* **2012**, *33*, 4362–4369.
180. Sang, Y.; Gu, Q.; Sun, T.; Li, F.; Liang, C. Filtration by a novel nanofiber membrane and alumina adsorption to remove copper(II) from groundwater. *J. Hazard. Mater.* **2008**, *153*, 860–866.
181. Ma, Z.; Kotaki, M.; Inai, R.; Ramakrishna, S. Potential of Nanofiber Matrix as Tissue-Engineering Scaffolds. *Tissue Eng.* **2005**, *11*, 101–109.
182. Pandey, S.; Lönnecke, P.; Hey-Hawkins, E. Cross-dehydrocoupling: A novel synthetic route to P-B-P-B chains. *Inorg. Chem.* **2014**, *53*, 8242–8249.
183. Fang, Y.; Giesecke, M.; Furó, I. Complexing Cations by Poly(ethylene oxide): Binding Site and Binding Mode. *J. Phys. Chem. B* **2017**, *121*, 2179–2188.
184. Rueden, C.T.; Schindelin, J.; Hiner, M.C.; DeZonia, B.E.; Walter, A.E.; Arena, E.T.; Eliceiri, K.W. ImageJ2: ImageJ for the next generation of scientific image data. *BMC Bioinformatics* **2017**, *18*, 529.
185. Harris, R.K.; Becker, E.D.; Cabral de Menezes, S.M.; Goodfellow, R.; Granger, P. NMR nomenclature: nuclear spin properties and conventions for chemical shifts. IUPAC Recommendations 2001. International Union of Pure and Applied Chemistry. Physical Chemistry Division. Commission on Molecular Structure and Spectroscopy. *Magn. Reson. Chem.* **2002**, *40*, 489–505.

186. Akltt, J.W. H. Nöth and B. Wrackmeyer. Nuclear magnetic resonance spectroscopy of boron compounds. No. 14 in the seriesNMR—Basic Principles and Progress, ed. by P. Diehl, E. Fluck and R. Kosfeld, Springer Verlag, 1978. 461 pages. Dm 162. *Org. Magn. Reson.* **1979**, *12*, III–III.
187. Clark, T.J.; Rodezno, J.M.; Clendenning, S.B.; Aouba, S.; Brodersen, P.M.; Lough, A.J.; Ruda, H.E.; Manners, I. Rhodium-catalyzed dehydrocoupling of fluorinated phosphine-borane adducts: Synthesis, characterization, and properties of cyclic and polymeric phosphinoboranes with electron-withdrawing substituents at phosphorus. *Chem. - A Eur. J.* **2005**, *11*, 4526–4534.
188. Dorn, H.; Rodezno, J.M.; Brünnhöfer, B.; Rivard, E.; Massey, J.A.; Manners, I. Synthesis, Characterization, and Properties of the Polyphosphinoboranes [RPH - BH 2]. *Macromolecules* **2003**, *36*, 291–297.
189. Nainan, K.C.; Ryschkewitsch, G.E. A new synthesis of amine- and phosphine-boranes. *Inorg. Chem.* **1969**, *8*, 2671–2674.
190. Jain, S.R.; Sisler, H.H. The chloramination of some ditertiary phosphines and arsines. *Inorg. Chem.* **1969**, *8*, 1243–1246.
191. Wu, T.-J.; Chiu, H.-Y.; Yu, J.; Cautela, M.P.; Sarmento, B.; das Neves, J.; Catala, C.; Pazos-Perez, N.; Guerrini, L.; Alvarez-Puebla, R.A.; et al. Nanotechnologies for early diagnosis, in situ disease monitoring, and prevention. In *Nanotechnologies in Preventive and Regenerative Medicine*; Uskoković, V., Uskoković, D.P.B.T.-N. in P. and R.M., Eds.; Elsevier, 2018; pp. 1–92 ISBN 978-0-323-48063-5.
192. Khayet, M.; García-Payo, C.; Matsuura, T. Superhydrophobic nanofibers electrospun by surface segregating fluorinated amphiphilic additive for membrane distillation. *J. Memb. Sci.* **2019**, *588*, 117215.
193. Blakney, A.K.; Ball, C.; Krogstad, E.A.; Woodrow, K.A. Electrospun fibers for vaginal anti-HIV drug delivery. *Antiviral Res.* **2013**, *100*, S9–S16.
194. Chen, S.; Cui, S.; Hu, J.; Zhou, Y.; Liu, Y. Pectinate nanofiber mat with high absorbency and antibacterial activity: A potential superior wound dressing to alginate and chitosan nanofiber mats. *Carbohydr. Polym.* **2017**, *174*, 591–600.
195. Hamano, F.; Seki, H.; Ke, M.; Gopiraman, M.; Lim, C.T.; Kim, I.S. Cellulose acetate nanofiber mat with honeycomb-like surface structure. *Mater. Lett.* **2016**, *169*, 33–36.
196. Maftoonazad, N.; Ramaswamy, H. Design and testing of an electrospun nanofiber mat as a pH biosensor and monitor the pH associated quality in fresh date fruit (Rutab). *Polym. Test.* **2019**, *75*.
197. Kim, J.W.; Kim, M.J.; Ki, C.S.; Kim, H.J.; Park, Y.H. Fabrication of bi-layer scaffold of keratin nanofiber and gelatin-methacrylate hydrogel: Implications for skin graft. *Int. J. Biol. Macromol.* **2017**, *105*.
198. Xie, Z.; Paras, C.B.; Weng, H.; Punnakitikashem, P.; Su, L.-C.; Vu, K.; Tang, L.; Yang, J.; Nguyen, K.T. Dual growth factor releasing multi-functional nanofibers for wound healing. *Acta Biomater.* **2013**, *9*, 9351–9359.
199. Ji, L.; Lin, Z.; Medford, A.J.; Zhang, X. Porous carbon nanofibers from electrospun polyacrylonitrile/SiO2 composites as an energy storage material. *Carbon N. Y.*

2009, *47*, 3346–3354.

200. Líbalová, H.; Costa, P.M.; Olsson, M.; Farcal, L.; Ortelli, S.; Blosi, M.; Topinka, J.; Costa, A.L.; Fadeel, B. Toxicity of surface-modified copper oxide nanoparticles in a mouse macrophage cell line: interplay of particles, surface coating and particle dissolution. *Chemosphere* **2018**, *196*, 482–493.
201. Geohegan, D.B.; Puretzky, A.A.; Duscher, G.; Pennycook, S.J. Time-resolved imaging of gas phase nanoparticle synthesis by laser ablation. *Appl. Phys. Lett.* **1998**, *72*, 2987–2989.
202. Kabashin, A. V.; Meunier, M.; Leonelli, R. Photoluminescence characterization of Si-based nanostructured films produced by pulsed laser ablation. *J. Vac. Sci. Technol. B Microelectron. Nanom. Struct.* **2001**, *19*, 2217–2222.
203. Kabashin, A. V; Singh, A.; Swihart, M.T.; Zavestovskaya, I.N.; Prasad, P.N. Laser-Processed Nanosilicon: A Multifunctional Nanomaterial for Energy and Healthcare. *ACS Nano* **2019**, *13*, 9841–9867.
204. Bailly, A.L.; Correard, F.; Popov, A.; Tselikov, G.; Chaspoul, F.; Appay, R.; Al-Kattan, A.; Kabashin, A. V.; Braguer, D.; Esteve, M.A. In vivo evaluation of safety, biodistribution and pharmacokinetics of laser-synthesized gold nanoparticles. *Sci. Rep.* **2019**, *9*, 1–12.
205. Nirwan, V.P.; Al-Kattan, A.; Kabashin, A.; Fahmia, A. Electrospun PEO/Chitosan Nanofibers Templated with Gold Nanoparticles Prepared with Laser and Wet Synthesis. In Proceedings of the 2018 IEEE 8th International Conference Nanomaterials: Application & Properties (NAP); IEEE, 2018; pp. 1–4.
206. Croisier, F.; Jérôme, C. Chitosan-based biomaterials for tissue engineering. *Eur. Polym. J.* **2013**, *49*, 780–792.
207. Hajiali, F.; Tajbakhsh, S.; Shojaei, A. Fabrication and Properties of Polycaprolactone Composites Containing Calcium Phosphate-Based Ceramics and Bioactive Glasses in Bone Tissue Engineering: A Review. *Polym. Rev.* **2018**, *58*, 164–207.
208. Contreras-Cáceres, R.; Cabeza, L.; Perazzoli, G.; Díaz, A.; López-Romero, J.M.; Melguizo, C.; Prados, J. Electrospun nanofibers: Recent applications in drug delivery and cancer therapy. *Nanomaterials* **2019**, *9*.
209. Zelepukin, I. V.; Popov, A.; Shipunova, V.O.; Tikhonowski, G. V; Mirkasymov, A.B.; Popova-Kuznetsova, E.A.; Klimentov, S.M.; Kabashin, A. V.; Deyev, S.M. Laser-synthesized TiN nanoparticles for biomedical applications: evaluation of safety, biodistribution and pharmacokinetics. *Mater. Sci. Eng. C.* **2020**.
210. Kim, M.; Hwang, S.; Yu, J.-S. Novel ordered nanoporous graphitic C 3 N 4 as a support for Pt–Ru anode catalyst in direct methanol fuel cell. *J. Mater. Chem.* **2007**, *17*, 1656–1659.
211. Rounaghi, S.A.; Vanpoucke, D.E.P.; Eshghi, H.; Scudino, S.; Esmaeili, E.; Oswald, S.; Eckert, J. Mechanochemical synthesis of nanostructured metal nitrides, carbonitrides and carbon nitride: a combined theoretical and experimental study. *Phys. Chem. Chem. Phys.* **2017**, *19*, 12414–12424.
212. Abdelrazek, E.M.; Hezma, A.M.; El-khodary, A.; Elzayat, A.M. Spectroscopic studies and thermal properties of PCL/PMMA biopolymer blend. *Egypt. J. Basic Appl. Sci.*

2016, *3*, 10–15.

213. Tian, J.; Wong, K.K.Y.; Ho, C.-M.; Lok, C.-N.; Yu, W.-Y.; Che, C.-M.; Chiu, J.-F.; Tam, P.K.H. Topical Delivery of Silver Nanoparticles Promotes Wound Healing. *ChemMedChem* **2007**, *2*, 129–136.
214. Ali, S.; Morsy, R.; El-Zawawy, N.; Fareed, M.; Bedaiwy, M. Synthesized zinc peroxide nanoparticles (ZnO2-NPs): a novel antimicrobial, anti-elastase, anti-keratinase, and anti-inflammatory approach toward polymicrobial burn wounds. *Int. J. Nanomedicine* **2017**, *Volume 12*, 6059–6073.
215. Grande, F.; Tucci, P. Titanium Dioxide Nanoparticles: a Risk for Human Health? *Mini-Reviews Med. Chem.* **2016**, *16*, 762–769.
216. Allegri, M.; Bianchi, M.G.; Chiu, M.; Varet, J.; Costa, A.L.; Ortelli, S.; Blosi, M.; Bussolati, O.; Poland, C.A.; Bergamaschi, E. Shape-related toxicity of titanium dioxide nanofibres. *PLoS One* **2016**, *11*.
217. Hamilton, R.F.; Buford, M.; Xiang, C.; Wu, N.; Holian, A. NLRP3 inflammasome activation in murine alveolar macrophages and related lung pathology is associated with MWCNT nickel contamination. *Inhal. Toxicol.* **2012**, *24*, 995–1008.
218. Gotman, I.; Gutmanas, E.Y.; Hunter, G. 1.8 Wear-Resistant Ceramic Films and Coatings ☆. In *Comprehensive Biomaterials II*; Elsevier, 2017; pp. 165–203 ISBN 9780081006924.
219. Hyde, G.K.; McCullen, S.D.; Jeon, S.; Stewart, S.M.; Jeon, H.; Loboa, E.G.; Parsons, G.N. Atomic layer deposition and biocompatibility of titanium nitride nano-coatings on cellulose fiber substrates. *Biomed. Mater.* **2009**, *4*, 025001.
220. Paschoal, A.L.; Vanâncio, E.C.; Canale, L. de C.F.; Silva, O.L. da; Huerta-Vilca, D.; Motheo, A. de J. Metallic Biomaterials TiN-Coated: Corrosion Analysis and Biocompatibility. *Artif. Organs* **2003**, *27*, 461–464.
221. Baronzio, G.F.; Hager, E.D. *Hyperthermia in Cancer Treatment: A Primer*; Springer US: Boston, MA, 2006; ISBN 978-0-387-33440-0.